UNBONDED MONOSTRANDS FOR CAMBER ADJUSTMENT

by

Vivek Sethi

Thesis presented to the faculty of the

Virginia Polytechnic Institute and State University

In partial fulfillment of the requirements for the degree of

Master of Science

in

Civil Engineering

Committee:

Carin L. Roberts-Wollmann, Co-Chair

Kamal B. Rojiani, Co-Chair

Richard E. Weyers

Feb 13, 2006

Blacksburg, VA

Keywords: Camber, Creep, Shrinkage, High strength concrete, Monte Carlo Simulation,

Prediction models, Probability distribution, Unbonded monostrands

UNBONDED MONOSTRANDS FOR CAMBER ADJUSTMENT

Vivek Sethi

Abstract

Prestressed concrete structural members camber upwards or downwards depending upon the location of application of prestress force. Identical members do not camber equally due to variability of the factors influencing it. Differential camber in the beams, if significant, results in excessively tall haunches or girder top flange extending into the bottom of the slab. For adjacent members like deck bulb-tees and box girders that are to be transversely post-tensioned the differential camber causes problems during the fit up process. This variation is undesirable and hinders the smooth progress of construction work if not properly accounted for at the design stage.

Various factors influence camber and camber growth in prestressed members. Some of the factors are concrete strength and modulus, concrete creep and shrinkage properties, curing conditions, maturity of concrete at release of prestress force, initial strand stress, climatic conditions in storage and length of time in storage. Combinations of these variables result in variation of camber of otherwise similar beams at the time they are erected.

One way to increase the precision of camber estimation is to use Monte Carlo simulation based upon the randomized parameters affecting the camber and camber growth. In this method, the parameters, in the form of a probability distribution function, are combined and passed through a deterministic model resulting in camber and camber growth prediction with narrowed probability bounds as compared to single definite value given by most contemporary methods. This outcome gives the expected range of cambers for a given girder design. After determining the expected range of camber, the ultimate goal is to provide guidelines for using unbonded monostrands for camber adjustment.

ACKNOWLEDGEMENT

Saying a thank you would not fully express my gratitude toward my professors who have been my mentors and guides for the last one and a half years. I would like to thank especially my committee chair and advisor Dr. Carin L. Roberts-Wollmann who showed faith in my capabilities and gave me an opportunity to work on this project. She was a constant source of inspiration and guidance and was always there to answer my every question. I would also like to thank my committee co-chair Dr. Kamal B Rojiani, without whose expertise and guidance in Statistical methods, this work would not have been a reality. I would also like to thank Dr. Richard E. Weyers for serving as a member of my committee and for his guidance on concrete materials.

I would like to express my gratitude toward my mother Sumitra Sethi, father VK Sethi, sister Swati and brother-in-law Harsh, without whose financial and emotional support, I could never be the person I am now.

I would like to say a special thanks to my roommate Surya, whose constant motivation and good food kept me working for long hours. I would like to thank my friends Manoj, Hasan, Ravi, Sumit, Vyas, for their encouragement and support.

Last but not least, I would like to thank God for giving me patience and perseverance to fulfill my dreams.

Table of Contents

List of Tables

List of figures

Chapter 1

Introduction

1.1 Introduction

Camber and camber growth are characteristic of all prestress members. Beams are observed to camber differently even though they have similar dimensions and concrete properties. This difference in camber of otherwise identical beams poses many problems during construction like increased haunch depths, jutting of beams into the bottom of the slab and increase in time for setting up the forms for cast in place deck slabs. Also for adjacent box girders and deck bulb-tees, the difference in camber causes problems during the fit up process. This unnecessarily increases the time and cost of construction.

Engineers over the years have improved their understanding of the behavior of concrete, but have been unable to precisely predict it. Concrete is a very complex material and its properties depend on materials used and environmental conditions under which it is produced and stored. These infinite combinations of materials and environmental conditions render it impossible to model precisely. The camber and camber growth in prestress members depends on various factors such as concrete strength and modulus, concrete creep and shrinkage properties, curing conditions, maturity of concrete at release of prestress force, initial strand stress, climatic conditions in storage and length of time in storage. Combination of these variable parameters results in variation of camber at the time of erection.

Lack of proper models to predict the behavior of concrete results in erroneous estimates of prestress losses and thus the camber in prestressed members. The variability in the concrete properties calls for the use of probabilistic methods to estimate a range of camber rather than calculating a discreet value as given by most contemporary methods.

The limits of the parameters affecting the camber and camber growth and their statistical distribution have been determined from experimental tests and published in literature. It is therefore possible to create a probability distribution function of the camber and camber growth in structural members based upon the random variation of the parameters and a model that can combine these parameters to calculate camber. This should give the range of camber expected for the structural member simulated by the model.

1.2 Implementing a Probabilistic Analysis

The overall analysis in this thesis consists of the application of two methods. The first being the transformed section analysis of concrete using the age adjusted effective modulus to plot the moment curvature relationships for calculation of camber and the second is randomizing the parameters affecting the above analysis using the Monte Carlo method to generate a probability distribution for the camber and camber growth.

1.2.1 Transformed Section Analysis

The stresses, strains and the prestress losses in the structural members are computed using either a net concrete section or a transformed section. The advantage of the transformed section analysis using the age adjusted effective modulus is that prestress losses are not calculated explicitly but are accounted for intrinsically in the method. The stresses and strains at various sections in the structural member are calculated using the transformed section analysis and then the force, moment and curvature in the net concrete section at various points is calculated. After that, the curvature diagram is plotted and then using the moment area method the deflection is calculated.

The camber growth is calculated using a change in curvature plot. The change in curvature is calculated using the age adjusted effective modulus approach by setting the necessary equilibrium, constitutive and compatibility relationships on the forces in the net concrete section. The parameters used to calculate the camber and camber growth are randomized from their probability distribution functions using the Monte Carlo method

and the probability distributions of camber and camber growth is generated. This probability distribution then gives a mean, an upper bound and a lower bound in which the camber is expected to fall for the member simulated. Thus its helps in establishing a confidence interval for the camber and camber growth rather than giving a discrete value as given by contemporary methods.

1.2.2 Monte Carlo Applications

The numerical method known as the Monte Carlo method is a statistical simulation technique to simulate a random or stochastic process. The Monte Carlo method is often used in simulations where the number of variables affecting the behavior of a system are too numerous and not sufficiently well understood for an analytical solution. The only requirement of the method is that the factors affecting the physical behavior of the system be described as probability distribution functions. Examples of the implementation of the Monte Carlo methods in civil engineering include the comparison of prestress loss methods in prestressed concrete beams (Ahlborn and Glibertson, 2003). Kirkpatrick (2001) determined the statistics of impact of chloride induced corrosion on service life of Virginia bridge decks using the Monte Carlo method. MacGregor (1979) used the method to develop the statistics of shear strength for slender reinforced beams in bending. Monte Carlo methods are also used in limit state applications where the reliability of high strength concrete is studied or where the reliability of partially prestressed beams is studied at those limit states (Naaman et al., 1982). The above examples use the Monte Carlo method to develop the statistics.

1.3 Objective and Scope

The objectives of this thesis are as follows:

1. To develop a simple probabilistic model for camber and camber growth of prestressed concrete members based on the transformed section analysis using the age adjusted effective modulus approach similar to the one used in NCHRP 496().

2. To utilize the probabilistic model in Monte Carlo simulation to simulate camber and camber growth characteristics of commonly used girder types produced by prestressing plants in Virginia. The probabilistic model should simulate camber and camber growth characteristics of all possible girder types commonly used in modern bridges. It is anticipated that the results of the simulation will provide expected values of camber and camber growth and a range in which they are expected to fall.

3. To confirm the validity of the model by comparing the results with the actual field data.

4. To study the feasibility of providing unbonded monostrands at the bottom of the girder, to adjust the camber upwards, as well as at the top of the girder to adjust the camber downwards. In addition, the influence of the monostrands tendons on the girder stresses and ultimate strength will also be studied.

5. To provide recommendations for future work.

1.4 Organization

This thesis is divided into six chapters. The first chapter introduces the problem statement and briefly describes the approach and the method of analysis used in this thesis. The second chapter is the theoretical development of the model and briefly reviews the literature associated with it. The method of analysis is described in the third chapter. The fourth chapter describes the method of random number generation and the statistics of the variables describing the model. Results of the simulation are presented in the fifth chapter. Discussion of these results and recommendations for future work are suggested in the sixth chapter.

Chapter 2

Literature review

2.1 Introduction

Concrete is an excellent compressive material but has poor tensile properties. Its tensile strength is approximately 10 percent of its compressive strength (Nilson, 1997). The tensile strength of concrete is unpredictable and is associated with small deformations prior to failure. These small deformations lead to a brittle failure, which is undesirable in design from safety and serviceability points of view. Therefore, reinforcing steel bars are placed in concrete members to improve their tensile performance and make the structure more ductile. Ordinary reinforcing steel is suitable for short span members. For medium and long spans, problems like excessive member size, steel quantities beyond those necessary to ensure ductile failure, and lack of economy are encountered.

The concept of prestressing concrete beams was invented in an effort to reduce excessive member sizes, span longer distances and improve the serviceability performance of ordinary reinforced concrete. The most common serviceability problems are crack widths and deflections. It is observed that crack widths are directly proportional to the magnitude of stress in reinforcing steel. Thus to limit crack widths, reinforcing steel is used at a much lower stress than it is capable of withstanding. The problems of large deflections and crack width are overcome by prestressing the steel at a high stress and applying most of the steel strain before the member is loaded.

The reasons why prestressed concrete is preferred over reinforced concrete are as follows:

- Longer spans
- Lighter members
- Efficient use of materials
- Control of cracking

- Smaller deflections
- Smaller dead load to live load ratio
- Greater carrying capacity for a given member size.

The development of prestressed concrete is credited to French engineer Eugene Freyssinet. He noticed the improvement in concrete performance that arises from prestressing. He was the first person who studied the effects of creep and shrinkage on prestressed concrete. His studies led him to realize that steel at high initial stress should be used to ensure that the prestress force lost due to time effects is not greater than the applied prestress to the steel. Thus, the use of high strength steel in prestressing began.

2.2 Problems with Prestressed Concrete

The use of prestressed concrete is very wide and varied. Its use is becoming more popular with time and slowly it is becoming a material of choice. In spite of many advances in the use of prestressed concrete, there have been only small advances in methods of predicting time dependent losses. There is a need for an all-encompassing model for predicting creep and shrinkage behavior in concrete, which is simple enough to be used by design engineers in practical applications. Research is still going on in this area but it is unlikely that this problem can be solved in near future. The reason that this problem cannot be solved so easily is the complex nature of concrete. Due to the complexity of predicting the creep and shrinkage of concrete, various code committees have developed predictive models which are conservative for design but sacrifice economy and efficiency (Bazant et al. 1984). It is for this reason that the precast industry and researchers are constantly endeavoring to develop a better model for the prediction of creep and shrinkage.

2.3 Prestress Losses

Prestress losses are divided into two categories:

- Instantaneous losses

- Time dependent losses

Instantaneous losses depend on the method of prestressing used:

In pretensioned concrete, the instantaneous losses are as follows:

- Elastic shortening

In post-tensioned concrete, the instantaneous losses are as follows:

- Frictions losses (curvature and wobble)
- Seating losses
- Elastic shortening (with multiple tendons)

Elastic shortening losses occur because of shortening of concrete in the elastic range due to applied stress. Friction losses occur only in post tensioning due to the friction between the tendon and the duct through which it is passed. Seating losses depend on the type of equipment used by the post-tensioning supplier and most manufacturers of post tensioning systems specify it as a standard value.

Time dependent losses are independent of the method of prestressing used, and they are as follows:

- Loss due to creep of concrete
- Loss due to shrinkage of concrete
- Loss due to relaxation of steel strand
- Thermal effects

Thermal effects on long-term prestress losses are neglected in design. They are significant in the regions where extreme temperature variations occur. Incorporating the effects of temperature in creep and shrinkage models is very difficult due to the complex nature of the problem (Bazant, 1985). In normal operating environments, the effect of temperature is insignificant and therefore it is neglected (Bazant et al. 1983).

For the other time dependent losses, various analytical models are used to predict the behavior. However, due to the material complexity of concrete, it is very difficult to develop a comprehensive model for predicting creep and shrinkage effects in concrete over time. Relaxation of prestressing steel is a type of creep effect and is defined as loss

of stress in steel at constant strain. This effect is predicted quite well by its analytical model because of the homogeneity of material.

Various internationally recognized models are available for predicting creep, shrinkage, elastic shortening and strand relaxation effects. Each method has its merits and drawbacks. For this thesis, the model recommended by NCHRP Report 496 (2003) for predicting creep, shrinkage and elastic shortening are used. The reason for using the NCHRP Report 496 model is that it is the only model designed specifically for high strength concrete (HSC) and is already included in the 2005 Interim AASHTO LRFD specification. The strand relaxation model is the Prestressed Concrete Institute Bridge Design Manual model (PCI, 1997). The AASHTO LRFD design methods are used in this thesis for design of girders. Major factors affecting the prestressed concrete and ultimately the camber are discussed in the following sections. The variation of stress versus time in a prestressed concrete girder is shown in Fig 2.1

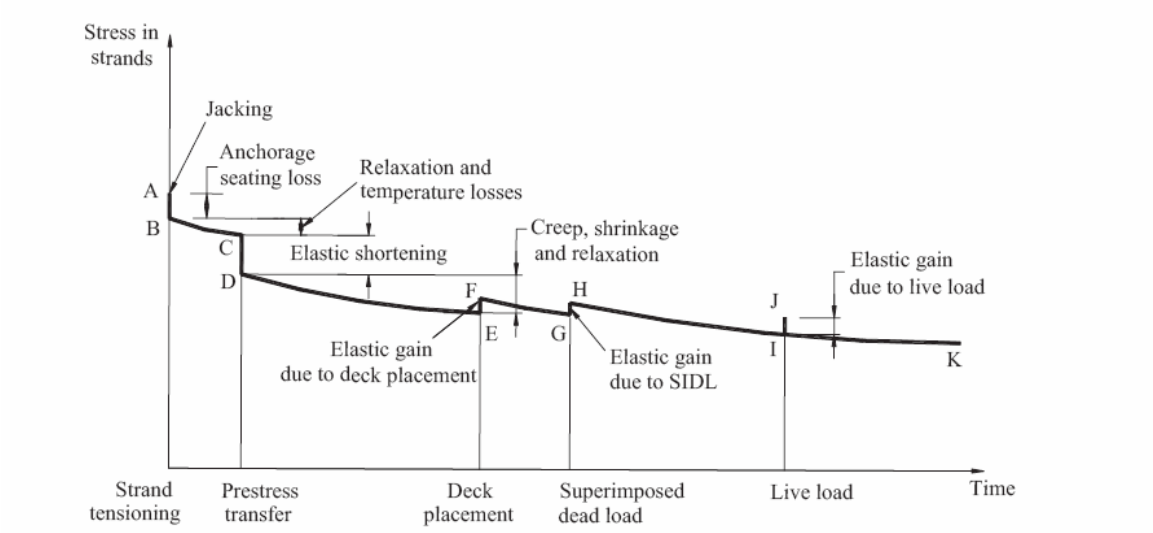

Figure 2.1 Stress versus time in the strands in a pretensioned concrete girder (NCHRP Report 496, 2003)

2.4 Camber

Camber is the upward deflection in flexural members due to an eccentrically applied prestressing force. Camber is subdivided into two categories i.e., initial camber and long-term camber. Initial camber is induced at transfer of the prestressing force at the time of release. It is the net upward deflection calculated by algebraically summing the smaller downward deflection caused by the beam self weight (Δ_{beam}) and the larger upward deflection (Δ_{ps}) caused by the prestressing force applied at an eccentricity 'e' below the center of gravity of the section. The components of camber due to self weight and prestressing force are given in Eqs. 2.1 and 2.2

$$\Delta_{beam} = \frac{5wL_s^4}{384E_cI} \tag{2.1}$$

$$\Delta_{ps} = \frac{PeL_s^2}{8E_cI} \tag{2.2}$$

for straight tendon profile

The magnitude of initial camber is the difference (Δ_{ps}- Δ_{beam}) between the above two values. Figure 2.2 illustrates the components of initial camber in the beams.

The long-term camber is extremely difficult to predict because of the large variability in the factors affecting it. Some of the factors affecting the camber growth are concrete strength and modulus, maturity of concrete at the time of transfer of prestress, creep, and shrinkage. The time dependent growth of camber is most affected by creep, which is caused by sustained applied loads such as prestress, and dead weight on the beam as shown in Figure 2.3.

Various methods are available for predicting initial and long-term camber in girders. Many studies have been done in the past to verify these methods with experimental

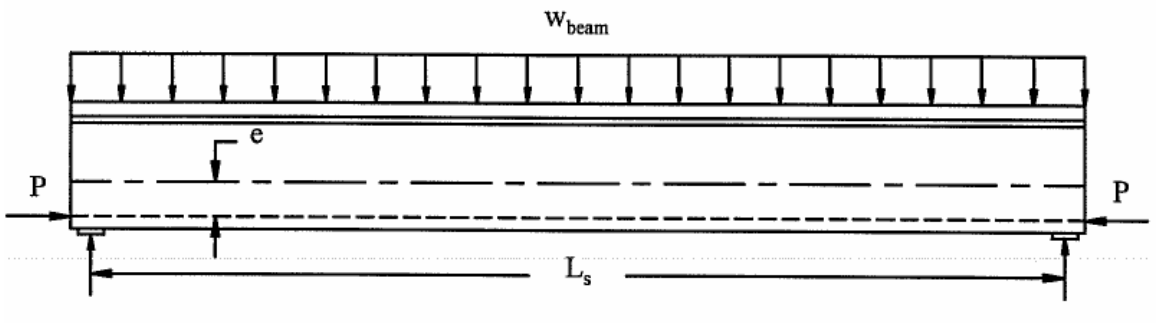

a) Loads applied to beam at release

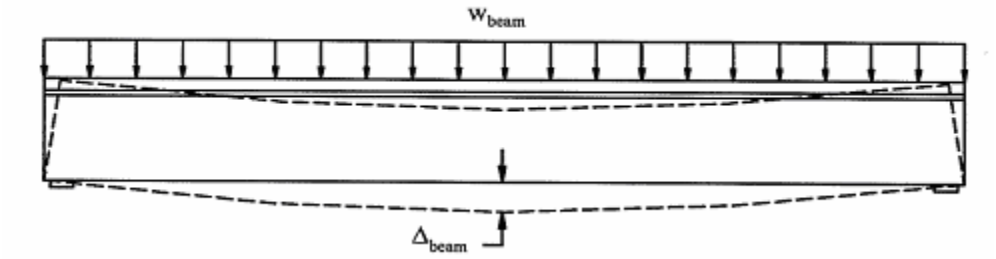

b) Deflections due to beam weight

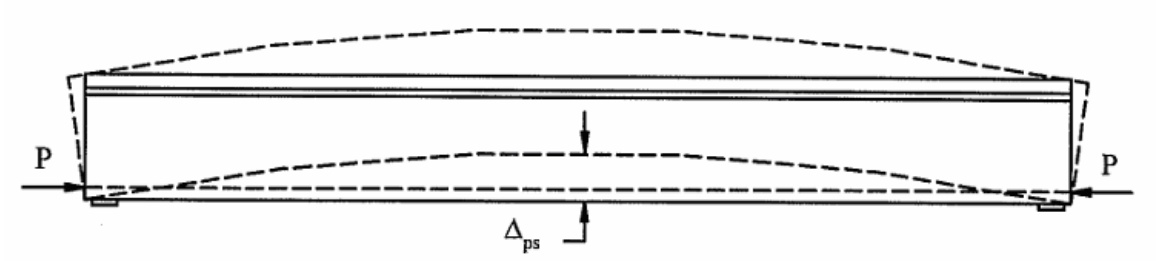

c) Camber due to prestressing force

Figure 2.2 Elastic components of beam camber and deflection immediately after release (Byle et al. 1997).

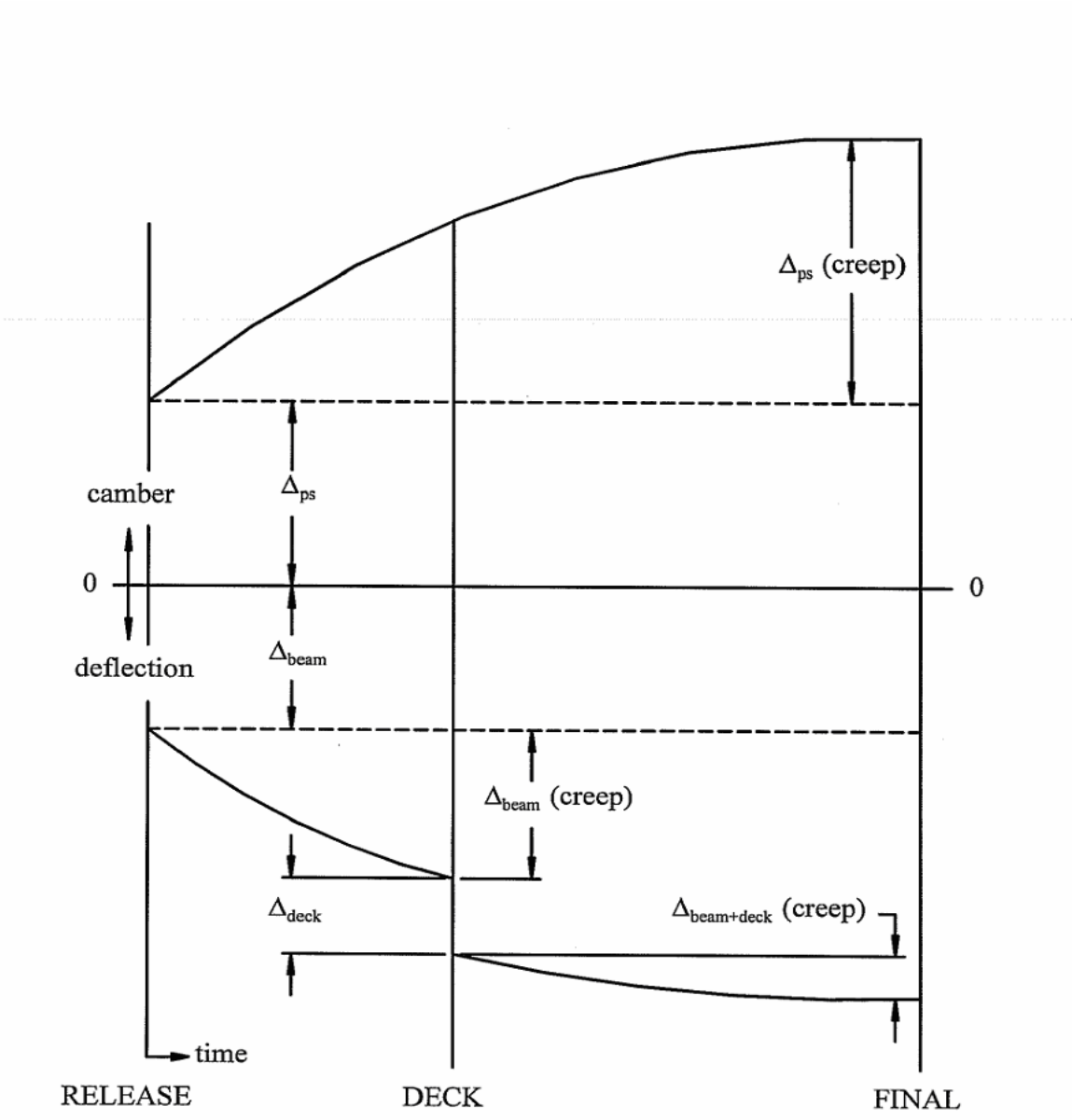

Figure 2.3 Components of time dependent camber and deflection (Byle et al. 1997).

results. Literature pertaining to these studies has been reviewed and a brief overview of these studies is given in the following paragraphs.

It has been observed that beams having identical cross sectional dimensions and material properties have significant variation in their cambers (Stallings et al. 2001). Kelly, Breen and Bradberry (1987) found that beams made of low strength concrete exhibited the greatest camber during erection, the greatest time dependent effects, and the least final camber at the end of their service life whereas beams made of high strength concrete exhibited opposite trends. Hinkle (2005) measured the camber of beams from the time of release until an age of 180 days. The experimental results showed the camber to increase until an age of 40 days, after which it stabilized for the duration of the measurement. Byle, Burns and Carrasquillo (1997) tracked camber and deflection from the time of release until the beams were in service. They compared the experimental results with the PCI method (PCI BDM, 1997) and the time step method (Branson, 1997) and they found the time step method to be a better predictor of camber when using time dependent material properties. Stallings and Eskildsen (2001) compared the experimentally measured values with theoretical values calculated using an incremental time step method. It was observed that when standard parameters of creep and shrinkage were used with an incremental time step method, it over predicted the camber by 24 percent. Upon using the parameters of HSC it under estimated the values by 6 percent on an average below the measured camber values. The larger error when standard parameters were used was attributed to over estimation of creep effects.

2.5 Parameters Affecting Camber

2.5.1 Modulus of Elasticity

Researchers over the years have worked to find a simple relationship for the modulus of elasticity of concrete. Neville (1997) asserted that there could be no simple relationship between the modulus of elasticity and compressive strength of concrete. The reason for this is that the modulus of elasticity of concrete is affected not only by the modulus of

elasticity of the aggregate but also the volumetric content of the aggregate in the mix. Current equations of modulus of elasticity given in various codes and specifications do not account for the bond between the aggregate and cement paste. Upon loading the concrete, micro cracking occurs at the interface of aggregates and cement paste and it is observed to affect the structural behavior of concrete. The stress-strain relationship of the constituent materials is observed to be linear but their combined response in concrete is nonlinear. The stress strain relationship for concrete is curvilinear and depends on the relative stiffness of aggregates and cement paste.

Due to the lower water cement ratio (w/c) in HSC mixes, the modulus of elasticity is found to be similar between the hardened cement paste and aggregate. Thus, concrete behaves as a more homogeneous material and its stress strain curve approaches linearity. Baalbaaki, Aitcin and Ballivy (1992) observed that the relationship between the modulus of elasticity and compressive strength are only valid for normal strength concrete. They also observed that predicting the modulus of elasticity of concrete based on the modulus of elasticity of aggregate worked well for granite and limestone aggregates, but not for quartzite and sandstone aggregates.

Various studies have been done to measure the accuracy of models for prediction of modulus of elasticity of concrete with the experimental results. The models that have been studied and a summary of the findings are as follows:

2.5.1.1 AASHTO LRFD Specification

The present AASHTO Equation 5.4.2.4-1 (AASHTO LRFD, 1998) given as Equation number 2.3 is applicable only for concrete having unit weights of 0.090kcf to 0.155kcf.

$$E_c = 33000 w_c^{1.5} \sqrt{f_c'} \text{ (kcf and ksi)} \qquad (2.3)$$

where E_c is the concrete modulus of elasticity,

f_c' is the concrete compressive strength of 4x8 cylinder at corresponding age, and

w_c is the unit weight of concrete.

The ACI 363 Committee report (ACI 363, 1992) observed that this equation tends to significantly over estimate the modulus of elasticity of concretes with compressive strengths higher than 6 ksi. Huo, Al-Omaishi, and Tadros (2001) observed a similar trend. NCHRP 496 (2003) also observed a similar trend where the above equation overestimated the modulus of elasticity for HSC.

2.5.1.2 ACI 363

The ACI 363 (ACI 363, 1992) equation for modulus of elasticity, given as Equation 2.4 below.

$$E_c = \left(\frac{w_c}{0.145}\right)^{1.5} \left(1000 + 1265\sqrt{f_c'}\right) \text{ (kcf and ksi)} \qquad (2.4)$$

where the E_c, f_c' and w_c are same as defined above.

This equation also over predicts the modulus for high strength concrete (Ahlborn et al. 1996). Myers and Carrasquillo (1999) have shown that modulus of elasticity of concrete appears to be a function of aggregate content and type. The above equation also does not include factors other than concrete self-weight and strength.

2.5.1.3 ACI 318

ACI 318 (ACI 318, 2002) also uses a similar equation as the AASHTO LRFD Equation 5.4.2.4-1 and similar trends of under prediction of modulus of elasticity have been reported by various researchers (Kahn et al. 1997).

2.5.1.4 NCHRP 496

This is the most recent equation given for predicting the modulus of elasticity of high strength concrete. It includes the effect of aggregate type, the equation is given as:

$$E_c = 33000 K_1 K_2 \left(0.140 + \frac{f_c'}{1000}\right)^{1.5} \sqrt{f_c'} \text{ (ksi)} \qquad (2.5)$$

where E_c, f_c' have the same meaning as above and

$$w_c = \left(0.140 + \frac{f_c'}{1000} \right)^{1.5}$$

K_1 = represents the difference between the national average and local average if test results are available

K_2 = represents whether an upper bound or lower bound is required. Note that f_c' is in ksi.

Tadros and Al-Omaishi (2003) have observed that this equation predicts the upper and lower bounds for the modulus of elasticity of the high strength concrete made in four states of Nebraska, New Hampshire, Texas and Washington very well. They have also given values of K_1 and K_2 depending on the types of aggregates available in these states. They have suggested that where the values of K_1 and K_2 are not available they should be taken as one.

Waldron (2004) measured the prestress losses for nine HSC girders in Virginia and compared the losses predicted by various methods. He found that the NCHRP 496 (2003) method to be one of the best predictors. The difference between measured and predicted losses was less than 5 ksi. This method has been incorporated in the 2005 Interim AASHTO LRFD Specifications. Thus, in this thesis this model is used for predicting the modulus of elasticity, creep and shrinkage of concrete.

2.5.2 Creep

Concrete creep is the most significant time and stress dependent effect in concrete. Considerable research has been done in the field of creep study. Despite this, there is no all-encompassing model which can predict creep and shrinkage accurately. This is due to material complexity of concrete, which renders the task of predicting accurately creep effects in concrete very difficult. Concrete after its formation is not in a state of equilibrium and undergoes change due to ongoing hydration reaction and moisture

diffusion through the member. Therefore, creep is separated in two components, basic creep and drying creep. Basic creep is the continued deformation under an applied stress occurring in a sealed specimen in a hydro-equilibrium environment. Drying creep occurs when a specimen is free to exchange moisture with the environment, inducing a drying stress in the specimen. In a prestressed girder, creep results in camber growth. The prolonged shortening of the bottom flange of the girder due to eccentrically applied prestress force causes the growth of camber in girders. The rate and extent of creep in prestressed girders depends on factors like time, maturity of the concrete at the time the time load is first applied, magnitude of applied stress, curing conditions, ambient relative humidity, mixture proportions, aggregate properties and w/c ratio.

Creep characteristics of concrete depend on the maturity of the concrete at the time it is first loaded. A more mature concrete specimen has better capacity to resist creep on application of load. HSC is found to be more sensitive to early age loading than normal strength concrete (Kahn et al 1997).

The magnitude of applied stress also influences creep characteristics of concrete. ACI 209 (ACI, 1992) suggests that the amount of creep is proportional up to an applied stress level of 40 percent of concrete strength. Shams and Kahn (2000) have suggested that, for HSC the amount of creep is proportional up to 60 percent of concrete compressive strength. According to AASHTO LRFD specifications (AASHTO, 1998) also, concrete strains are proportional to applied stress equal to 60 percent of concrete compressive strength.

ACI 209 (ACI, 1992) and AASHTO LRFD specifications indicate that at relative humidity of 40 percent, the ultimate creep coefficient is 36 percent higher than at a relative humidity of 80 percent. The ambient relative humidity affects the amount of drying creep.

Concrete creep is also affected by curing conditions. It has been observed that steam curing can reduce creep by 30 to 50 percent by accelerating the hydration of cement

(Neville, 1997). Researchers have also observed that concrete cured at high temperature exhibits more creep than concrete cured at lower temperature because of increased porosity and internal cracking (Mokhtarzadeh and French, 2000). Air cured specimens of concrete are found to exhibit more creep than moist cured specimens (Kahn, et. al. 1997).

The constituent materials and their mix proportions also affect the creep characteristics of concrete. The majority of creep occurs in the cement paste surrounding the aggregate. Therefore, the type of cement used also affects the creep. Rapid hardening cement produces a stiffer paste quickly and thus they exhibit lesser creep than slower hardening cement. (Neville, 1970). Aggregate properties like grading, particle size, shape, stiffness, surface roughness and absorption also affect creep. Concrete made with stiffer aggregates is found to exhibit lesser creep as the cement paste transfers the load applied to the aggregates (Mokhtarzadeh and French, 2000). Alexander (1996) found that aggregates with low absorption tend to produce lesser creep. Several researchers have observed that concrete with high compressive strength and lower w/c ratio exhibits lower creep than normal strength concrete (Alexander et al, 1996).

2.5.2.1 Mathematical Model of Creep of Concrete

Concrete can be approximated as an aging linear visco-elastic material for which the uniaxial relationship between stress and strain can be expressed as a Stieltje's integral (Bazant, 1975) as opposed to other forms such as Rieman's integral or Volterra's integral which do not include discontinuous stress histories. The Time Step method for calculating creep strains is a numerical equivalent of Stieltje's integral.

$$\varepsilon_t - \varepsilon_t^o = \int_0^t J(t, t_o) d\sigma(t_o) \qquad (2.6)$$

where

$d\sigma$ is the increment or decrement of stress occurring in different time steps, and

$d\sigma(t_o)$ is the stress applied at time zero or the time of loading,

ε_t is the total normal strain of an axially loaded specimen and is the sum total of creep, shrinkage, thermal and inelastic strain,

ε_t° is the instantaneous elastic strain at the time of loading,

$J(t,t_o)$ is the creep compliance defined as the strain at time t including the instantaneous elastic strain caused by a unit stress since time t_o.

The following assumptions are made to use the preceding function:

1. The water content history of concrete is disregarded.
2. Temperature effects on creep are disregarded.

The above assumptions allow the stress or strain at any time to be considered as a function of the previous stress or strain alone.

McHenry (McHenry, 1943) realized the importance of the above equation in the principal of superposition as applied to concrete. The principal of superposition states that the stress or strain response due to two subsequent stress or strain histories is the sum of the individual responses. Experimental evidence and past studies have shown that this method models the time dependent behavior of concrete very well (Branson, 1977).

Other forms of the above equation are given below.

Rieman's Integral

$$\varepsilon(t) - \varepsilon(t_o) = \int_0^t J(t,t') \left(\frac{d\sigma(t)}{dt'} \right) dt' \tag{2.7}$$

if $\sigma(t)$ is a continuous function.

Volterra's Integral

$$\sigma(t) = \int_0^t E_R(t,t') \left[d\varepsilon(t') - d\varepsilon^o(t') \right] \tag{2.8}$$

where

$E_R(t,t')$ is the relaxation modulus or stress at time t caused by a unit constant strain introduced at time $t' \leq t$. Creep properties are completely described by either $J(t,t')$ or $E_R(t,t')$.

Several engineering societies and specification committees use the following form to describe the creep compliance $J(t,t')$.

$$J(t,t') = \frac{1+\phi(t,t')}{E(t')} = \frac{1}{E(t')} + C(t,t') \quad (2.9)$$

Φ(t,t') is the ratio of creep strain to elastic strain under constant stress and is called the creep coefficient.

C(t,t') is the specific creep

Engineering societies have made the following approximations.

$$\phi(t,t') = \phi_u(t')\phi(t-t') \quad (2.10)$$

where

Φ(t,t') is the ratio of creep strain to elastic strain under constant stress and is called the creep coefficient,

Φ_u (t') is the ultimate creep coefficient,

Φ(t- t') is the reduction factor for the ultimate creep coefficient and is a function of time.

The creep coefficient is a function of the ultimate creep value, reduced by a factor that is a function of time. Various researchers and technical committees have proposed a number of different models. The function of these models is to determine $\phi(t,t')$. The NCHRP 496 model is used in this thesis and will be discussed in the following sections.

2.5.2.2 NCHRP 496 Creep Model

Tadros et al. (2003) have proposed this model. This is the only model specifically developed for HSC. The NCHRP 496 creep model uses a similar approach as to that used in PCI BDM. The PCI BDM model was also developed by Tadros et al. (1985). The model used here uses the age adjusted effective modulus concept (Bazant, 1972). The effective modulus is defined as follows.

$$E_c^*(t,t_o) = \frac{E_c(t_o)}{1+\chi(t,t_o)C(t,t_o)} \quad (2.11)$$

where

$E_c(t_o)$ is the elastic modulus of concrete at transfer,

$\chi(t,t_o)$ is the aging coefficient,

$C(t,t_o)$ is the creep coefficient,

NCHRP 496 recommends the use of the following equation for predicting creep in HSC.

$$\psi(t,t_i) = 1.90\gamma_{cr}K_1K_2 \tag{2.12}$$

where

$\psi(t,t_i)$ is the creep strain at time t

K_1 and K_2 represents the average, upper and lower bound values of the creep coefficient for local materials

1.90 is the ultimate creep coefficient

γ_{cr} is the product of the applicable correction factors.

$$\gamma_{cr} = k_{td}k_{la}k_sk_{hc}k_f \tag{2.13}$$

The applicable correction factors are as follows:

$\mathbf{k_{td}}$ is the time development correction factor and is given by

$$\mathbf{k_{td}} = \frac{t}{61 - 4f_{ci}' + t} \tag{2.14}$$

where t is the age of concrete after loading, in days.

$\mathbf{k_{la}}$ is the loading factor and is given by

$$\mathbf{k_{la}} = t_i^{-0.118} \tag{2.15}$$

where t_i is the age of concrete when load is initially applied for accelerated curing and the age of concrete (in days) minus 6 days for moist curing.

$\mathbf{k_s}$ is the size factor

$$\mathbf{k_s} = \frac{1064 - 94V/S}{735} \tag{2.16}$$

where V/S is the volume to surface area ratio

$\mathbf{k_{hc}}$ is the humidity factor for creep

$$\mathbf{k_{hc}} = 1.56 - 0.008H \tag{2.17}$$

where H is the relative humidity, in percent

$\mathbf{k_f}$ is the concrete strength factor

$$\mathbf{k_f} = \frac{5}{1 + f_{ci}'} \tag{2.18}$$

where f_{ci}' is the specified compressive strength at prestress transfer (ksi).

Equation (2.12) and the correction factors given in Equations (2.13) through (2.18) are based on research done on HSC girders in four states, Texas, Washington, New Hampshire and Nebraska.

Several other models such as ACI 209, AASHTO LRFD, B3, Sakata, GL2000, Shams and Kahn, AFREM are available for predicting the creep and shrinkage in concrete. However, none of these models are as all encompassing and accurate. Most of them either over predict or under predict the creep strains. Various researchers have conducted studies to verify the best predictor of experimentally measured values. However, there has been no consensus amongst them. Townsend (2003) reports that the ACI 209 modified method is the best predictor of creep strain of all models considered. Waldron (2004) reports that the AASHTO LRFD model is the best for predicting creep strains. According to Myerson (2001), the Sakata model is the best predictor of creep strain. Huo et al. (2001) have found that the ACI 209 model over predicts creep strains. Due to availability of a vast amount of literature with conflicting opinions about the best predictor of creep and shrinkage model, no conclusion about the best model can be drawn. Therefore in this thesis the NCHRP Report 496 model is used since it was adopted in 2005 Interim AASHTO LRFD specification. Most designers in industry use these specifications so it was the most logical choice.

2.5.3 Shrinkage

The volumetric change in a concrete specimen in the absence of load is called shrinkage. Shrinkage has three components, drying shrinkage, autogenous shrinkage and

carbonation. Drying shrinkage takes place when excess water, not consumed during the hydration process, diffuses into the environment. Autogenous shrinkage occurs because the volume of hydrated cement is less than the solid volume of dry unhydrated cement. Carbonation occurs when carbon dioxide present in the atmosphere reacts with calcium hydroxide in the cement paste, in the presence of moisture, and results in a decrease in the volume of concrete.

Shrinkage is also a time dependent effect and like creep it also shortens the concrete member, thus reducing the strand stress. Shrinkage depends on many factors like ambient relative humidity, curing conditions, size and shape of the member and concrete mix proportions. Drying shrinkage occurs due to the difference between the ambient relative humidity and the internal relative humidity of concrete. It only occurs when the ambient relative humidity is lesser than the latter. According to ACI 209 and AASHTO LRFD specifications, shrinkage will increase 67 percent when ambient relative humidity decreases from 80 percent to 40 percent.

Myers (1986) observed that higher strength concrete had lower shrinkage strains as compared to normal strength concrete. This can be attributed to the lower w/c ratio. Moisture content in concrete is a significant factor affecting the amount of shrinkage especially drying shrinkage. Lower water content in concrete means that less water is available for diffusion and thus less drying shrinkage will occur (Shah and Ahmad, 1994). Researchers have also observed that accelerated curing at high temperatures reduces shrinkage in concrete specimens. Specimens cured using heat to accelerate the curing process exhibit 75 percent less shrinkage (Mak, et al., 1997).

All of the models mentioned above for creep have a shrinkage model too. Similar to creep there is no consensus as to which model is the best predictor of concrete shrinkage. Townsend (2003) found ACI 209 modified model to be the best predictor of shrinkage strains. According to Myerson (2001), the Sakata model is the best predictor of shrinkage strains. Waldron (2004) found GL2000 to be the best model for predicting shrinkage

strains. Due to a lack of consensus on the best model for prediction of shrinkage strains, the NCHRP 496 model is used in this thesis.

2.5.3.1 NCHRP 496 Shrinkage Model

Tadros et al. (2003) have proposed this model. This is the only model specifically developed for HSC.

NCHRP 496 recommends the use of following equation for predicting shrinkage strains in HSC.

$$\varepsilon_{sh} = 480.0x10^{-6}\gamma_{sh}K_1K_2 \qquad (2.19)$$

where

ε_{sh} is the shrinkage strain at time t

K_1 and K_2 represents the average upper and lower bound values of the creep coefficient for local materials.

$480x10^{-6}$ is the ultimate shrinkage strain

γ_{sh} is the product of the applicable correction factors.

$$\gamma_{sh} = k_{td}k_sk_{hc}k_f \qquad (2.20)$$

The applicable correction factors are as follows:

$\mathbf{k_{td}}$ is the time development correction factor and is given by

$$\mathbf{k_{td}} = \frac{t}{61 - 4f_{ci}' + t} \qquad (2.21)$$

where t is the age of concrete after loading, in days.

f'_{ci} is the concrete strength at release, ksi

$\mathbf{k_s}$ is the size factor and is given by

$$\mathbf{k_s} = \frac{1064 - 94V/S}{735} \tag{2.22}$$

where V/S is the volume to surface area ratio (inches).

$\mathbf{k_{hc}}$ is the humidity factor for creep and is given by

$$\mathbf{k_{hc}} = 2.00 - 0.0143H \tag{2.23}$$

where H is the relative humidity, in percent

$\mathbf{k_f}$ is the concrete strength factor and is given by

$$\mathbf{k_f} = \frac{5}{1 + f_{ci}'} \tag{2.24}$$

where f_{ci}' is the specified compressive strength at prestress transfer (ksi).

This formula and the above correction factors are based on research on HSC girders in four states, Texas, Washington, New Hampshire and Nebraska.

2.5.4 Prestressing Steel Relaxation

Stress relieved strand is the most commonly used prestressing steel nowadays. The most commonly used strand is the seven-wire strand. It is fabricated by intertwining six wires around a central core wire of slightly larger diameter.

Prestressing steel is high strength steel with minimum ultimate tensile strength ranging from 250 ksi to 300 ksi depending upon the grade of strand used. Strands with diameters of 0.5 in. and 0.6 in. are most commonly used in bridge girders. They are initially stressed to a level of up to 80 percent of their ultimate tensile strength and at transfer the stress remaining in these stands is close to 75 percent of their ultimate tensile strength (Collins et al. 1991). At such high stresses the steel creeps, but since it is at a constant

strain, it is termed as relaxation. The amount of relaxation in steel depends on the stress; the higher the stress the greater the relaxation. The relationship between the stress and relaxation is not linear.

Generally, two types of strands are used in prestressing applications, normal relaxation and low relaxation. Low relaxation strand is predominantly used nowadays because of the low stress loss characteristics it exhibits. Low relaxation strands are stress relieved by stretching them at an appropriate temperature during the manufacturing process.

Relaxation losses in prestressing steel are also dependent on temperature. Elevated temperature results in an increased relaxation loss. Steam curing is done at high temperatures which results in rapid relaxation in the tendons. This must be accounted for in the calculation of the initial camber if the elevated temperatures (>80° C) are maintained for an extended period. Due to prolonged exposure to high temperature, cold worked strand suffers permanent reduction in strength. Short-term temperature increases do not affect the strength of steel adversely and subsequent cooling restores the strength (Naaman, 1982). In a prestressed concrete member, the tendon stress is gradually reduced, not only by relaxation losses, but also by the time dependent effects of creep and shrinkage in the concrete.

Magura et al. (1964) have developed the following relationship to predict the stress in prestressing steel at any time t.

$$f_{ps}(t) = f_{pi}\left[1 - \frac{\log(t)}{K}\left(\frac{f_{pi}}{f_{py}} - 0.55\right)\right] \tag{2.25}$$

where

t is in hours and not less than one hour

Log(t) is the logarithm to the base 10

$\frac{f_{pi}}{f_{py}} \geq 0.55$

f_{pi} is the strand stress at the beginning of the desired interval in ksi

f_{py} is the yield stress of the strand in ksi

K=45 for low relaxation steel

K=10 for normal relaxation steel

For the stress loss due to pure relaxation:

$$\Delta f_{pr}(t) = f_{pi} - f_{ps}(t) = f_{pi}\left[\frac{\log(t)}{K}\left(\frac{f_{pi}}{f_{py}} - 0.55\right)\right] \tag{2.26}$$

The Prestressed Concrete Institute () suggests the use of following equation to compute relaxation losses in low relaxation strands which are used for girders in this study.

$$\Delta f_{rel} = f_{pi}\left(\frac{\log(t_n) - \log(t_r)}{45}\right)\left(\frac{f_{pi}}{f_{py}} - 0.55\right) \tag{2.27}$$

where Δf_{rel} is loss in stress due to relaxation in ksi,

t_n is the time at the end of the desired interval in hours,

t_r is the time at the beginning of the desired interval in hours, .

f_{pi} is the strand stress at the beginning of the desired interval in ksi,

f_{py} is the yield stress of the strand in ksi.

$$\frac{f_{pi}}{f_{py}} \geq 0.55$$

2.5.5 Age at Release

Kelly, Breen and Bradberry (1987) found that maturity of concrete at the time of release had very little effect on the camber growth.

2.5.6 Thermal Effects

The camber in a prestressed beam is significantly affected by ambient conditions during storage and time of measurement. Various conditions like wind, relative humidity, solar radiations, and composite material and section properties of the girder can influence the internal temperature of the girder. A structural member experiences a thermally induced strain and expands uniformly if the temperature increase is uniform. However due to the

precompressed tensile zone the bottom flange is restrained and the compressive flange is free to expand. This induces a curvature in the girder. Also according to the field data gathered, the temperature increase is not uniform. Girders experience higher temperatures in the top flange than in the bottom flange thereby creating a thermal gradient. Researchers have observed temperature gradients as high as 77° F in prestressed girders. The temperature variation also affects steel relaxation losses in prestressed girders (Naaman, 1982). In a study done by Byle, Burns and Carrasquillo (1997) at the University of Texas an empirical analysis method was used to correlate the temperature gradient with camber in the girders. NCHRP 276 Report outlines an analytical method for investigating thermal effects in concrete superstructures. Barr et al., (2005) observed that temperature variation during the casting of girders also affects the camber.

2.6 Monte Carlo Method

The Monte Carlo method is applied in this thesis to model the variability in camber of prestressed girders. The Monte Carlo method is used to generate a probability distribution function for camber and camber growth. The probability distribution function generated by the Monte Carlo method will serve two purposes. The first being the prediction of limits of expected behavior of camber and camber growth in prestressed girders. This will help the designer in establishing a confidence interval on the expected camber. Secondly it will help the designer in estimating the amount of camber to be adjusted upwards or downwards depending on the significance level chosen by the designer.

2.6.1 Theory of Monte Carlo Method

The theory of the Monte Carlo method is given in a number of references (Gentle, 2003 and Grewal, 2004). The expected value of a continuous random variable is given by Equation 2.28.

$$E(x) = \int_{-\infty}^{\infty} xf(x)dx \tag{2.28}$$

where x is the random variable and f(x) is its probability distribution function.
For a continuous function of multiple variables, the expected value of the function can be written as

$$E(g(x_1, x_2, ..., x_n) = \int_{-\infty}^{\infty} \int_{-\infty}^{\infty} ..... \int_{-\infty}^{\infty} g(x_1, x_2, ..., x_n) f(x_1, x_2 ..., x_n) dx_1 dx_2 .... dx_n \qquad (2.29)$$

where $g(x_1,x_2\ldots,x_n)$ is a function of variables, and $f(x_1,x_2\ldots,x_n)$ is the multivariate probability distribution function (PDF) of variables x_1 to x_n . Integrating such expressions is a very complicated task mathematically. Some functions can be evaluated numerically. The multivariate probability distribution functions when plotted give a three dimensional bell shaped curve. Predicting values of a variable that are dependent on other variables requires knowledge of conditional probability and the task becomes all the more complicated as the number of variables increases. Therefore knowledge of mathematical functions that define multivariate PDF or even the PDF's of the variables is very scant. This makes the task of determination of camber and camber growth very difficult considering the fact that they are dependent on a number of variables and non-linear functions. Therefore, the numerical approach called the Monte Carlo simulation is used.

It has been assumed that all the variables affecting camber and camber growth, used for the Monte Carlo simulation in this thesis are independent and have PDFs that can be approximated by a normal distribution. In the case where insufficient data is available, the mean value is approximated on the distribution of a variable an approximation is made and it is assumed to be normally distributed. The variable whose distribution was known was taken from past technical literature.

In the Monte Carlo method, a set of random values for each of the variables is generated. These values are then passed to the simulation model. Once the distribution parameters are determined, it is possible to determine a set of probable values or establish a confidence interval on the expected value. For the purpose of the study, the value expected is camber and camber growth. The output from the simulation model is a set of values for camber and camber growth. These values are then used to determine the

statistical parameters of an assumed distribution such as a uniform distribution or a normal distribution.

2.6.2 Monte Carlo Approximation of Exact Integrals

The mean value of a continuous random variable is defined as before by Equation (2.28). The variance of a variable is given by

$$VAR(x) = E(x^2) - \left[E(x)\right]^2 = \int_{-\infty}^{\infty} x^2 f(x)dx - \left[\int_{-\infty}^{\infty} xf(x)dx\right]^2 \tag{2.30}$$

The Monte Carlo approximation of the above expression is given as follows:
It is assumed that the variables x_1 through x_n are sampled randomly from the PDF f(x), a function G may be defined as :

$$G = \sum_{n=1}^{N} \lambda_n g_n(x_n) \tag{2.31}$$

where g_n may be a different function of x_n and λ_n is a real number. Each g_n is a random variable and the sum of $g_n(x_n)$ is also a random variable. The expectation of the value G becomes:

$$E(G) = \langle G \rangle = E\left[\sum_{n=1}^{N} \lambda_n g_n(x_n)\right] = \sum_{n=1}^{N} \lambda_n g_n(x_n) \tag{2.32}$$

where $\lambda_n = \frac{1}{N}$

The variance of the function G is:

$$VAR(G) = E(G^2) - \left[E(G)\right]^2 = \sum_{n=1}^{N} \lambda_n{}^2 VAR(g_n(x)) = \frac{1}{N} VAR(g(x)) \tag{2.33}$$

That is, as N, the number of samples of x increases, the variance of the mean value of G decreases as $\left[N\right]^{-1}$. This leads to the central idea of Monte Carlo evaluation of integrals.

An integral may be approximated by a sum as follows:

$$E(g(x)) = \int_{-\infty}^{\infty} g(x) f(x) dx = E\left[\frac{1}{N}\sum_{n=1}^{N} g(x_n)\right] \quad (2.34)$$

The form of the above expression is described as follows:

Draw a series of random variables, x_n, from f(x). Evaluate each g(x) for each x_n. The arithmetic mean of all the values of g is an estimate of integral. The variance of this estimate decreases as the number of terms N increases. As the number of dimensions of an integral decreases, the Monte Carlo method at times can be the only way to evaluate that integral(Gentle, 2003). The evaluator is in control of the accuracy of the result. Greater accuracy can be obtained by either increasing the number of samples N, by using a variance reduction technique, or a combination of both.

The Monte Carlo method in this thesis is primarily used for the following. First, it is used to check the efficacy of the camber prediction model used in this thesis. Second, it is used to provide a confidence interval on the camber for a particular girder with given section and material properties. Third, it is used to perform a sensitivity analysis to determine which factors most affect the camber and camber growth.

2.7 Conclusions

In this chapter, a review of literature on the factors affecting camber and camber growth was presented. Several models are available for predicting creep and shrinkage of concrete. However, there is no consensus as regards which model is the most accurate. Some of the models discussed here are for normal strength concrete. Only the NCHRP 496 model has been specifically developed for high strength concrete. However, even this model is not very accurate and there is considerable difference in the predicted and actual measured values of camber and prestressed losses. Thus, a probabilistic model using the Monte Carlo methods is preferred over a deterministic model. A probabilistic model will provide a range of camber values rather than a single discreet value.

Chapter 3

Method of Analysis

3.1 Introduction

All current methods for predicting camber calculate a single discrete value. However, from the field data available it has been observed that camber of beams having identical design material properties, cross sectional dimensions and cast in similar ambient weather conditions have a significant variations in camber. Therefore, to account for variation in camber, a probabilistic approach is required. The advantage of a probabilistic method over contemporary methods is that it accounts for the variation in the factors affecting camber. Thus it gives a range of camber values that can be expected for a girder with given sectional and material properties. This will help the designer in establishing a confidence interval for the camber of the beam that is being designed.

The method of analysis used in this study is the transformed section analysis proposed by Tadros et al. (2003) for calculating initial camber. For predicting camber growth, the Age Adjusted Effective Modulus method suggested by Trost (1967) and Bazant (1975) is used. The advantage of the method proposed in this study is that it uses data presented in the AASHTO LRFD specifications. The primary drawback of the method is that it requires the designer to have statistical information on time and on the factors affecting camber. It also requires a little more computational effort and time on the part of designer but this problem is overcome by the use of a computer. A program implementing the above two methods was developed as part of this study. In addition, the elements of the Monte Carlo Simulation method were incorporated in the program.

3.2 Description of Model

The computer program used in this study is based on the method described in the following section. The camber at release is calculated using the curvature diagram of the beam. Camber growth is calculated using the change in the curvature diagram, where change in curvature occurs due to time dependent effects such as creep and shrinkage in concrete and relaxation in steel strands. The Moment Area method is used to calculate the midspan defections from the curvature diagram. The beams examined in this study have both straight and harped tendons; therefore, the moment area method is the most straightforward method for determination of midspan deflections.

The method used in this thesis is divided into two phases. Phase one deals with calculation of camber at transfer. To increase the accuracy of the calculations in this study, the effects of self-weight and prestressing force are considered simultaneously. The curvature calculated for phase one is the algebraic sum of the curvature due to self-weight and prestressing force. Self-weight is an important factor because of the large cross sectional area of the members studied. The curvature, including the effects of both self-weight and prestressing force, is calculated at various locations in the beam and the moment area method is used to calculate the midspan deflection.

After transfer, the beam is exposed to the environment and undergoes shrinkage. The other time dependent effects of concrete creep and relaxation of prestressing strands have already begun. The age adjusted effective modulus approach is now used to set up equilibrium, compatibility and constitutive relationships for calculating the change in curvature due to the time dependent effects of creep, shrinkage and relaxation of steel strands. The advantage of using the age adjusted effective modulus approach is that it accounts for the variation in creep due to maturity of concrete and changing prestress force. This is important because creep of concrete is smaller under a continuously decreasing effective prestress force than under a constant applied load. The equations developed in this phase are then used to calculate the change in curvature due to time

dependent effects at various locations. Then the change in the curvature diagram is plotted and change in deflection is calculated using the moment area method.

3.2.1 Instantaneous Deflections (Phase 1)

The method used in phase one is described in detail in the following steps:

1. Calculate the jacking force.

$$P_j = 0.75 f_{pu} A_{strand} nstrand \tag{3.1}$$

where

f_{pu} is the specified ultimate tensile strength of prestressing steel, ksi,

A_{strand} is the cross sectional area of strand, $in.^2$,

nstrand is the number of strands.

2. Calculate the net and transformed section properties of the beam.

$$A_n = A_g - A_{ps} \tag{3.2}$$

$$y_{bn} = \frac{A_g y_{bg} - A_{ps} y_{cg}}{A_n} \tag{3.3}$$

$$I_n = I_g - A_{ps}(y_{bn} - y_{cg})^2 \tag{3.4}$$

$$A_{tr} = A_g + (n_{pci} - 1)A_{ps} \tag{3.5}$$

$$y_{btr} = \frac{A_g y_{bg} + (n_{pci} - 1)A_{ps} y_{cg}}{A_{tr}} \tag{3.6}$$

$$I_{tr} = I_g + A_g(y_{btr} - y_{bg})^2 + (n_{pci} - 1)A_{ps}(y_{btr} - y_{cg})^2 \tag{3.7}$$

where

A_n is the net area of concrete section of the beam, $in.^2$,

A_g is the gross sectional area of the beam, $in.^2$,

A_{ps} is the total area of prestressing strands, $in.^2$,

y_{bn} is the distance of the center of gravity of the net concrete section of the beam from the extreme fiber of the bottom flange, in.,

y_{bg} is the distance of the center of gravity of the gross section of the beam from the extreme fiber of the bottom flange, in.,

y_{cg} is the distance of the center of gravity of the prestressing strands from the extreme fiber of the bottom flange, in.,

I_n is the second moment of area of the net concrete section of the beam, $in.^4$,

A_{tr} is the area of the equivalent transformed section of the beam, $in.^2$,

$$n_{pci} = \frac{E_p}{E_{ci}} \tag{3.8}$$

n_{pci} is the modular ratio

E_p is the modulus of elasticity of prestressing strands, ksi,

E_{ci} is the modulus of elasticity of concrete at release, ksi,

y_{btr} is the distance of the center of gravity of the equivalent transformed section of the beam from the extreme fiber of the bottom flange, in.,

I_{tr} is the second moment of area of the equivalent transformed section, $in.^4$.

3. Calculate the self weight moment and prestressing force at release by subtracting the loss in prestressing force due to relaxation

$$M_{sw} = \frac{wx(l-x)}{2} \tag{3.9}$$

$$P_{rel} = P_j - P_{relaxation} \tag{3.10}$$

where

M_{sw} is the self weight moment, in.-k,

w is the weight per unit length of the beam, k/in.,

L is the length of the beam, in.,

P_{rel} is the effective prestressing force at release, k,

$P_{relaxation}$ is the loss is prestressing force due to relaxation of strands and is calculated using the relaxation loss model suggested by PCI (PCI BDM, 1997) as described in Equation (2.27).

4. Calculate the stresses at the extreme fibers, incorporating the effects of self-weight in addition to the prestressing force and moment

$$f_{top} = \frac{P_{rel}}{A_{tr}} - \frac{P_{rel}e(h - y_{btr})}{I_{tr}} + \frac{M_{sw}(h - y_{btr})}{I_{tr}} \tag{3.11}$$

$$f_{bot} = \frac{P_{rel}}{A_{tr}} + \frac{P_{rel}ey_{btr}}{I_{tr}} - \frac{M_{sw}y_{btr}}{I_{tr}} \tag{3.12}$$

where

f_{top} is the stress at extreme top fiber of the beam,

e is the eccentricity of the prestressing strands with respect to the center of gravity of the equivalent transformed section,

h is the height of the section,

f_{bot} is the stress at the extreme bottom fiber of the beam.

5. Calculate the stress at the level of the centroid of the prestressing strand pattern

$$f_{cgp} = \frac{P_{rel}}{A_{tr}} + \frac{P_{rel}e^2}{I_{tr}} - \frac{M_{sw}e}{I_{tr}} \tag{3.13}$$

where

f_{cgp} is the stress at the centroid of prestressing strand pattern properties.

6. Calculate the values of strains at the extreme fibers of the beam and the centroid of the prestressing strand pattern using Hooke's law

$$\varepsilon_{top} = \frac{f_{top}}{E_{ci}} \tag{3.14}$$

$$\varepsilon_{bot} = \frac{f_{bot}}{E_{ci}} \tag{3.15}$$

$$\varepsilon_{ps} = \frac{f_{cgp}}{E_{ci}} \tag{3.16}$$

7. Calculate initial curvature

$$\phi = \frac{\varepsilon_{bot} - \varepsilon_{top}}{h} \tag{3.17}$$

8. Calculate initial forces in the prestressing strands

$$P_i = P_{rel} - (\varepsilon_{ps}.E_p.nstrand.A_{strand}) \quad (3.18)$$

where

$\varepsilon_{ps}.E_p.nstrand.A_{strand}$ is the elastic shortening loss, kips.

9. Calculate the initial force in the concrete at the net center of gravity

$$f_{conc} = \frac{P_{rel}}{A_{tr}} - \frac{P_{rel}e(y_{bn} - y_{btr})}{I_{tr}} + \frac{M_{sw}(y_{bn} - y_{btr})}{I_{tr}} \quad (3.19)$$

$$P_{conc} = f_{conc}.A_n \quad (3.20)$$

10. Check equilibrium by checking

$$P_i = P_{conc} \quad (3.21)$$

11. Calculate the moment in the net concrete section

$$M_{conc} = \phi.E_{ci}.I_n \quad (3.22)$$

To calculate the initial camber, the above steps are repeated at various locations in the beam and the curvature diagram is plotted. Then initial camber at release can be calculated using the moment area method.

3.2.2 Time Dependent Camber Changes (Phase II)

After getting the initial camber, the long term camber is calculated by using the equations developed for the second phase. The method used in the second phase is described in detail in the following steps:

1. The sum of the changes in the forces in the concrete and the prestressing strands must be zero

$$\Delta N_g + \Delta N_{ps} = 0 \quad (3.23)$$

where

ΔN_g is the change in axial force in the girder, kips,

ΔN_{ps} is the change in force in prestressing strands, kips.

2. The sum of the changes in the moments in the section must be zero

$$\Delta M_g + \Delta N_{ps} e = 0 \tag{3.24}$$

ΔM_g is the change in the moment in the net concrete section, in.-k,

e is the eccentricity of strand pattern about the net section centroid, in.

3. The change in girder strain at the centroid can be calculated as follows

$$\Delta\varepsilon_g = \frac{N_g^{\ o}}{E_g A_g}\phi_g + \frac{\Delta N_g}{E_g A_g}(1+\mu\phi_g) + \varepsilon_{shg} \tag{3.25}$$

where

$\Delta\varepsilon_g$ is the change in girder strain at the centroid of the girder,

$N_g^{\ o}$ is the initial axial force in the net concrete section, kips,

E_g is the modulus of elasticity of concrete at release, kips,

A_g is the net area of concrete section, in (A_n),

Φ_g is the creep coefficient at time t corrected using the correction factors given in NCHRP 496,

μ is the aging coefficient =0.8,

ε_{shg} is the shrinkage strain at time t corrected using the factors given in NCHRP 496.

4. The change in the steel strain can be calculated as follows

$$\Delta\varepsilon_{ps} = \frac{\Delta N_{ps} - \Delta N_{relax}}{A_{ps} E_p} \tag{3.26}$$

where

ΔN_{relax} is the change in prestressing force due to relaxation, kips.

5. The change in the curvature can be calculated as follows

$$\Delta x = \frac{M_g^{\ o}}{E_g I_g}\phi_g + \frac{\Delta M_g}{E_g I_g}(1+\mu\phi_g) \tag{3.27}$$

where

Δx is the change in curvature of the cross section,

I_g is the second moment of area of the net concrete section (I_n),

$M_g^{\ o}$ is the initial moment in net concrete section.

6. The following compatibility equation relates the strains and the curvature:

$$\Delta\varepsilon_{ps} - \Delta xe = \Delta\varepsilon_g \tag{3.28}$$

The above equations are solved using the Gaussian elimination method to calculate the change in curvature. The above steps are then repeated to calculate the change in curvature at various locations. These calculated values at various locations are used to plot the change in the curvature diagram and the change in deflection is computer using the moment area method.

3.3 Program Operation

It has been stated that the objective of this thesis is to determine bounds on camber in the prestressed beams being analyzed by developing a PDF of the camber for these girders. The model described in the preceding section was programmed into the computer and the Monte Carlo algorithm was implemented to develop the PDF of camber and camber growth. The Monte Carlo algorithm was implemented after the program was checked by entering nominal design values for a girder and checking the solution with hand calculations for the same girder. The program developed for this study was written in Visual Basic.Net.

3.4 Implementing the Monte Carlo Procedure

The Monte Carlo procedure is a process to randomize the input variables to the camber prediction model. For example, in the model described above, 15 input variables are randomized. The number of simulations depends on the discretion of the user. The procedure for implementing the Monte Carlo method is outlined below.

1. Determine the statistics of the input variables.
2. Determine or assume a PDF for each input variable.
3. Generate a set of random numbers for each input variable using step one and two. The number of values generated depends on the number of trials.

4. For each trial, a set of input values is entered into the simulation model and the response of the girder in terms of camber and camber growth values is obtained.
5. These values are then used to determine the PDF and statistics of camber and camber growth.

This procedure simulates many of the possible material and environmental conditions that the girder may be subjected to and thereby simulates the girder response to these conditions in the form of camber and camber growth values.

3.5 Member Modeling and Input

Member modeling in this study means representing the data pertaining to the member being studied in a form that can be easily read into the simulation program. The number of sections of interest along the length of member depends on the amount of change in curvature along the length. If the curvature of the beam changes too frequently then the number of sections required would be more but otherwise only those sections would be of interest wherever there is a significant change in slope of the curvature diagram. For this study the input variables for the program at each section of interest, are the cross sectional dimensions of the beam, grade of strand, area of strand, number and pattern of strands at each section, concrete strength at release and at 28 days and age at release. For the variables that are considered to be random, it is necessary to establish their mean, standard deviation, lower limit and upper limit. The program generates random values for these variables from a standard normal distribution by calling a subroutine GAUSS, which generates random numbers from a standard normal distribution. A standard normal distribution is a normal distribution having a mean value of zero and a standard deviation of one. The GAUSS subroutine internally calls the Visual Basic.Net RND function that returns a uniformly distributed number from zero to one. The uniformly distributed number generated by the RND function is transformed to a normally distributed number using the Box-Mueller algorithm. If the upper and lower limit of a variable is specified then the generated number is checked against these limits. If it satisfies the limits, it is accepted or otherwise it is rejected. When random values for all sixteen variables are

generated and stored, the program uses these 16 values as input for the algorithm developed for the model described above.

The main program uses these values and calculates section properties, forces, moments and finally the curvature at each section of interest. The program then proceeds to calculate the deflection using the algorithm based on the moment area method. All the values of the deflection calculated for each simulation are stored in arrays. The forces and moments developed at each net concrete section are then used in the algorithm for Phase II of the model. Here, the random values of the ultimate creep and shrinkage coefficients are corrected using correction factors specified in NCHRP 496. The set of equations used in the second phase are then solved by the Gaussian Elimination method by calling a subroutine GAUSSELIM for each specified section. The change in curvature due to time dependent effects at each section is calculated by solving this set of equations. The moment area method is used to calculate the change in deflection. The change in deflection and the values used to calculate it for each iteration are stored in an array.

The input values and the values of initial camber and change in camber calculated using the program are stored in an array and then transferred to MS Excel. Here a statistical analysis is performed on the stored variables to determine properties such as the mean, standard deviation and kurtosis. This is done to verify the accuracy of random number generator and the transformation routines. Results indicate that the random number generator and transformation routine worked really well. The difference between the assumed and calculated statistical parameters of the variables was found to be insignificant at 15000 simulations.

The same statistical analysis is carried out on the values of camber and change in camber to determine their statistical parameters and to plot their probability distribution using the Excel histogram function. The result of this analysis is the outcome expected in this thesis. It helps to compare the mean value of the predicted camber and camber growth to those calculated using the deterministic analysis. In addition, the probability distribution plotted helps in establishing a confidence interval and provides a range of values within

which camber and camber growth is expected to fall. The predicted range can be used to determine the number of monostrands required to adjust the camber up or down so that it is equal to the mean value.

Chapter 4

Statistical Parameters and Random Number Generation

4.1 Introduction

In this chapter, the statistical parameters of the variables needed for the probabilistic analysis of camber and camber growth are presented. The statistical parameters of most of the variables were available in the literature. Assumptions were made for those variables where no data was available regarding their bounds or statistical distributions, assumption were made and noted in here.

4.2 Statistical Parameters

4.2.1 Concrete Strength Variability

Researchers have only developed models for the 28-day characteristic strength of concrete. All the published statistical information pertaining to this model is based on the work of Mirza et. al.(1978). According to Mirza et. al.(1978) the mean 28-day compressive strength of concrete in a structure for a minimum acceptable curing is given by Equation 4.1

$$f_{cr}^{'} = 0.675 f_c^{'} + 1100 \leq 1.15 f_c^{'} \text{ psi} \quad (4.1)$$

The variability in the concrete strength is given by the following equation:

$$v^2 = v_{ccyl}^{\ 2} + 0.0084 \quad (4.2)$$

where

v_{ccyl} is the coefficient of variation of compression test cylinder.

The probability distribution function of concrete strength can be considered to be Normal (Naaman, 1982).Based on the above equations, various researchers have chosen statistical parameters for modeling concrete strength variability at transfer and 28 days. Mwanza (1993) and Mwanza and Scanlon (2000) have chosen the mean as given in the above equation and a coefficient of variation (COV) of 0.176. Steinberg (1995) has taken the COV as 0.15 for concrete at transfer and a COV of 0.18 for concrete strength at 28

days. Ahlborn and Gilbertson (2003) have chosen the mean as 1.10f'c and a COV of 0.20 for concrete strength at transfer and a COV of 0.174 for concrete strength at 28 days. In the above research, the PDF of the concrete strength was taken to be normal. The data given by Ahlborn and Gilbertson is used in this thesis.

4.2.2 Variability of Prestressing Steel Parameters

4.2.2.1 Modulus of Elasticity of Prestressing Steel

The nominal value of the modulus of elasticity of prestressing strands is given as 28500 ksi. For pretensioning and post tensioning operations in the field it is generally specified to use the value given by the manufacturer for that particular batch of strands. Mirza et. al.(1978) have given the mean value of the elastic modulus of prestressing steel as $1.011E_p$ where E_p is the nominal value of elastic modulus of prestressing steel. They have also given the distribution of this variable as normal. Kikuchi et. al. (1978) have given the COV of this variable as 2.11 percent. Mwanza and Scanlon (2003) have used a COV of 1 percent. Steinberg (1995) uses the same value for the mean and the COV. Ahlborn and Gilbertson (2003) have used the nominal value as the mean value and COV of 2 percent. For this thesis, same values were used.

4.2.2.2 Prestressing Steel Area

The variability in the area of prestressing steel arises due to manufacturing tolerances. It has been observed that manufacturers using strict quality control procedures generally tend towards the positive tolerances. It has also been observed from extensive statistical studies that ratio of actual area to required area is always greater than one. Therefore, the following equation is used to for calculating the mean area of prestressing steel.

$$A_{ps} = 1.01176 A_{psn} \tag{4.3}$$

where

A_{psn} is the design or nominal value of the area of prestressing strand.

A_{ps} is the actual area of prestressing strand

The COV of this variable is given as 1.25 percent, the prestressing strand area is normally distributed (Naaman, 1982).

4.2.2.3 Depth of Prestressing Strands

Strand placement in pretensioning or post tensioning is done using templates, which are fabricated according to the exact dimensions as specified in design. This leads to lower variability in their position. These small variabilities have a negligible effect on camber. Mirza et. al. (1978) have suggested that the mean value of depth of prestressing strands is normally distributed and is equal to the nominal value plus $1/16^{th}$ of an inch. The COV varies from a value of 4 percent to a value given by 0.68/member depth where member depth is in ft. Ahlborn et. al.(2003). have also used the same values. Kikuchi et. al.(1978). have given the mean depth as the nominal depth plus $1/8^{th}$ of an inch with a standard deviation of 11/64 inches. The values suggested by Mirza et. al.(1978) are used in this thesis.

4.2.2.4 Ultimate Tensile Strength of Prestressing Steel

It is generally observed that the ultimate tensile strength of prestressing strands is higher than that specified for the strand. It is also variable and unpredictable. There this variable is also considered random in this study. Ahlborn and Gilbertson (2003) have used a mean value of 281 ksi for Grade 270 strand whose minimum ultimate tensile strength is 270 ksi. The distribution for this variable is also assumed as normal and COV is given as 2.5 percent. These values reported by Ahlborn et. Al(2003). is quoted in paper by Mirza et. al. (1980). The same values are used in the thesis.

4.2.2.5 Jacking Stress in Prestressing Strands

The nominal value of jacking stress is taken as 0.75fpu (AASHTO LRFD, 1998). This value can be variable since it depends on many factors like the jacking force transferred to the strands and the ultimate tensile strength of strands. However, there are practical limits on the value of this variable. The maximum jacking stress in the strand should not exceed 0.80fpu. The PCI BDM (PCI, 1997) has specified an upper and lower limit for this variable. The values of upper and lower limits as reported in Ahlborn and Gilbertson (2003) are 212.7 and 192.5 respectively. The distribution is assumed as normal and the mean value is given as 202.5 ksi, which is equal to 0.75fpu for Grade 270 strand. This thesis also uses the same values.

4.2.3 Ultimate Shrinkage Coefficient

Many researchers have shown that the shrinkage of HSC mix is lower than the Normal strength mix. For normal strength mixes, the ultimate shrinkage strain had a mean value of 780e-6 in/in and lower, upper bound values 415e-6 in/in and 1070e-6 in/in respectively (ACI 209, 1992). For HSC mixes, the mean value is taken as 480e-6 in/in, a lower bound value of 250e-6 in/in and upper bound value of 700e-6 in/in (NCHRP 496, 2003). These values are derived from data given in NCHRP 496. The distribution for the shrinkage values is assumed approximately normal based on the work of Bazant (Bazant et al., 1984). The COV is found by assuming the above-specified limits at a 5 percent significance level. It means that the probability of shrinkage strain values falling between the above two values is 0.95. It also signifies the ratio of the area under the normal curve. The statistical Z –tables were used to calculate the COV and at the 5 percent significance level the COV was found to be 27.7 percent and thus a standard deviation of 1.33e-4 in/in. was found.

4.2.4 Ultimate Creep Coefficient

Similar to shrinkage, the creep of HSC mix is also lower as compared to Normal Strength concrete mix. For normal strength concrete, the ultimate creep coefficient is 2.35e-6 in/in. The lower bound of this variable is 1.30e-6 in/in. and upper bound value is 4.15e-6 in/in. (ACI 209, 1992). According to the data given in NCHRP 496 (2003), the mean value of this variable is 1.90e-6 in/in with a lower bound of 1.25e-6in/in. and an upper bound of 2.50e-6 in/in. Bazant has found that the probability distribution function of the creep coefficient can be approximated as normal. Mirza et. al. (1978) have suggested that the distribution of this variable can be approximated as log normal. For the study done in this thesis the distribution is assumed to be normal with a mean of 1.90e-6 in/in. The COV of this variable is calculated using the statistical Z-tables at a 5 percent significance level and it is found to be 19.1 percent.

4.2.5 Curing Time and Loading Age

In this study curing and loading age are considered to be the same. According to Ahlborn and Gilbertson (2003), the mean for this variable is taken as 36 hours with an upper and lower bound of 48 and 24 hours respectively. The COV is 20.2 percent. The distribution is approximated as normal. This thesis uses the same data. The sensitivity analysis done in this thesis showed that the curing time and loading age do not have a significant effect on camber.

4.2.6 Humidity

The humidity is also modeled as a random variable in this thesis. The mean value of 70 percent is chosen with an upper bound of 100 percent and a lower bound of 40 percent. The distribution was approximated as normal and statistical Z-tables were used to calculate the COV by assuming the lower and upper bounds at a 5 percent significance level. The COV was found to be 12.3 percent. Ahlborn and Gilbertson (2003) have used

the mean as 75 percent with an upper bound of 89 percent and a lower bound of 60 percent. The COV used in their study is 11.8 percent.

4.2.7 Cross Sectional Area

The cross sectional area of the member is also variable. However, there is less variability because the most prestressed concrete members are precast and produced in plant conditions. This thesis uses the same approach as used by Ahlborn and Gilbertson (2003). The upper and lower bound of the cross sectional area is found from the dimension tolerances given in PCI Bridge Design Manual. After determining the upper and lower bounds, the mean is chosen as the mean of the distribution. The distribution is approximated as normal. Then using the upper and lower bound values at a 5 percent significance level and the statistical Z-tables the COV is found.

4.2.8 Perimeter

A similar approach, as described above for the cross sectional area is also used for computing the statistics of the perimeter. The distribution is assumed normal. Statistical Z-tables are used to calculate the COV.

4.2.9 Moment of Inertia

A similar approach to that described in the previous two sections is used to determine statistical parameters of the moment of inertia.

4.2.10 Ratio of Volume to Surface Area

This variable is not directly used for camber calculation but it is used in the correction factors applied to the time dependent effects of creep and shrinkage. The V/S ratio is

calculated using the ratio of area of the member to the perimeter of the member. Since both these variables are treated as random variables, they are directly used to calculate this ratio.

4.2.11 Unit Weight of Concrete

The mean value of the unit weight of concrete is assumed as 0.150kcf. According to Ahlborn and Gilbertson (2003) and Mwanza and Scanlon (2003) the distribution of unit weight of concrete is normal with a COV of 1.25 percent.

4.3 Practical Application of Theory of Monte Carlo

Just implementing the Monte Carlo procedure to perform simulation does not necessarily guarantee good results. The implementation of Monte Carlo in practical applications requires the use of certain techniques to ensure that simulation produces the desired results. The technique used in this thesis is outlined below.

4.3.1 Variance Reduction Techniques

Several variance reduction techniques are available and the most commonly used are listed here. These are Jackknifing, Antithetic Variates, Stratification, Common Random Numbers, Control Variates, Importance Sampling and Conditional Monte Carlo (Gentle, 2003).

The factor that is common to all above-mentioned techniques is that they reduce the variance and thereby increase the accuracy of the solution without increasing the number of trials. This was beneficial in the past when the computational capabilities were limited and accuracy was desired by limiting the number of runs. With the advent of better computational capabilities these variance reduction techniques are only used in very complex and large simulations. For medium or small simulations model like the one in

this study even a personal computer is powerful enough to handle the number of computations. Thus, convergence is achieved by increasing the number of runs rather than applying these variance reduction techniques.

In the development phase of the program used in this study, several trials with different number of runs were done to determine the minimum number required to achieve good convergence. It was determined that around 15000 runs of simulation were required to reduce the variance and achieve the results with desired precision. It was observed that the difference between the actual and calculated values of the statistical parameters of the variables was less than 1 percent. A similar approach was used for determining the number of runs required to achieve the desired precision in the outcome of the model. It was observed that for 20000 simulations the difference in the results when compared to 15000 simulations was insignificant. Therefore, the number of iterations for the simulation was chosen as 15000. The total time needed for generating the random numbers and performing the computations was less than 2 minutes on a laptop computer.

It is possible to get an error estimate of the simulation by invoking the Central Limit Theorem, which gives the following expression (Grewal, 2004).

$$P\left(\left|\frac{1}{N}\sum_{j=1}^{N} X_j - m\right| \rangle \frac{3v}{\sqrt{N}}\right) = 0.997 \tag{4.4}$$

where

N is the number of samples or runs,

x_j represents the N sampled values,

m is the mean value of N samples,

v is the standard deviation of the N variables.

The equation written above is read as follows: For the 99.7 percent confidence interval, the approximation to m is correct with an error not exceeding $\frac{3v}{\sqrt{N}}$ (Grewal, 2004). The error can then be modified by either using the variance reduction technique or increasing

the number of runs. The increase in the number of runs was considered a better choice for this study.

4.3.2 Transformation of Variables

Random number generators in any programming language are programmed to generate random numbers in the interval zero to one with a uniform distribution. The reason for this is that random numbers generated from a standard uniform distribution can be used to obtain random numbers from other distributions through a transformation process. Therefore, it finds its application in Monte Carlo simulations because it involves use of random numbers from a particular distribution.

4.3.3 Random Number Generator

Random numbers generated by a random number generator are not truly random. Therefore, they are called pseudo random numbers. In one dimension, these numbers appear random but in three-dimensional space, these random numbers are not exactly random but appear in some kind of pattern (Gentle, 2003). The non-randomness exhibited by the numbers in three-dimensional space can be in the form of parallel lines or spirals. The quality of random number generator depends on how long is its period, which is the number of random numbers without being repeated and how truly random are the numbers generated by it.

Various types of random number generators are available in the literature (Gentle, 2003). They are divided into two types a) Linear Congruential Generators and b) Non Linear Congruential generators. There are several types of linear congruential generators such as Multiple Recursive generator, Matrix Congruential Generator, Add-with-carry, Subtract-with- borrow and Multiply-with-carry generators. The random number generator used in this thesis is the Linear Congruential Generator built in Visual Basic.Net. However, its type is not known. It is recommended that this generator is suitable for normal

applications but not for cryptography applications. The random numbers generated by this generator are in interval zero to one and are uniformly distributed. The PDF desired is a Gaussian so a transformation is done using a Box-Mueller algorithm (Gentle, 2003).

$$X_i = (-2\ln U1)^{0.5} COS(2\pi U2) \tag{4.5}$$

$$X_{i+1} = (-2\ln U1)^{0.5} SIN(2\pi U2) \tag{4.6}$$

where U1 and U2 are uniformly distributed random numbers and X_i and X_{i+1} are the corresponding normally distributed random numbers from a standard normal distribution. The standard normal distribution is designated as N(0,1) and has a mean of zero and standard deviation of one.

4.3.4 Rejection Techniques

The term rejection technique refers to the process of sampling from a known PDF. A trial random number is selected. Then this number is subjected to either one or more tests if one or more than one random variable is involved. The proposed number may be accepted if it passes the test, or rejected if it fails. If a trial random number is rejected then the cycle is repeated until a random number is accepted.

In this study the random number generated is already sampled from a standard normal distribution. This distribution has to be shifted to the desired distribution as none of the parameters used in the study in this thesis have a standard normal distribution. In addition, some of the variables have a truncated normal distribution. In a truncated normal distribution, the tails are shortened. Values, sampled from a standard normal distribution but lying outside the truncation limits should be rejected. Then the number generated from an N(0,1) distribution must be resampled until it is accepted.

In a truncated distribution, the Z variable has a minimum and maximum value. For example, the jacking stress in a grade 270 strand cannot be less that 192.5 ksi and cannot be higher than 202.5 ksi. The standard normal distribution has infinitely long tails but it must be truncated to reflect the practical limits on the variable. The jacking stress of

prestressing strands can then assume any value between the two end points and with a maximum expectancy around the mean value. Let a and b be the lower and upper limits of the distribution upon back transforming the Z variable to a standard normal distribution. The equations for the upper and lower limits are as follows:

$$LowerLimit: \frac{a-m}{\sigma} \tag{4.7}$$

$$UpperLimit: \frac{b-m}{\sigma} \tag{4.8}$$

where the upper and lower limits are for the generated random number ξ. If the generated random number is lower or higher than the lower and upper limit respectively then it is rejected and the process is repeated until acceptance.

The transformation of the random variable from a standard normal distribution back to its usual form is given as follows:

$$Z = m + \sigma\xi \tag{4.9}$$

where

Z is the desired random variable,

m is the mean value of random variable,

σ is the standard deviation of the random variable,

ξ is the value of the N(0,1) distributed random variable.

The actual variables and their statistical parameters are listed in the Table 4.1. Fifteen different variables, all with a normal or truncated normal distribution were input into the computer program. Another three were generated as a combination of these fifteen variables. All of the variables were randomly generated 15000 times over the limits specified in the table and stored in an array and then each row of this array was used as input for the model for every iteration of simulation. The only disadvantage of this technique is that it may have a low efficiency i.e. it may reject many numbers before it accepts one. However, this cannot be considered a significant disadvantage given the powerful computational capabilities now available on the desktop.

Table 4.1 Camber parameters and their statistical distributions

Variable	Nominal Value	Mean Value	Coefficient of Variation	Distribution Type
f_{pu}	270 ksi	281ksi	0.025	Normal
γ_c	γ_{cn}	γ_{cn}	0.030	Normal
E_p	28500 ksi	28500ksi	0.020	Normal
A_{ps}	A_{psn}	$1.01176A_{psn}$	0.0125	Normal
E		0 to +1/16 in.	0.04 to 0.68	Normal
f_{pj}	202.6 ksi High/Low 212.7/192.5	202.6 ksi	0.030	Truncated Normal
f'_c	f'_c	1.1 f'_c	0.174	Normal
f'_{ci}	f'_{ci}	1.1 f'_{ci}	0.200	Normal
RH	70 percent High/Low 100/40	70 percent	0.123	Truncated Normal
A_g	Design cross sectional area High/Low depends on dimensional tolerances	Mean of high and low value	Computed	Truncated Normal
Perimeter	Design Perimeter High/Low Depends on dimension tolerances	Mean of high and low value	computed	Truncated Normal
I_g	Design MOI High/Low Depends on dimension tolerances	Mean of high and low value	computed	Truncated Normal
t, time	36 hours High/Low 48/24	36 hours	0.202	Truncated Normal
Ultimate Shrinkage Coefficient	480e-6 in/in High/Low 250e-6/700e-6	480e-6 in/in	0.277	Normal
Ultimate Creep Coefficient	1.90e-6 in/in High/Low 1.25e-6/2.5e-6	1.90e-6 in/in	0.191	Normal

Chapter 5

Evaluation of Variability of Camber in Prestressed Concrete Bridge Girders

5.1 Introduction

The study done in this thesis is primarily focused on I girders. The girders studied in this thesis are PCBT's used by VDOT. The study was divided into four phases. The first phase included the development of a computer program implementing the Monte Carlo method on the model. This phase was completed by performing a parametric study to check the efficacy of the model and to determine the behavior of the probabilistic model in comparison to the deterministic solution calculated using the AASHTO LRFD specifications. After verifying the accuracy of the model, it was tested against actual field data. The values predicted by the model after simulations were compared to experimentally measured values. This constituted the second phase of the study. In the third phase, a sensitivity analysis was done to determine which variables of the model had a significant effect on the predicted camber and camber growth. For the fourth and the last phase of this study, a feasibility study was performed to check whether the objective of controlling camber using unbonded monostrands could be achieved. The following sections discuss the various phases of this study and the results obtained.

5.2 Parametric Study

The parametric study was done for two main purposes, the first was to check the accuracy and effectiveness of the model and the second was to determine the difference between the probabilistic solution given by the model and the deterministic solution calculated using the AASHTO LRFD specification. The study was done on the commonly available PCBT sections in Virginia. VDOT provided the data sheet specifying the concrete strength, span length, spacing of beams, and depth of slab and distance of harping point

for the PCBT's. These beams were designed using the AASHTO LRFD specifications to calculate the strand pattern and initial camber. The Monte Carlo simulation was performed using the same data and the results were compared to the AASHTO LRFD method values. For camber growth, the AASHTO LRFD method does not include time dependent effects for calculating long-term camber, therefore those values could not be compared. The AASHTO LRFD equations used to calculate the camber at release and at the time of erection are shown in Equations (5.1) to (5.2). The net camber at transfer and at the time of erection is the algebraic sum of deflections calculated using Equations (5.1) and (5.2). It was observed in this study that the average value predicted by the probabilistic method was 15- 20 percent higher than that calculated by the deterministic method. The reason for over prediction by the MCS method as compared to AASHTO method could be the inclusion of elastic shortening loss along the full length of girder and the over prediction of modulus of elasticity of HSC by the AASHTO method. Tables 5.1 to 5.9 show the comparison between the deterministically and probabilistically determined values of camber at release. A sheet showing a reference PCBT section with its section properties and a table showing the number of strands used in sections depending on the span length and concrete strength is attached in Appendix A.

$$\Delta_p = \frac{P_i}{E_{ci} I}\left(\frac{e_c L^2}{8} - \frac{e' a^2}{6}\right) \text{ in.} \qquad (5.1)$$

where

Δ_p is the upward deflection due to an eccentrically applied prestressing force,

P_i is the total prestressing force after transfer,

e_c is the eccentricity of the prestressing force at midspan,

e' is the difference between the eccentricity of prestressing steel at midspan and end of the beam,

a is the distance from the end of the beam to the harp point,

L is the overall beam length,

E_{ci} is the modulus of elasticity of concrete at transfer,

I is the gross moment of inertia of the precast beam.

$$\Delta_g = \frac{5wL^4}{384E_{ci}I} \text{ in.} \quad (5.2)$$

where

Δ_g is the downward deflection due to beam self weight at transfer or erection,

w is the beam self weight,

E_{ci} is the modulus of elasticity of precast beam at transfer,

I is the gross moment of inertia,

L is the overall beam length at transfer and c/c of bearing length at the time of erection.

PCBT 29

Table 5.1 Comparison between Deterministic and Probabilistic solution of camber at release for PCBT 29 girder.

Concrete Strength (psi)	Span Length (ft)	Number of Strands	Mean Camber from MCS (in.)	AASHTO Camber (in.)	MCS/AASHTO
5000					
6000	40	12	0.335	0.308	1.09
	45	14	0.480	0.423	1.13
7000	40	12	0.309	0.269	1.15
	50	16	0.586	0.526	1.11
8000	40	12	0.287	0.263	1.09
	60	24	1.115	0.933	1.20

PCBT 37

Table 5.2 Comparison between Deterministic and Probabilistic solution of camber at release for PCBT 37 girder.

Concrete Strength (psi)	Span Length (ft)	Number of Strands	Mean Camber from MCS (in.)	AASHTO Camber (in.)	MCS/AASHTO
5000	40	12	0.273	0.237	1.15
	55	20	0.785	0.673	1.17
6000	40	12	0.249	0.220	1.13
	60	18	0.679	0.590	1.15
7000	40	12	0.229	0.202	1.13
	75	28	1.350	1.117	1.21
8000	40	14	0.262	0.233	1.12
	80	34	1.725	1.517	1.14

PCBT 45

Table 5.3 Comparison between Deterministic and Probabilistic solution of camber at release for PCBT 45 girder.

Concrete Strength (psi)	Span Length (ft)	Number of Strands	Mean Camber from MCS (in.)	AASHTO Camber (in.)	MCS/AASHTO
5000	40	14	0.260	0.227	1.15
	70	20	0.800	0.690	1.16
6000	40	14	0.237	0.208	1.14
	85	28	1.319	1.132	1.17
7000	40	16	0.254	0.226	1.12
	95	38	2.050	1.781	1.15
8000	40	16	0.232	0.212	1.09
	100	44	2.345	2.047	1.15

PCBT 53

Table 5.4 Comparison between Deterministic and Probabilistic solution of camber at release for PCBT 53 girder.

Concrete Strength (psi)	Span Length (ft)	Number of Strands	Mean Camber from MCS (in.)	AASHTO Camber (in.)	MCS/AASHTO
5000	40	16	0.245	0.214	1.14
	90	26	1.128	0.955	1.18
6000	40	16	0.223	0.197	1.13
	105	38	1.962	1.664	1.18
7000	40	18	0.234	0.208	1.13
	115	50	2.823	2.439	1.16
8000	40	18	0.217	0.195	1.11
	115	50	2.648	2.301	1.15

PCBT 61

Table 5.5 Comparison between Deterministic and Probabilistic solution of camber at release for PCBT 61 girder.

Concrete Strength (psi)	Span Length (ft)	Number of Strands	Mean Camber from MCS (in.)	AASHTO Camber (in.)	MCS/AASHTO
5000	40	18	0.232	0.203	1.14
	110	36	1.852	1.477	1.25
6000	40	18	0.211	0.186	1.13
	120	44	2.320	1.873	1.24
7000	40	20	0.207	0.184	1.13
	125	50	2.644	2.377	1.11
8000	40	20	0.193	0.172	1.12
	125	48	2.339	2.002	1.17

PCBT 69

Table 5.6 Comparison between Deterministic and Probabilistic solution of camber at release for PCBT 69 girder.

Concrete Strength (psi)	Span Length (ft)	Number of Strands	Mean Camber from MCS (in.)	AASHTO Camber (in.)	MCS/AASHTO
5000	40	18	0.232	0.203	1.14
	120	40	1.968	1.657	1.19
6000	40	20	0.191	0.170	1.12
	130	48	2.481	2.024	1.23
7000	40	20	0.176	0.156	1.13
	135	50	2.460	2.013	1.22
8000	40	22	0.183	0.165	1.11
	135	50	2.310	1.902	1.21

PCBT 77

Table 5.7 Comparison between Deterministic and Probabilistic solution of camber at release for PCBT 77 girder.

Concrete Strength (psi)	Span Length (ft)	Number of Strands	Mean Camber from MCS (in.)	AASHTO Camber (in.)	MCS/AASHTO
5000	40	20	0.182	0.163	1.12
	130	50	2.560	2.174	1.18
6000	40	20	0.166	0.146	1.14
	135	44	1.973	1.657	1.19
7000	40	22	0.170	0.151	1.13
	140	48	2.136	1.810	1.18
8000	40	22	0.158	0.142	1.11
	140	46	1.849	1.568	1.18

PCBT 85

Table 5.8 Comparison between Deterministic and Probabilistic solution of camber at release for PCBT 85 girder.

Concrete Strength (psi)	Span Length (ft)	Number of Strands	Mean Camber from MCS (in.)	AASHTO Camber (in.)	MCS/AASHTO
5000	40	20	0.160	0.140	1.14
	135	38	1.490	1.420	1.05
6000	40	22	0.161	0.140	1.15
	145	46	1.881	1.638	1.15
7000	40	22	0.149	0.131	1.14
	150	50	2.032	1.730	1.17
8000	40	24	0.152	0.124	1.23
	150	50	1.905	1.601	1.19

PCBT 93

Table 5.9 Comparison between Deterministic and Probabilistic solution of camber at release for PCBT 93 girder.

Concrete Strength (psi)	Span Length (ft)	Number of Strands	Mean Camber from MCS (in.)	AASHTO Camber (in.)	MCS/AASHTO
5000	40	22	0.157	0.137	1.15
	145	46	1.930	2.017	0.96
6000	40	22	0.142	0.126	1.13
	155	50	2.031	1.679	1.21
7000	40	24	0.145	0.129	1.12
	155	48	1.735	1.437	1.21
8000	40	26	0.147	0.132	1.11
	150	48	1.626	1.352	1.20

5.3 Comparison of Field Data

The comparison of field data was the most important phase of this study. The reason for its importance is that one of the aims of this study is to develop a tool for designers, with which they can better predict the camber and avoid the delays caused in construction due to its variability. The field data required for this study was provided by Bayshore Concrete. They provided the data for the commonly used PCBT 45 section. The data provided included the date of casting, age at release, concrete strength at release, length of beam, number of bottom straight strands, number of draped strands and measured camber at mid span. Table 5.10 presents the data provided by Bayshore Concrete. Monte Carlo Simulation was performed for these girders and probability distribution was generated for camber and camber growth. A representative graph for the probability density function of camber and camber growth is as shown in Figure 5.1. Results of the simulation for the beams are shown in Figure A.1 to A.42 in Appendix A. A comparison of range of camber at release predicted by simulation and experimentally measured values is shown in Table 5.11. Unfortunately, long-term field data for these girders was not available to compare the predicted camber growth values.

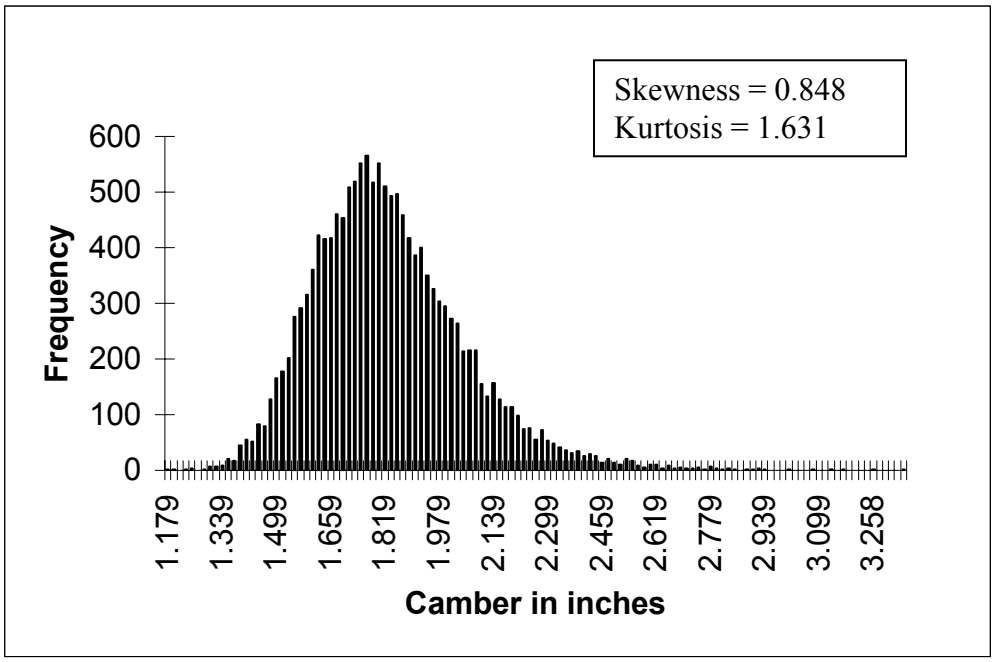

Figure 5.1 Graph showing the probability density function of camber at release for beam number 1

Table 5.10 Field data provided by Bayshore Concrete for a PCBT 45 girder

Beam Number	Date of casting	Beam Length (ft)	Concrete Strength at Release Psi	Age at Release (days)	Camber at release (inches)	Number of Bottom Strands	Number of Draped Strands
1	11/19/05	89.625	7809	2	2.375	28	4
2	11/19/05	89.600	7831	2	2.500	28	4
3	11/16/05	89.071	7732	2	1.375	28	4
4	11/16/05	89.670	8100	2	1.440	28	4
5	11/14/05	106.350	7452	1	3.625	36	8
6	11/14/05	107.250	7357	1	3.250	36	8
7	11/10/05	108.150	8341	1	2.875	36	8
8	11/10/05	107.540	7942	2	3.000	36	8
9	11/8/05	106.450	7592	1	2.810	36	8
10	11/8/05	105.875	7641	1	2.688	36	8
11	11/3/05	106.920	6983	1	2.560	36	8
12	11/3/05	106.290	7747	1	2.560	36	8
13	10/29/05	108.150	8566	2	2.940	36	8
14	10/29/05	107.540	7914	2	2.875	36	8
15	10/27/05	91.770	7698	1	1.500	26	4
16	10/21/05	89.560	8519	3	1.690	26	4
17	10/21/05	94.770	8772	3	1.750	26	4
18	10/19/05	93.650	7553	1	1.690	26	4
19	10/19/05	93.080	7532	1	1.375	26	4
20	10/12/05	94.400	8317	2	1.500	26	4
21	10/12/05	93.920	7684	2	1.500	26	4

Table 5.11 Comparison of predicted range of camber at release values to experimentally measured camber at release

Beam Number	MCS Predicted Range (in.)	Mean (in.)	Measured Value (in.)	Standard Deviation
1	1.357-2.775	1.821	2.375	0.223
2	1.354-2.779	1.817	2.500	0.223
3	1.357-2.598	1.819	1.375	0.219
4	1.330-2.736	1.787	1.440	0.220
5	2.063-4.107	2.794	3.625	0.336
6	2.085-4.143	2.826	3.250	0.340
7	1.955-3.950	2.666	2.875	0.326
8	2.003-4.021	2.725	3.000	0.332
9	2.043-4.078	2.769	2.810	0.334
10	2.031-4.057	2.751	2.688	0.332
11	2.140-4.224	2.894	2.560	0.344
12	2.020-4.042	2.739	2.560	0.331
13	1.926-3.907	2.630	2.940	0.326
14	2.007-4.027	2.730	2.875	0.332
15	1.382-2.380	1.860	1.500	0.228
16	1.280-2.483	1.725	1.690	0.215
17	1.313-2.733	1.784	1.750	0.225
18	1.417-2.895	1.912	1.690	0.235
19	1.413-2.886	1.905	1.375	0.234
20	1.350-2.791	1.830	1.500	0.229
21	1.406-2.891	1.900	1.500	0.234

Hinkle (2005) measured the initial and long-term camber for two sets of girders used in the Cooper River Bridge in Charleston, SC. Figure 5.2 shows the dimensions of the girder. Each set of girders was grouped according to strand pattern and length. The strand pattern and the details of the group for both sets is shown in Figure B1, B2, and Table B1 and B2 respectively in Appendix B. The girders in a set were chosen on the basis that their length did not differ by more than 6 inches. The design strength of concrete at release was given as 6100 psi and at 28 days as 9000 psi (Hinkle, 2005). A Monte Carlo simulation was done using this data and the results, in the form of graphs, are as shown in Figures 5.3 to 5.8. Table 5.12 shows the comparison between the actual field values measured by Hinkle (2005) and the range predicted by the Monte Carlo Simulation.

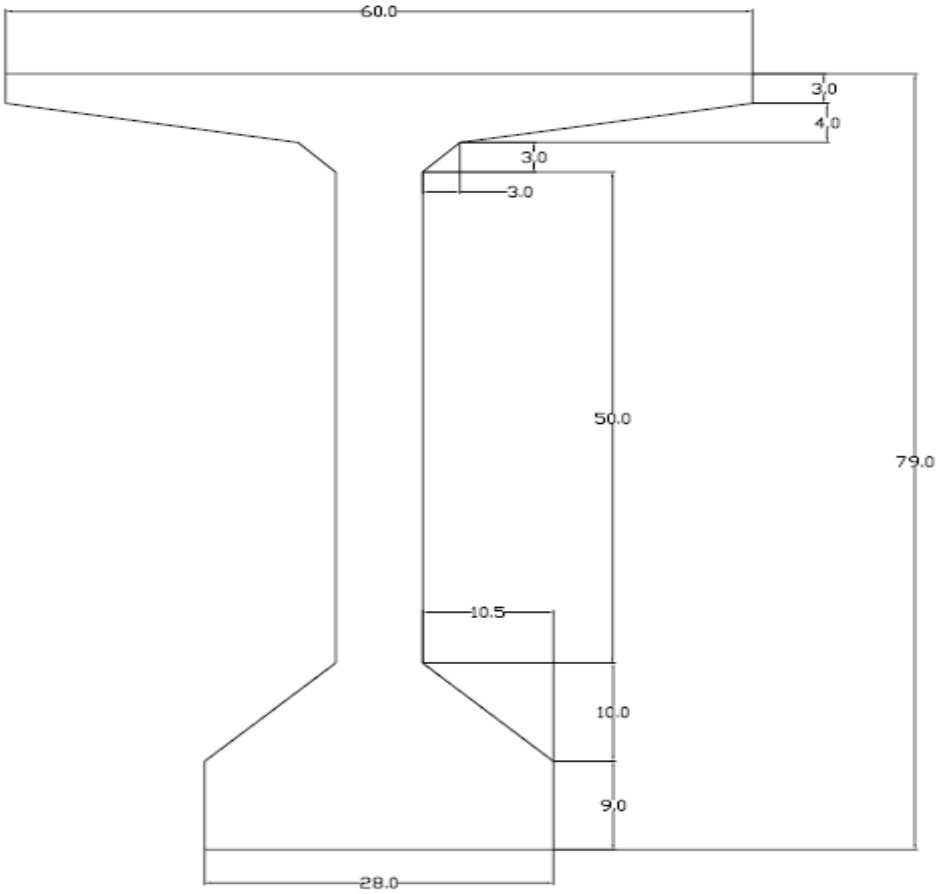

Figure 5.2 Dimensions of the 79 in. modified bulb tee used in the Cooper River Bridge, Charleston, SC (Hinkle, 2005)

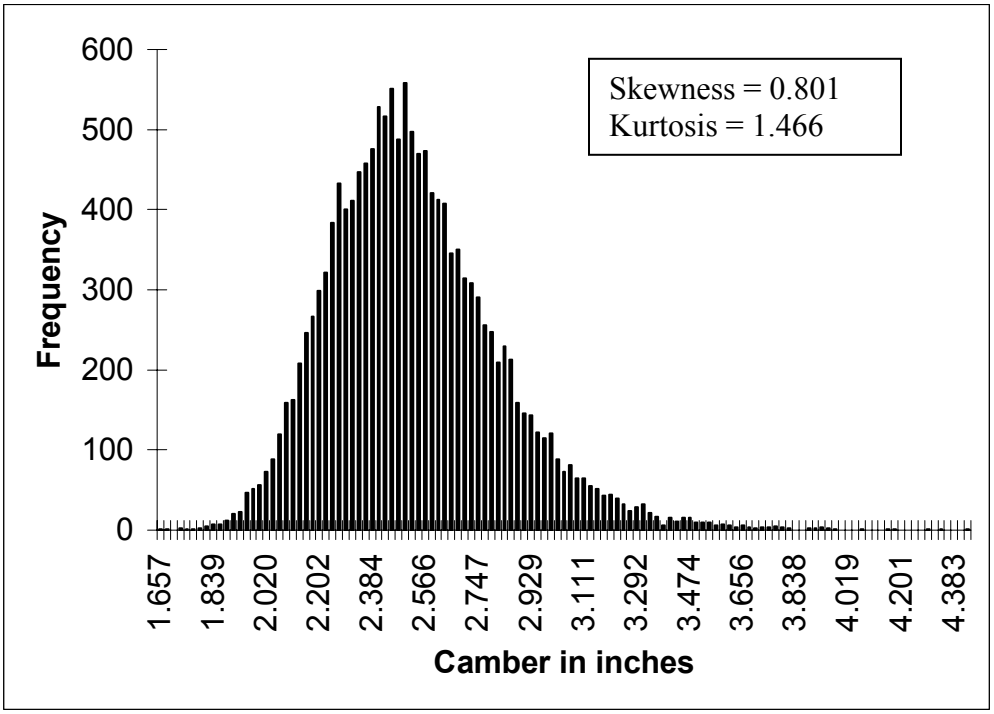

Figure 5.3 Graph showing the probability density function of camber at release for beam sample 1

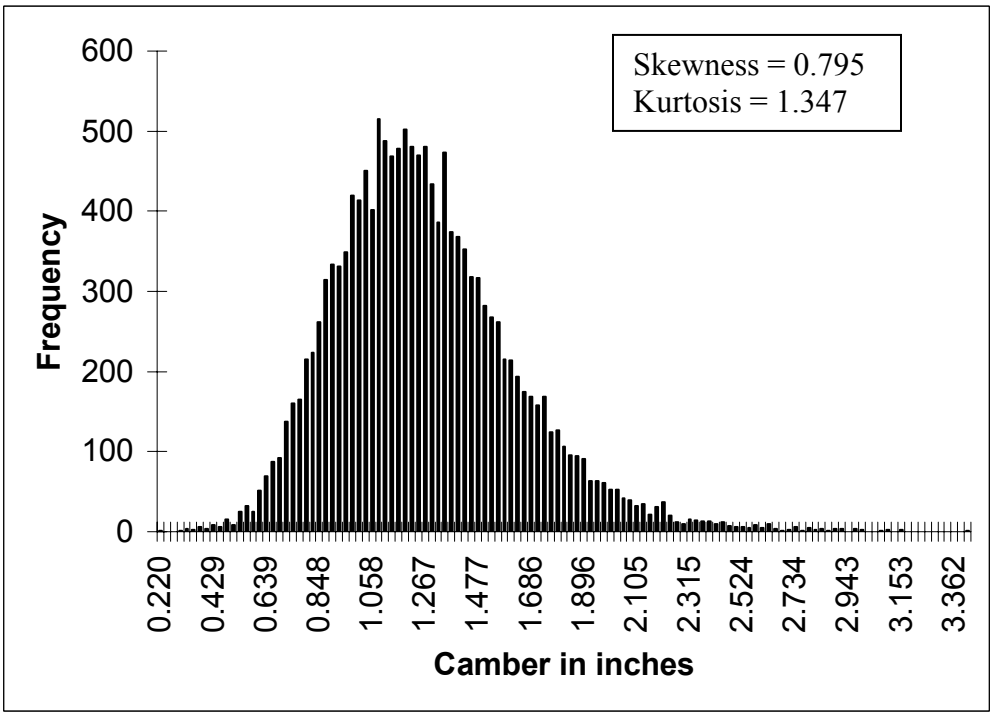

Figure 5.4 Graph showing the probability density function of camber growth at 60 days for beam sample 1

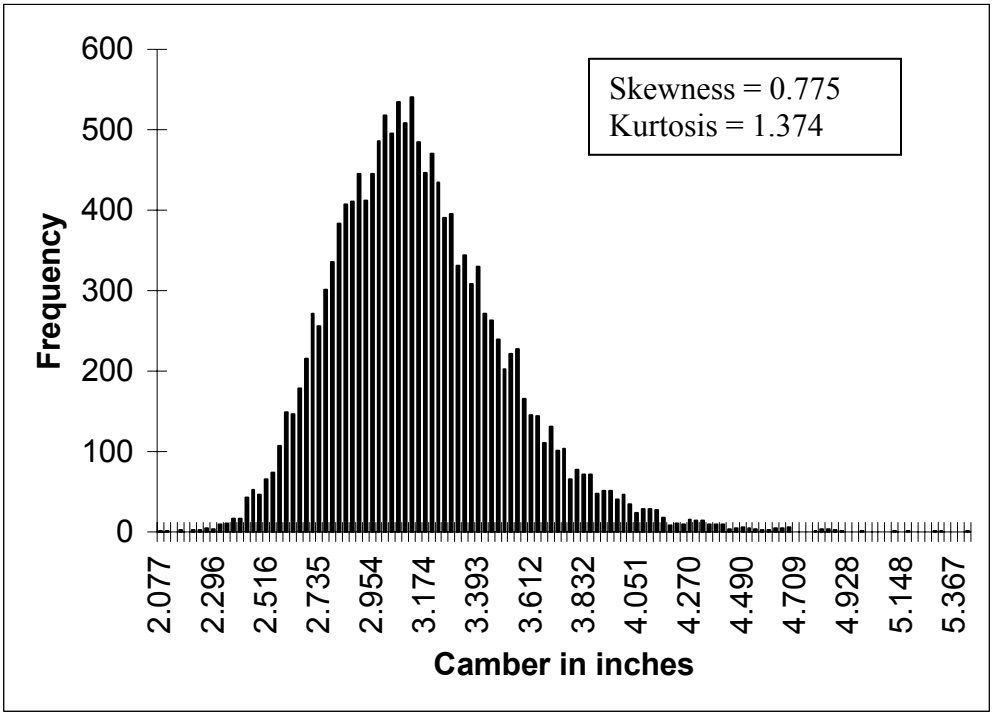

Figure 5.5 Graph showing the probability density function of camber at release for beam sample 2

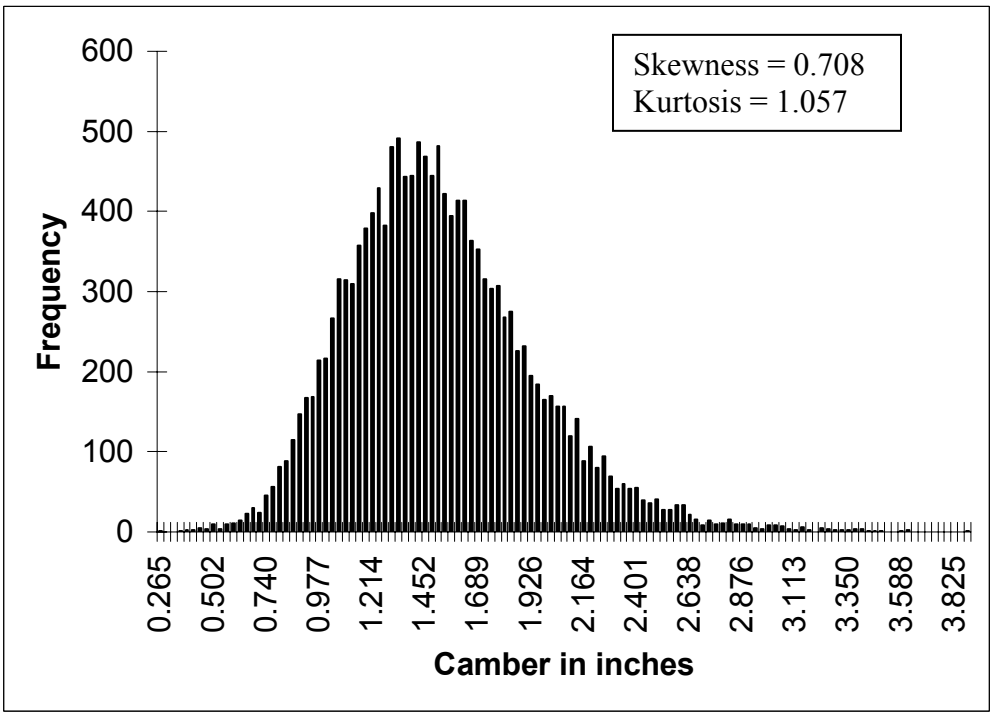

Figure 5.6 Graph showing the probability density function of camber growth at 60 days for beam sample 2

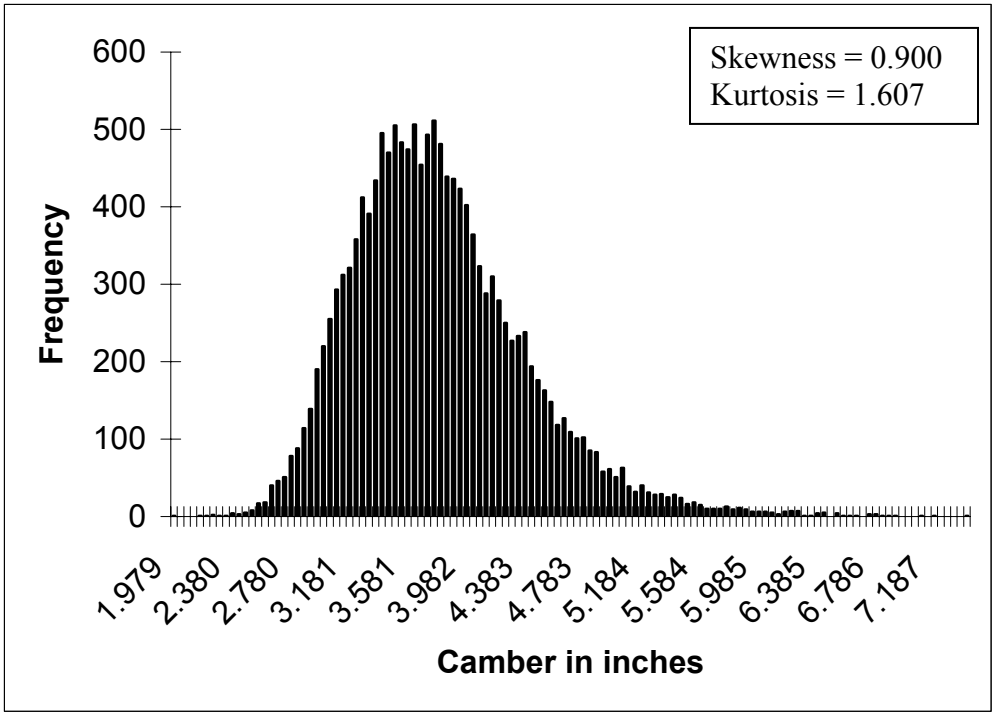

Figure 5.7 Graph showing the probability density function of final camber at 60 days for beam sample 1

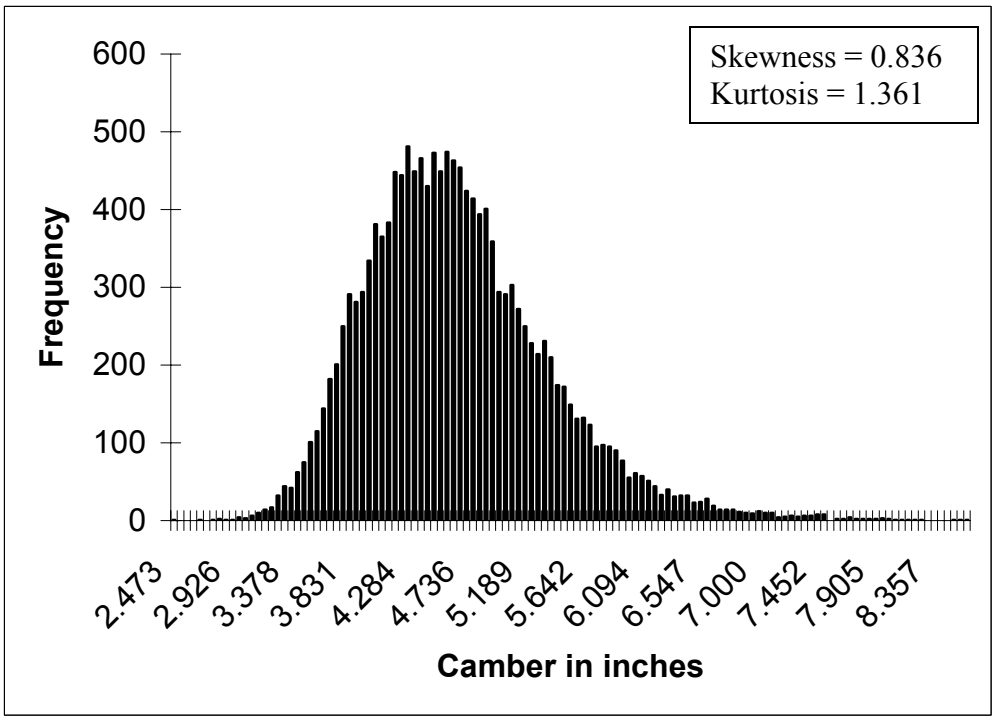

Figure 5.8 Graph showing the probability density function of final camber at 60 days for beam sample 2

Table 5.12 Comparison between the MCS predicted values and experimentally measured values of camber at release and camber growth for Cooper River bridge girders

Sample Number	Camber Type	MCS Predicted Range	Measured Camber			
			Beam Number			
			1	2	3	4
1	Camber at release	1.884-3.701	1.60	1.80	2.50	2.75
	Camber Growth (60 days)	0.482-2.576	0.50	0.50	0.40	0.35
	Camber (60 days)	2.335-5.896	2.10	2.30	2.90	3.10
2	Camber at release	2.351-4.545	2.50	2.50	2.75	2.90
	Camber Growth (60 days)	0.562-2.935	0.75	0.90	0.50	0.60
	Camber (60 days)	2.900-6.890	3.25	3.45	3.25	3.50

Upon observing the data in Table 5.11 and 5.12, it is observed that the beams have a significant variation in camber even though they were having similar concrete strengths and were cast in similar environmental conditions. It is also noted that MCS method was able to predict this variation. For PCBT 45 section in Table 5.11, no long-term camber change data was available so no conclusion could be drawn for the long-term change in camber. Referring to Table 5.12 little data was available for long-term change in camber and it was observed that the camber growth and final camber values predicted by the MCS method were at the lower end of the range.

5.4 Sensitivity Analysis

In the third phase of this study, a sensitivity analysis was done in order to determine which of the 15 parameters mentioned in Table 4.1 affected the camber and camber growth the most. An assumption was made that all the variables are statistically

independent. The model used in this thesis does not use the concrete strength at 28 days for calculations. Therefore, the number of variables used in the sensitivity analysis is only 14. The number of runs used per variable was the same as the number of iterations performed for the simulation that is 15000 runs were used.

One variable was varied while holding the others constant. The results for camber and camber growth are tabulated in Table 5.13. The average value of camber and camber growth respectively for 15000 different values of the variable are given in the second and third column of Table 5.13. The coefficient of variation of camber and camber growth respectively for the variable are shown in columns four and five. It is expected that the value of camber and camber growth would tend towards the Monte Carlo expected value when all variables are treated as random and to the deterministic value when all values are considered to be deterministic. Column six and seven present a weighting factor signifying the relative importance of each variable in predicting camber and camber growth.

From Table 5.13 it is evident which parameters have the greatest effect on camber and camber growth. From statistical theory, the variability due to all the variables combined should be equal to the sum of variability of individual variables (Grewal, 2004). The expression depicting the above statement is given as Equation 5.3.

$$(V_{all})^2 = \sum_{i=1}^{n} (V_{individual\ variables})^2 \tag{5.3}$$

Note: This equation is true only if all the variables are normally distributed.
The sum at the bottom of columns six and seven shows that this relation is indeed satisfied.

From Table 5.13, it can be seen that the concrete strength at release and the unit weight of concrete account for about 75 percent of the variability in camber. The reason for concrete strength at release accounting for so much variability is that it also affects the modulus of elasticity of concrete, which is a major variable affecting the camber and

Table 5.13 Results of Sensitivity Study

Variable	**Mean of camber at release**	**Mean of Camber growth**	**COV Camber**	**COV Camber Growth**	**Initial** $\frac{V^2}{V_{all}^2}$	**Growth** $\frac{V^2}{V_{all}^2}$
All	1.899	1.054	0.12332	0.30178	1	1
None	1.759	0.911	0	0	0	0
Ultimate Tensile Strength	1.875	0.983	0.03969	0.04721	0.09631	0.02438
Concrete Unit Weight	1.875	0.984	0.01752	0.02223	0.01878	0.00540
E Prestressing Steel	1.875	0.984	0.00215	0.00846	0.00028	0.00078
Area, Prestressing Steel	1.875	0.984	0.01861	0.01811	0.02118	0.00358
Jacking Stress	1.759	0.911	0.03932	0.04737	0.09452	0.02454
Concrete Strength, release	1.785	0.947	0.11041	0.20590	0.74523	0.46365
Humidity	1.759	0.911	7.59961E-07	0.05238	3.53E-11	0.03000
Area of Girder	1.753	0.906	0.01205	0.02138	0.00888	0.00500
Perimeter of Girder	1.759	0.911	7.59961E-07	0.00127	3.53E-11	1.79E-05
Moment of Inertia	1.760	0.911	0.01555	0.01416	0.01478	0.00219
Loading Age	1.759	0.946	7.59961E-07	0.02056	3.53E-11	0.00462
Ultimate Shrinkage Coeff.	1.759	0.911	7.59961E-07	0.03601	3.53E-11	0.01418
Ultimate Creep Coeff.	1.759	0.908	7.59961E-07	0.19634	3.53E-11	0.42160
CG Strands	1.759	0.911	0.00056	0.00056	1.96E-05	3.55E-06
SUM					1	1

camber growth. In order to generalize the simulation program, jacking stress was made a function of ultimate tensile strength. Therefore, in the sensitivity analysis the contribution of variability in ultimate tensile strength to the total variability in camber and camber growth is attributed to jacking stress. The variability in jacking stress in prestressing steel, accounts for 19 percent of the variability in camber. Around 2 percent of the variability in prediction of camber at release is accounted by the variability in the area of prestressing steel. The moment of inertia of the girder accounts for another 1 percent. Other factors such as the modulus of elasticity of prestressing steel, age of concrete at loading, cross sectional area, perimeter of the section and environmental conditions modeled as ambient humidity, variability of creep and shrinkage coefficients have very little effect on the variability of camber at release.

For camber growth the concrete strength at release accounts for about 46 percent of the total variability in camber growth. The reason for this high contribution of concrete strength is that it also affects the modulus of elasticity of concrete which in turn accounts for the maturity of concrete with age by the use of age adjusted effective modulus. The contribution to the variability in concrete creep and shrinkage from various types of concrete is 43 percent. Approximately 5 percent of the total variability in the growth of camber is accounted by the variation in jacking stress.

Relative humidity accounts for a further 3 percent of the total variability. The remaining part is accounted by other factors such as modulus of elasticity of prestressing strands, area of prestressing strands, cross sectional area, perimeter and moment of inertia of the beam. The variability in the center of gravity of strands is found to have an insignificant effect on the ultimate variability in camber and camber growth.

The curing time and loading age of the girder were set equal and were expected to have a significant effect on the variability of camber and camber growth. However, the results showed otherwise and their effect on the ultimate variability was insignificant.

5.5 Feasibility Study for Using Unbonded Monostrands

The final objective of this thesis is to find an economically feasible solution for camber control. The solution proposed in this thesis is to use unbonded monostrands for controlling camber. The options analyzed in this study were to use the unbonded monostrands in the bottom and top flange of the girder to bring the camber up or down depending on the need. However, the option of using monostrands in the bottom flange to bring the camber up to the desired value was discarded. The reason for this was that there was no space available to insert the anchorages. Secondly, the lower camber can be made up with a deeper haunch depth. For camber greater than the mean predicted value, it is suggested that unbonded monostrands to be used in the top flange of the girder to bring the camber down to the desired value. The feasibility study done for this thesis concentrated on three aspects of using unbonded monostrands in the top flange.

The first aspect of the study was to determine an arrangement of anchorages in the top flange. The arrangement decided upon depended on the strand pattern used in the girders. For girders having no draped strands, the middle two anchorages had their long edges placed vertically. The other two anchorages had their long edges horizontal. The number of anchorages and their distance from the centerline of the girder cross section depended on the fact that the minimum cover required around 0.6 in. diameter strands is two inches. The top flange is tapered towards the edge and to meet the cover requirement of the strands only four anchorages could be placed. In the girders that had draped strands, the anchorages were placed horizontally. The two arrangements are shown in Figures 5.9 and 5.10 respectively. The anchorage used for this feasibility study is Type S6 manufactured by M/S VSL. A data sheet showing the dimensions of anchorages is attached in Appendix A.

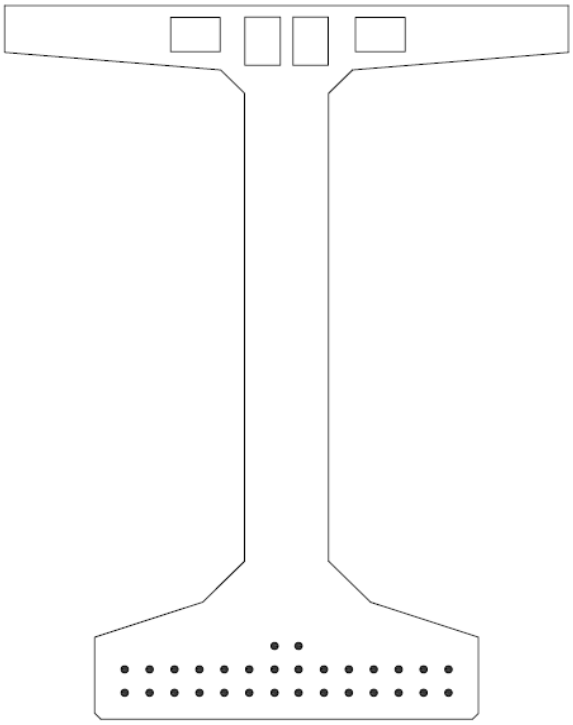

Figure 5.9 Sketch showing the arrangement of Type S6 monostrand anchorages in a PCBT girder having no draped strands.

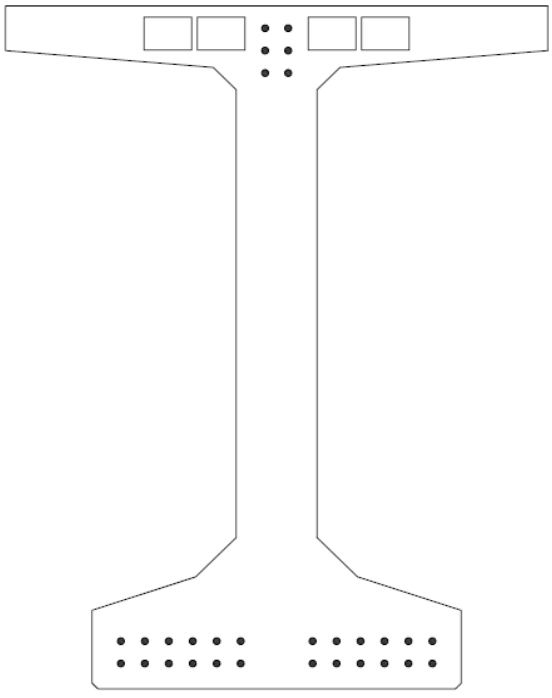

Figure 5.10 Sketch showing the arrangement of Type S6 monostrand anchorages in a PCBT girder having draped strands.

After determining the arrangement of anchorages the second aspect studied was the stresses developed in the anchorage zone. The two stresses that are most important in the anchorage zone are the bearing stresses directly under the plate and the bursting stresses in the orthogonal direction of applied compressive force of the tendon (Wollmann et al. 2000). The allowable bearing stress was calculated using the equation based on the provisions in the AASHTO Standard Specification for highway bridges. The equation used in this study is as shown in Equation 5.4. Note the conversion to allowable stress form from the LRFD form.

$$f_{cpi} = 0.5 f_{ci}' \sqrt{\frac{A}{A_g}} \leq 1.0 f_{ci}' \tag{5.4}$$

where

f_{cpi} is the allowable bearing stress on concrete during tendon stressing,

f'_{ci} is the concrete cylinder strength at the time of tendon stressing,

A is the distribution area,

A_g is the gross bearing plate area.

The above equation is valid if no local zone confinement reinforcement is provided. The average bearing stress under $P_{jack} = 0.8 A_{ps} f_s'$ is given as shown in Equation (5.5)

$$f_{bi} = \frac{P_{jack}}{A_b} \leq f_{cpi} \tag{5.5}$$

where

f_{bi} is the average bearing stress under the plate,

A_b is the net bearing plate area.

The bursting stress in the anchorage zone is calculated by assuming rectangular section behavior. For rectangular sections the Guyon's equations (Wollmann et al. 2004) are used for calculating the bursting force and maximum bursting stress (Wollmann et al. 2004). The equation used for calculating the bursting force and stress are as shown in Equations 5.6 to 5.8.

$$T_{burst} = \frac{P}{4}\left(1 - \frac{b}{h}\right) \tag{5.6}$$

$$\max\ f_t = \frac{0.45P}{h \times t}\left(1 - \frac{b}{h}\right) \tag{5.7}$$

$$\max\ f_t = \frac{T_{burst}}{0.55h \times t} \tag{5.8}$$

where

b is the bearing plate width,

h is the member height,

t is the member width,

P is the tendon force,

T_{burst} is the bursting force, and

max f_t is the maximum bearing stress.

The above-mentioned equations are used to calculate stresses for the four anchorages used in the top flange. In addition, the compressive force at the end of the local zone is also checked and as per AASHTO provisions it should not be greater than $0.5f'_c$. A sample design calculation for the top flange of a PCBT section used by VDOT is attached as Appendix C.

The third aspect of this study was to determine how much camber could be controlled by using the four unbonded monostrands. The approach used in this part of the feasibility study was to assume the distribution of long-term camber growth as normal and then take two standard deviations to the right of the mean. The two standard deviations to the right of the mean would give the camber in excess of what is generally expected. In addition, it would account for the values of camber greater than the mean that have a 90 percent chance of falling between mean and the max possible value of camber predicted by the simulation. A study was done using the sections and span lengths used for the parametric study and the results are presented in the Tables 5.14 to 5.22. The results are discussed in the next chapter. A systematic procedure for calculating the camber controlled by unbonded monostrands placed in top flange is shown in Appendix C.

PCBT 29

Table 5.14 Comparison between expected variation and correction achieved due to unbonded monostrands for PCBT 29 girder.

Concrete Strength	Span Length (ft)	Number of Strands	Number of 0.6 in. Strands	2σ of Camber growth from Mean (in.)	Camber Corrected (in.)	Corrected/2σ
5000						
6000	40	12	4	0.181	0.186	1.02
	45	14	4	0.248	0.236	0.95
7000	40	12	4	0.156	0.170	1.08
	50	16	4	0.274	0.267	0.97
8000	40	12	4	0.136	0.158	1.16
	60	24	4	0.445	0.356	0.80

PCBT 37

Table 5.15 Comparison between expected variation and correction achieved due to unbonded monostrands for PCBT 37 girder.

Concrete Strength	Span Length (ft)	Number of Strands	Number of 0.6 in. Strands	2σ of Camber growth from Mean (in.)	Camber Corrected (in.)	Corrected/2σ
5000	40	12	4	0.166	0.148	0.89
	55	20	4	0.411	0.281	0.68
6000	40	12	4	0.140	0.134	0.95
	60	18	4	0.334	0.302	1.15
7000	40	12	4	0.120	0.123	1.02
	75	28	4	0.544	0.431	0.79
8000	40	14	4	0.127	0.113	1.12
	80	34	4	0.629	0.454	0.72

PCBT 45

Table 5.16 Comparison between expected variation and correction achieved due to unbonded monostrands for PCBT 45 girder.

Concrete Strength	Span Length (ft)	Number of Strands	Number of 0.6 in. Strands	2σ of Camber growth from Mean (in.)	Camber Corrected (in.)	Corrected/2σ
5000	40	14	4	0.158	0.113	0.71
	70	20	4	0.406	0.348	0.85
6000	40	14	4	0.134	0.102	0.76
	85	28	4	0.549	0.462	0.84
7000	40	16	4	0.131	0.094	0.72
	95	38	4	0.736	0.529	0.72
8000	40	16	4	0.115	0.087	0.76
	100	44	4	0.773	0.542	0.70

PCBT 53

Table 5.17 Comparison between expected variation and correction achieved due to unbonded monostrands for PCBT 53 girder.

Concrete Strength	Span Length (ft)	Number of Strands	Number of 0.6 in. Strands	2σ of Camber growth from Mean (in.)	Camber Corrected (in.)	Corrected/2σ
5000	40	16	4	0.148	0.091	0.61
	90	26	4	0.501	0.458	0.91
6000	40	16	4	0.125	0.082	0.66
	105	38	4	0.712	0.562	0.79
7000	40	18	4	0.120	0.075	0.62
	115	50	4	0.896	0.618	0.69
8000	40	18	4	0.105	0.069	0.66
	115	50	4	0.829	0.572	0.69

PCBT 61

Table 5.18 Comparison between expected variation and correction achieved due to unbonded monostrands for PCBT 61 girder.

Concrete Strength	Span Length (ft)	Number of Strands	Number of 0.6 in. Strands	2σ of Camber growth from Mean (in.)	Camber Corrected (in.)	Corrected/2σ
5000	40	18	4	0.139	0.074	0.53
	110	36	4	0.712	0.562	0.79
6000	40	18	4	0.118	0.067	0.57
	120	44	4	0.789	0.603	0.76
7000	40	20	4	0.107	0.062	0.58
	125	50	4	0.840	0.600	0.71
8000	40	20	4	0.093	0.057	0.61
	125	48	4	0.738	0.556	0.75

PCBT 69

Table 5.19 Comparison between expected variation and correction achieved due to unbonded monostrands for PCBT 69 girder.

Concrete Strength	Span Length (ft)	Number of Strands	Number of 0.6 in. Strands	2σ of Camber growth from Mean (in.)	Camber Corrected (in.)	Corrected/2σ
5000	40	18	4	0.120	0.062	0.51
	120	40	4	0.731	0.562	0.77
6000	40	20	4	0.106	0.056	0.53
	130	48	4	0.825	0.595	0.72
7000	40	20	4	0.091	0.052	0.57
	135	50	4	0.777	0.589	0.76
8000	40	22	4	0.087	0.048	0.55
	135	50	4	0.720	0.546	0.76

PCBT 77

Table 5.20 Comparison between expected variation and correction achieved due to unbonded monostrands for PCBT 77 girder.

Concrete Strength	Span Length (ft)	Number of Strands	Number of 0.6 in. Strands	2σ of Camber growth from Mean (in.)	Camber Corrected (in.)	Corrected/2σ
5000	40	20	4	0.110	0.054	0.49
	130	50	4	0.897	0.564	0.63
6000	40	20	4	0.093	0.049	0.53
	135	44	4	0.680	0.551	0.81
7000	40	22	4	0.087	0.044	0.50
	140	48	4	0.696	0.543	0.78
8000	40	22	4	0.076	0.041	0.54
	140	46	4	0.595	0.503	0.84

PCBT 85

Table 5.21 Comparison between expected variation and correction achieved due to unbonded monostrands for PCBT 85 girder.

Concrete Strength	Span Length (ft)	Number of Strands	Number of 0.6 in. Strands	2σ of Camber growth from Mean (in.)	Camber Corrected (in.)	Corrected/2σ
5000	40	20	4	0.098	0.046	0.47
	135	38	4	0.555	0.530	0.95
6000	40	22	4	0.090	0.042	0.47
	145	46	4	0.631	0.552	0.87
7000	40	22	4	0.077	0.038	0.50
	150	50	4	0.647	0.542	0.84
8000	40	24	4	0.073	0.035	0.48
	150	50	4	0.598	0.502	0.84

PCBT 93

Table 5.22 Comparison between expected variation and correction achieved due to unbonded monostrands for PCBT 93 girder.

Concrete Strength	Span Length (ft)	Number of Strands	Number of 0.6 in. Strands	2σ of Camber growth from Mean (in.)	Camber Corrected (in.)	Corrected/2σ
5000	40	22	4	0.095	0.041	0.43
	145	46	4	0.685	0.536	0.78
6000	40	22	4	0.080	0.037	0.46
	155	50	4	0.663	0.554	0.84
7000	40	24	4	0.075	0.034	0.45
	155	48	4	0.563	0.509	0.90
8000	40	26	4	0.070	0.031	0.44
	150	48	4	0.519	0.471	0.91

From the Tables 5.14 to 5.22 it is evident that for larger sections like PCBT 53 to PCBT 93, a larger correction in camber was possible for longer spans as compared to smaller spans. However, the smaller sections from PCBT 29 to PCBT 37 exhibit an opposite trend. The PCBT 45 section doesn't show a particular trend and no conclusion can be derived on the trend of correction achieved for that section.

Chapter 6

Findings and Recommendations

6.1 Findings

The major findings based on the results of the research reported in this thesis are presented in the following paragraphs.

Monte Carlo simulation of camber in prestressed girders showed that it is possible to predict the range of camber. The parametric study done as part of the thesis showed that the mean value predicted by Monte Carlo simulation, was about 15 to 20 percent higher than that calculated using the deterministic AASHTO LRFD method. This indicates that the simulation has an average bias of about 17 percent when compared with the deterministic solution. The probable reason for the higher value of the camber obtained from the Monte Carlo simulation could be that the AASHTO LRFD method over predicts the modulus of elasticity for high strength concrete whereas the modulus of elasticity equation used in this study is specifically developed for high strength concrete. Another reason is that it also assumes some elastic shortening for the entire beam. It was also observed that the probability distribution of the camber was not exactly normal even though all the variables used for prediction of camber are assumed to have a normal distribution. The skewness and kurtosis of the distribution of camber were on an average 0.8 and 1.7 respectively. The values of skewness and kurtosis are relative values to the normal distribution as measured by Excel. Positive value of skewness indicates a longer right tail of the distribution and a positive value for kurtosis indicates that the distribution is more peaked as compared to the normal distribution. A Chi squared goodness of fit test was also done on the probability distribution of camber to check if it can be approximated as normal. The results of the test showed that the distribution can be approximated as lognormal rather than normal distribution.

In Table 5.2, beams 1, 2, 3 and 4 can be grouped into one sample and beams 5, 6, 7 and 9 into another sample. The grouping is done according to their similar span lengths,

material properties, cross sectional area and strand patterns. The deterministic solution predicted the same value for all the beams in a sample while measured values were highly variable. Comparison of field values and predicted ranges indicated that the Monte Carlo method used in this thesis could predict the upper and lower bound values for the group quite accurately.

The long-term change in camber data for PCBT 45 was not available; therefore, those values predicted by the method were not compared to field data. The little data available from Hinkle's (2005) work was compared to the predicted values, and it was found that the experimentally measured values were on the lower bound of the predicted range.

The results of the sensitivity analysis showed that the variability in concrete strength at release accounted for a significant part in the variability of camber at release. This is partly because of the fact that the modulus of elasticity of concrete also depends on concrete strength. The variability in jacking force also has a significant effect on the variability in initial camber. For change in camber over time, the certainty in predicting creep and shrinkage of concrete was a major contributing factor in the change of camber over time. Concrete strength was also a significant factor, since it affects the change in modulus of elasticity of concrete and maturity of concrete with age. Environmental effects like relative humidity and curing time also influence the camber to a moderate extent.

The feasibility study for using unbonded mono strands also showed that monostrand anchorages in the top flange can be used with minimal additional reinforcement. Stresses in the anchorage zone were found to be less than the allowable stresses. For the commonly used PCBT sections, only four anchorages could be accommodated in the top flange. Also, 0.6-in. diameter strands were used for correcting the deviation from mean camber. The value selected as the limit for camber correction was two standard deviations above the mean. It was observed that more correction was possible for larger girders with longer spans than with smaller spans. However, smaller girders showed an opposite trend. The amount of correction achieved by the unbonded monostrands varied

over the section sizes and span lengths. In some cases, for example the smaller sections, it was possible to reduce excess camber more than was desired, whereas in other cases the correction was only up to 50 percent of the desired value.

6.2 Recommendations for Future Research

1. The study done in this thesis was primarily focused on I-girders. However this model can also be used for other shapes of girders. Therefore, for future work, the model should be generalized and tested for other shapes.

2. Due to the complex nature of the thermal effects on the girder at the time of casting as well as storing, it was not possible to include these effects in the model in the initial phase of this study. It is recommended that corrections for thermal effects to be included in the model and that the predicted values be checked with field-measured values.

3. Little data was available on long-term changes in camber. The long-term camber change values predicted by the model were compared to limited field data. It is recommended that the long-term data for change in camber be collected and compared to the predicted values generated from the model.

4. Uncertainty in the prediction of creep and shrinkage is a major source of error and variability in the model. Due to the lack of an accurate model for predicting creep and shrinkage, it is very difficult to predict long-term change in camber values. In addition, the error in the values predicted by the NCHRP 496 Report model is unknown. Therefore, for future research, the error in the NCHRP 496 model for prediction of creep and shrinkage should be calculated and should be incorporated in the model to reduce the variability in the prediction of long-term camber change.

5. Past research has shown that environmental conditions have a significant affect on camber. However, the sensitivity analysis does not reflect the significance of the environmental conditions on the variability in camber. A probabilistic analysis incorporating spectral analysis should be performed to model environmental conditions.

6. The feasibility study for use of mono strands to control camber showed that it is possible to place anchorages in the top flange and control the camber up to 70- 90 percent of the correction required. The method of analysis for the anchorage zones employed in this thesis is an approximate linear elastic method given by Guyon (Wollmann et al. 2004) which is valid only for rectangular sections. However the top flange of the girders is tapered and it is not accurate to model the flange as a rectangular section. For future work, a detailed Strut and Tie modeling or a detailed finite element analysis of the anchorage zone should be done to accurately assess the amount of stress developed.

7. Placement of unbonded monostrands in the girder would increase the material and labor cost of the girder. A detailed cost analysis for the placement of unbonded monostrands to asses the economic impact on the total cost of the girders should be done as a future work to this study.

References

1. American Association of State Highway and Transportation Officials (AASHTO), (1996).Standard Specification for Highway Bridges: Sixteenth Edition. Washington, D.C.
2. American Association of State Highway and Transportation Officials (AASHTO), (1998).*LRFD* Specification for Highway Bridges: Second Edition. Washington, D.C.
3. American Association of State Highway and Transportation Officials (AASHTO), (1989).Guide Specifications "Thermal effects in Concrete Bridge Superstructures (NCHRP R-276)". Washington, D.C.
4. American Concrete Institute (ACI), (1992). "Prediction of creep, shrinkage, and temperature effects in concrete structures." *Manual of Concrete Practice, ACI 209R-92,* Farmington Hills, MI.
5. American Concrete Institute (ACI), (1992). "State-of-the-art report on high strength concrete." Manual of Concrete Practice, ACI 363R-92, Farmington Hills, MI.
6. American Concrete Institute (ACI), (2002). "Building code requirements for structural concrete and commentary." Manual of Concrete Practice, ACI 318-02, Farmington Hills, MI.
7. Ahlborn, T. M., French, C. E., and Leon, R. T. (1995), "Applications of high-strength concrete to long-span prestressed bridge girders." Transportation Research Record, 1476, pp 22-30.
8. Alexander, M. G. (1996). "Aggregates and the deformation properties of concrete." *ACI Materials Journal,* November-December, pp 569-577.
9. Ahlborn, T. M., French, C. E., and Shield, C. K. (2000). "High-Performance Concrete Prestressed Bridge Girders: Long Term and Flexural Behavior," Report 2000-32, Minnesota Department of Transportation, St. Paul, MN p. 91.
10. Ahlborn, T. M., Gilbertson, C.G., (2003). "Probabilistic Comparison of Prestress Loss Methods in Prestressed Concrete Beams", PCI Journal, September-October, pp 52-63.

11. Baalbaki, W., Aitcin, P-C., and Ballivy, G., (1992). "On Predicting Modulus of Elasticity in High-Strength Concrete," ACI Materials Journal, Sep-Oct, Vol. 89, No. 5, pp 517-520.
12. Bazant, Z.P., (1975). "Theory of Creep and Shrinkage in Concrete Structures: A Précis of Recent Development", Mechanics Today, V.2, pp1-93.
13. Bazant, Z.P., Chern, J.C., (1984). "Bayesian Statistical Prediction of Concrete Creep and Shrinkage", ACI Journal, July-August, pp 319-330.
14. Bazant, Z.P., Panula, L., (1980). "Creep and Shrinkage Characterization for Analyzing Prestressed Concrete Structures", PCI Journal, May-June, pp 86-122.
15. Bazant, Z.P., Wittman, F.H., (1983). "Creep and Shrinkage in Concrete Structures", john Wiley & Sons Ltd.
16. Branson, D.E., (1977). "Deformations of Concrete Structures" McGraw-Hill Book Company.
17. Byle, K.A., Burns, N.H., Carrasquillo, R.L., (1997). "Time Dependent Behavior of Prestressed High Performance Concrete Bridge Beams" Center for Transportation Research , University of Texas at Austin, October.
18. Collins, M. P. and Mitchell, D., (1991). "Prestressed Concrete Structures", Prentice Hall, Englewood Cliffs, NJ.
19. Gentle, J. E., (2003). "Random Number Generation and Monte Carlo Methods", Springer.
20. Grewal, B.S., (2004). "Higher Engineering Mathematics", Khanna Publishers.
21. Hinkle, S., (2005). "Thesis Draft", Master's Thesis, Via Dept. of Civil and Environmental Engineering, Virginia Polytechnic Institute and State University, Blacksburg, VA.
22. Huo, X.S., Al-Omaishi, N., and Tadros, M.K., (2001). "Creep, Shrinkage, and Modulus of Elasticity of High Performance Concrete," *ACI Material Journal*, Vol. 98, No. 6, November-December, pp. 440-449.
23. Kahn, A. A., Cook, W. D., and Mitchell, D., (1997). "Creep, shrinkage, and thermal strains in normal, medium, and high strength concrete during hydration." ACI Materials Journal, 94(2), 156-163.

24. Kelly, D.J., Breen, J.E., Bradberry, T.E., (1987). "Time Dependent Deflections of Pretensioned Beams" Center for Transportation Research, University of Texas at Austin, August.
25. Kikuchi, D. K., and Mirza, S. A., and MacGregor, J. G., (1978). "Strength Variability of Bonded Prestressed Concrete Beams, Structural Engineering Report No. 68", University of Alberta, 196 pp.
26. Kirkpatrick, T.J., (2001). "Impact of Specification Changes on Chloride Induced Corrosion Service Life of Virginia Bridge Decks." Master's Thesis, Via Dept. of Civil and Environmental Engineering, Virginia Polytechnic Institute and State University, Blacksburg, VA.
27. Magura, D. D., Sozen, M. A., and Siess, C. P., (1964). "A Study of Relaxation in Prestressing Reinforcement", PCI Journal, V. 9, No. 2, pp 13-57.
28. Mak, S. L., Foster, G., Chirgwin, G., and Ho, D. W. S., (1997). "Properties of high performance heat-cured slag cement concrete for bridge structures." Proceedings of the 3rd CANMET/ACI International Conference, Kuala Lumpur, Malaysia, 821-830.
29. McHenry, D., (1943). "A New Aspect of Creep in Concrete and its Applications to Design", ASTM Proceedings, V. 43, pp 1069-1084.
30. Mirza, S.A., Hatznikolas, M., Macgregor, J.G., (1978). "Statistical Descriptions of the Strength of Concrete", ASCE Journal of Structural Division
31. Mirza, S.A., Kikuchi, Dennis, K., Macgregor, J.G., (1980). "Flexural Strength Reduction Factor for Bonded Prestressed Concrete Beams", ACI Journal V 77, No. 4, July-August, pp 237-246
32. Mirza, S.A., Macgregor, J.G., (1979). "Statistical Study of Shear Strength of Reinforced Concrete Slender Beams", ACI Journal, November, pp 1159-1177.
33. Mokhtarzadeh, A. and French, C., (2000). "Time-dependent properties of high-strength concrete with consideration for precast applications." *ACI Materials Journal,* 97(3), pp 263-271.
34. Mwanza, P., (1993). "Bayesian Prediction of Prestress Losses in Prestressed Concrete Girders Using a Monte Carlo Generated Prior", M. S. Thesis in Civil Engineering, The Pennsylvania State University, 194 pp.

35. Mwanza, P., and Scanlon, A., (2000). “Monte Carlo Simulation of Prestress Loss in Prestressed Bridge Girders.” Proceedings of the 28th Annual Conference of the Canadian Society for Civil Engineering, London, Ontario, 4 pp.
36. Myers, J. J. and Carrasquillo, R. L., (1999). “Production and Quality Control of High Performance Concrete in Texas Bridge Structures,” Research Report 580/589-1, Center for Transportation Research, University of Texas, Austin, TX 176 pp.
37. Myerson, R., (2001). “Compressive Creep of Prestressed Concrete Mixtures with and without Mineral Admixtures” Master’s Thesis, Via Dept. of Civil and Environmental Engineering, Virginia Polytechnic Institute and State University, Blacksburg, VA
38. Naaman, A.E., (1982). “Prestressed Concrete Analysis and Design”, McGraw-Hill Book Company.
39. Naaman, A.E., Siriaksorn, A., (1982). “Reliability of Partially Prestressed Concrete Beams at Serviceability Limit States”, PCI Journal, November-December, pp 66-85.
40. Neville, A.M., (1997). “Aggregate Bond and Modulus of Elasticity of Concrete” ACI Materials Journal, January-February, pp 71-74.
41. Neville, A. M., (1970). “Creep of Concrete: Plain, Reinforced, and Prestressed Concrete”, North-Holland Publishing Company, Amsterdam, Holland.
42. Nilson, A.H. (1997). “Design of Prestressed Concrete”, John Wiley and Sons Ltd.
43. Precast/Prestressed Concrete Institute (PCI), (1997). “Bridge Design Manual”, Chicago, IL.
44. Shah, S. P. and Ahmad, S. H., (1994). “High Performance Concrete: Properties and Applications”, McGraw-Hill, New York.
45. Shams, M. K. and Kahn, L. F., (2000). “Time-dependent behavior of high-strength concrete: task 3, use of high strength/high performance concrete for precast prestressed concrete bridges in Georgia.” Structural Engineering, Mechanics, and Materials Research Report No. 00-1, Georgia Institute of Technology, Atlanta GA.
46. Stallings, J. M. and Eskildsen, S., (2001). "Camber and Prestress Losses in High Performance Concrete Bridge Girders," Highway Research Center, Harbert Engineering Center, Auburn University, Auburn, AL, May, 116 pp.
47. Steinberg, Eric P., (1995). “Probabilistic Assessment of Prestress Loss in Pretensioned Prestressed Concrete.” PCI Journal, November-December, pp 76-85.

48. Tadros, M. K., Al-Omaishi, N., Seguirant, S. J., and Gallt, J. G., (2003). "Prestress losses in pretensioned high-strength concrete bridge girders." *NCHRP Report 496*, National Cooperative Highway Research Program, Transportation Research Board, National Research Council.
49. Townsend, B., (2003). "Creep and shrinkage of a high strength concrete mixture." Master's Thesis, Via Dept. of Civil and Environmental Engineering, Virginia Polytechnic Institute and State University, Blacksburg, VA.
50. Trost, H., (1967). "Auswirkungen des superprositionspringzips auf kriech-und relaxations probleme bei Beton and Apannbeton." *Beton and Stahlbetonbau*, 62(10) 230-238.
51. Waldron, C.J., (2004). "Investigation of Long-Term Prestress Losses in Pretensioned High Performance Concrete Girders" PhD Dissertation, Via Dept. of Civil and Environmental Engineering, Virginia Polytechnic Institute and State University, Blacksburg, VA.
52. Wollmann, G.P., Wollmann, C.L.R., (2000). "Anchorage Zone Design" Chapter 8 Post Tensioning Manual, Sixth Edition.

APPENDIX A

The Appendix A contains the graphs representing the probability density function for camber and camber growth of PCBT 45 used by VDOT. In addition, it contains data sheets showing the dimension details and number of strands used in PCBT sections depending upon the spacing of girders, span length and concrete strength.

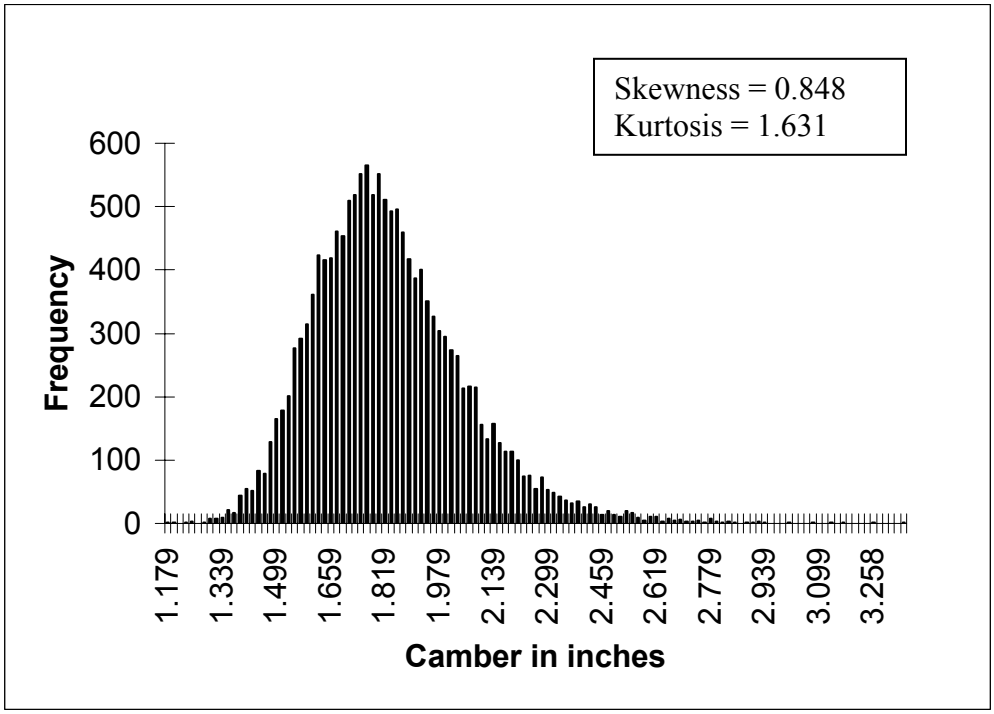

Figure A.1 Graph showing the probability density function of camber at release for beam number 1

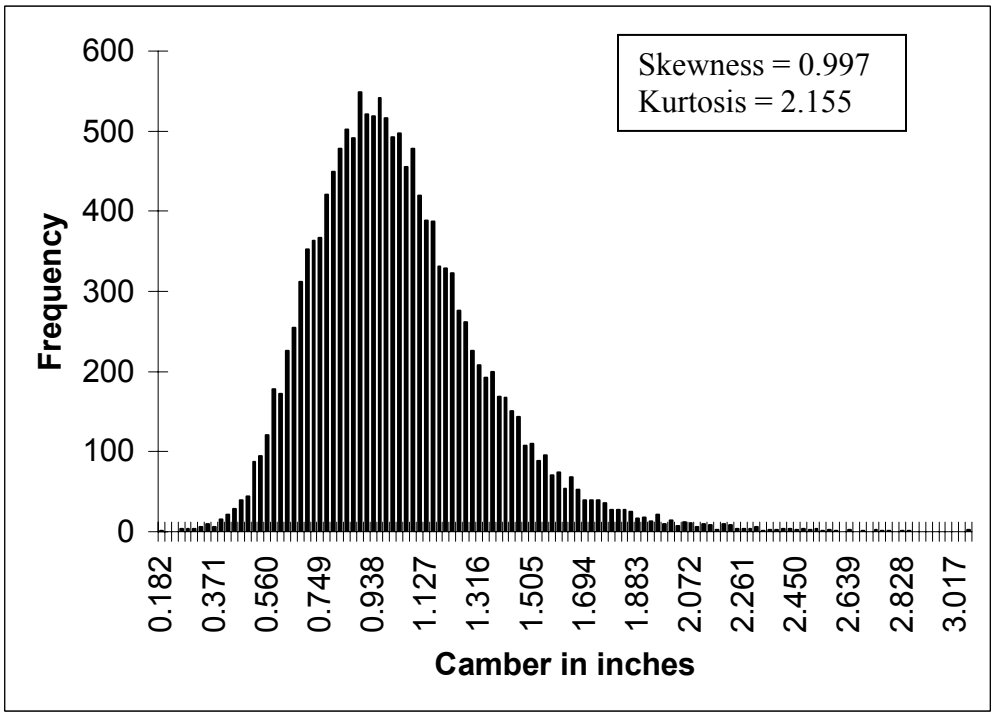

Figure A.2 Graph showing the probability density function of camber growth at 90 days for beam number 1

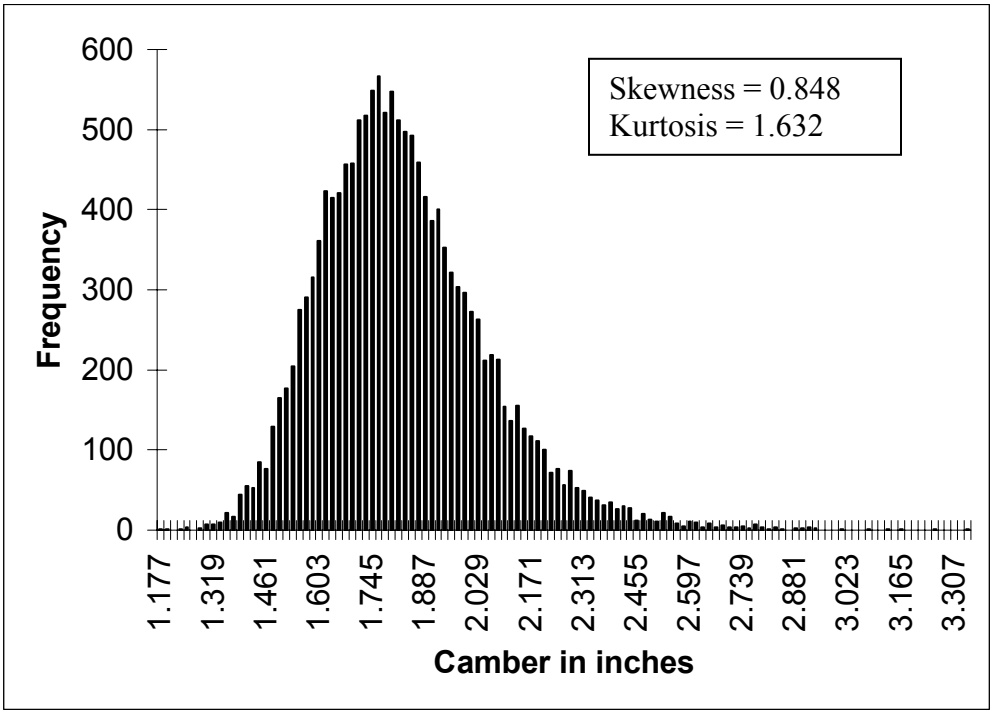

Figure A.3 Graph showing the probability density function of camber at release for beam number 2

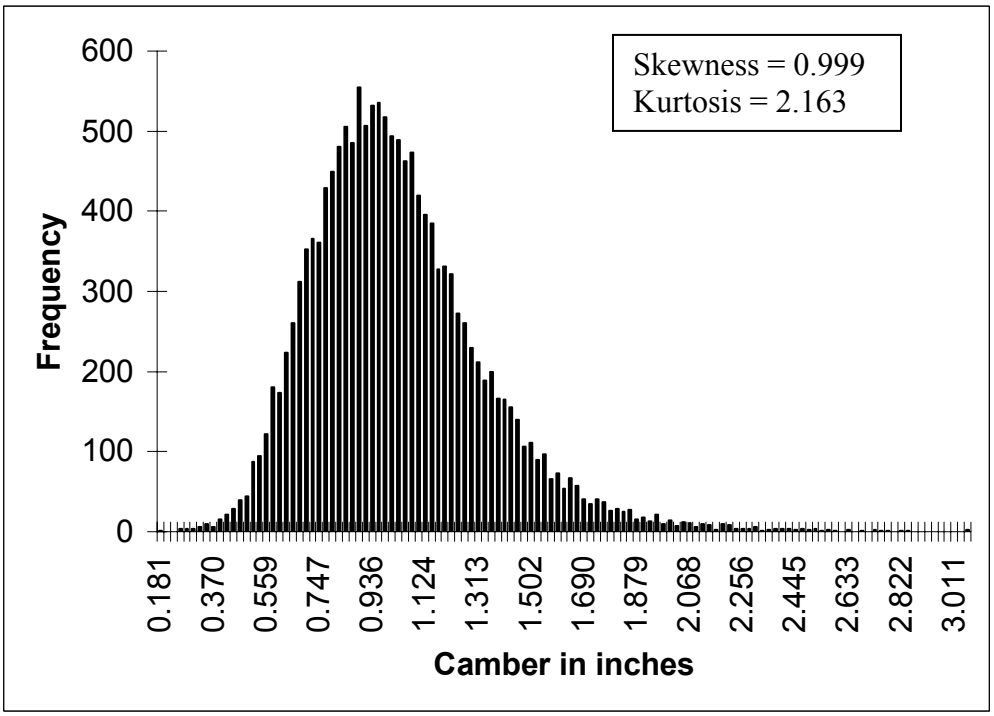

Figure A.4 Graph showing the probability density function of camber growth at 90 days for beam number 2

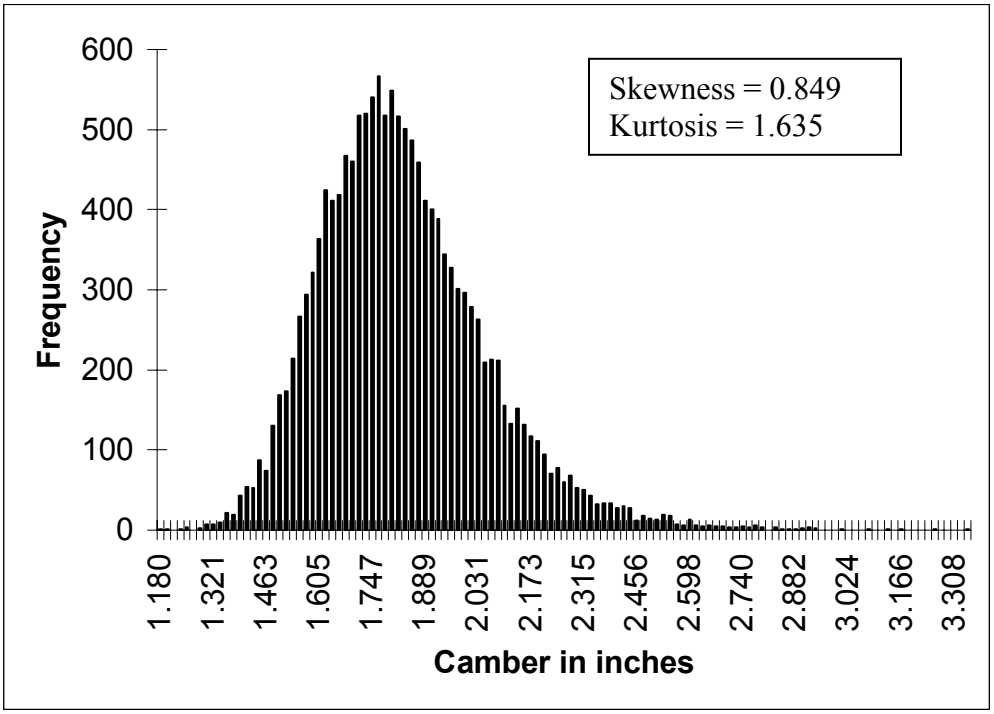

Figure A.5 Graph showing the probability density function of camber at release for beam number 3

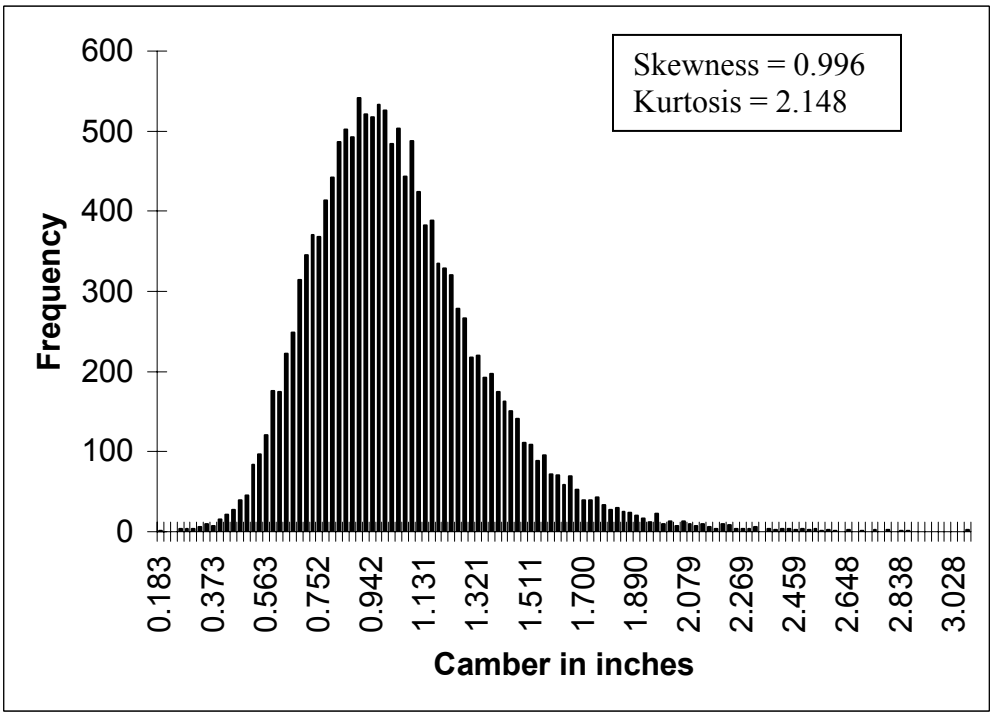

Figure A.6 Graph showing the probability density function of camber growth at 90 days for beam number 3

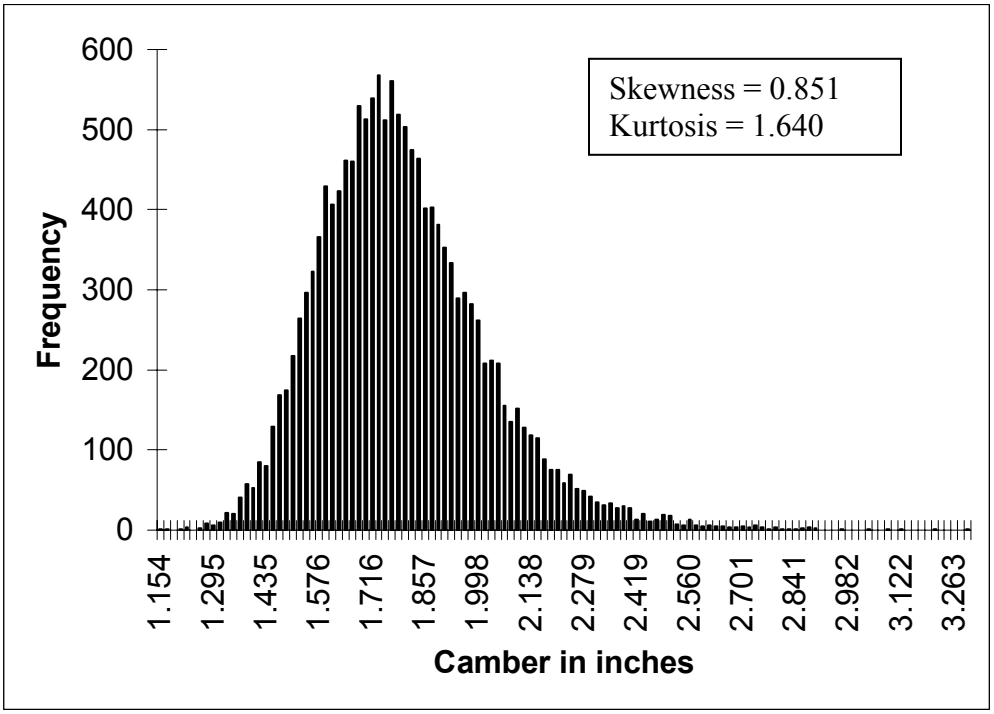

Figure A.7 Graph showing the probability density function of camber at release for beam number 4

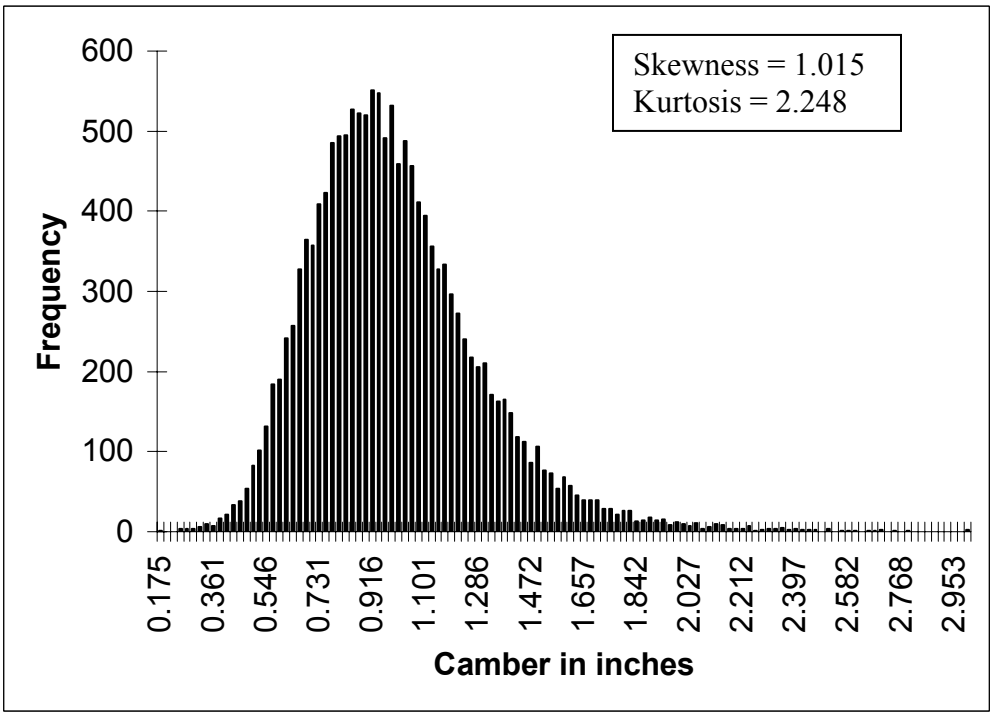

Figure A.8 Graph showing the probability density function of camber growth at 90 days for beam number 4

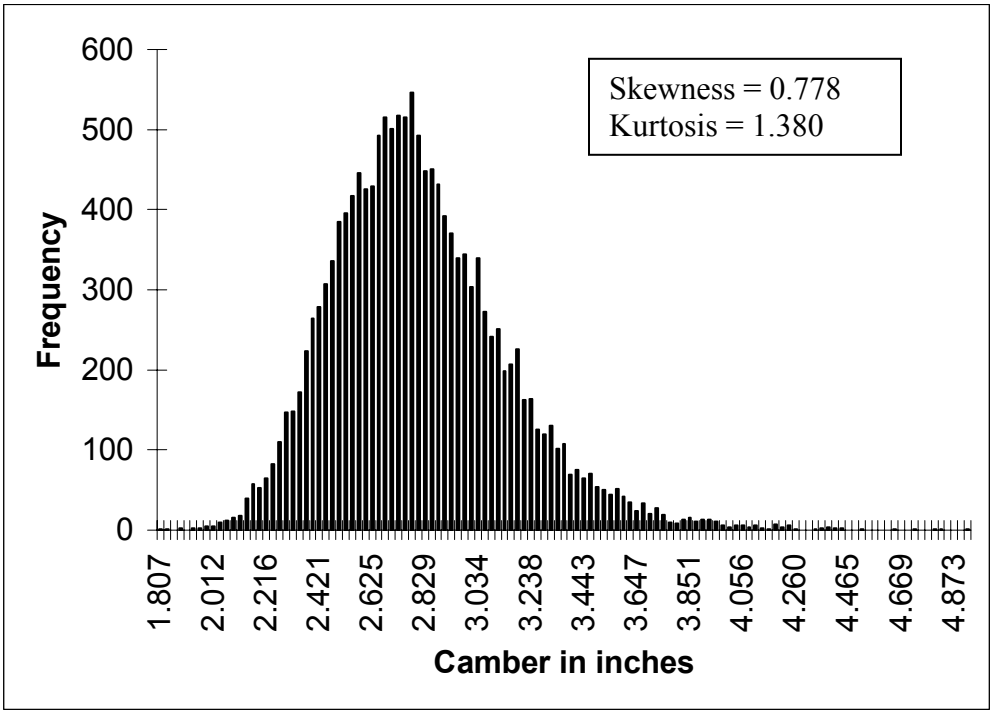

Figure A.9 Graph showing the probability density function of camber at release for beam number 5

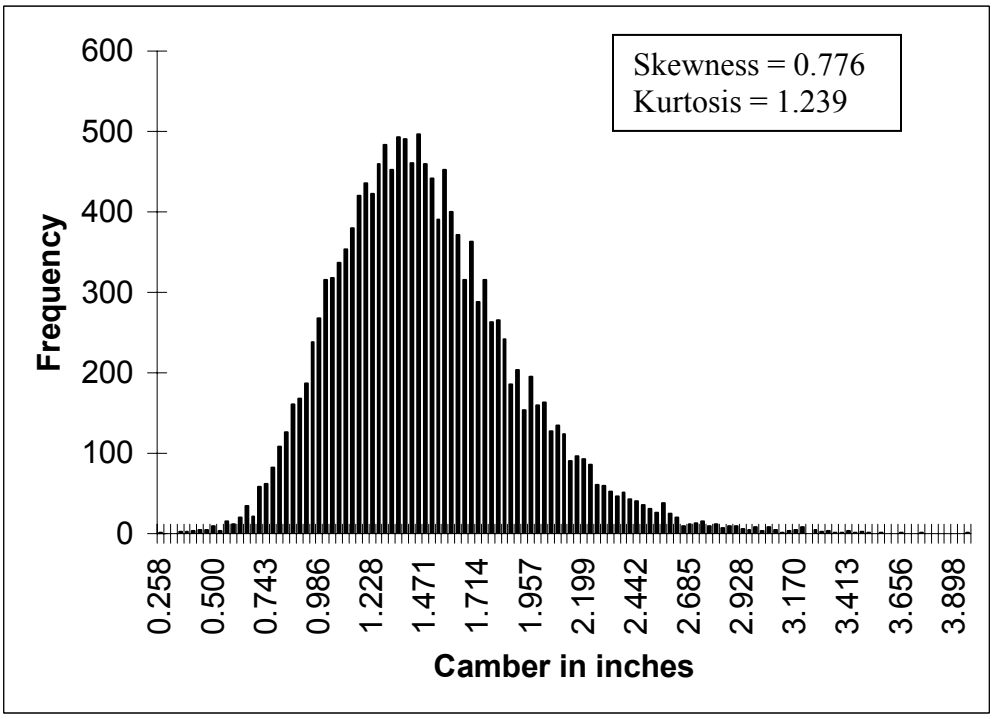

Figure A.10 Graph showing the probability density function of camber growth at 90 days for beam number 5

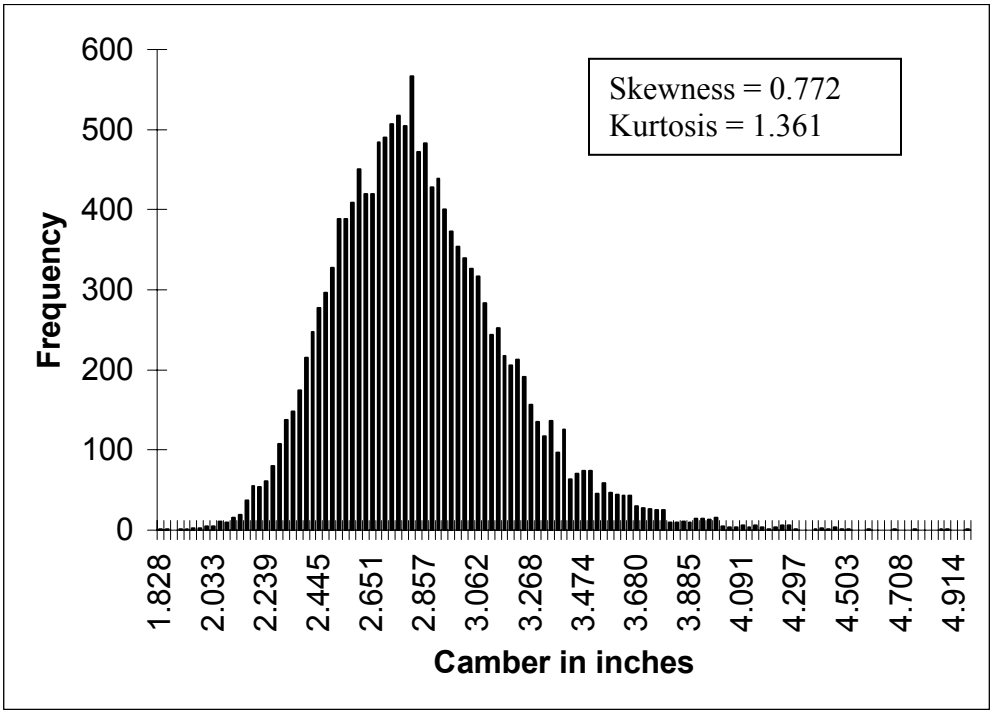

Figure A.11 Graph showing the probability density function of camber at release for beam number 6

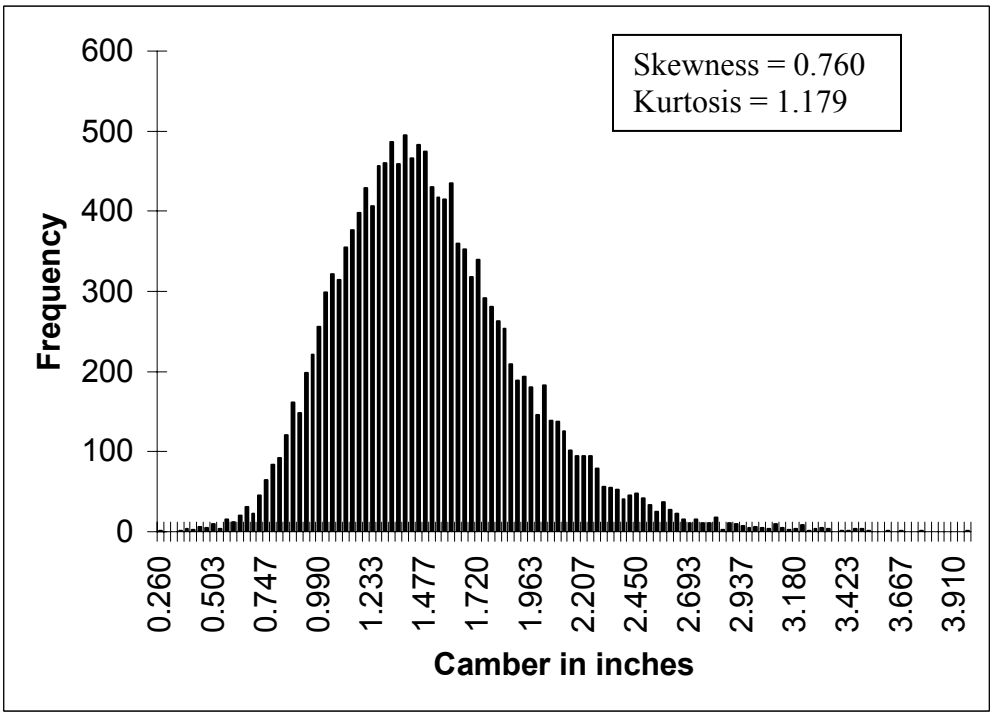

Figure A.12 Graph showing the probability density function of camber growth at 90 days for beam number 6

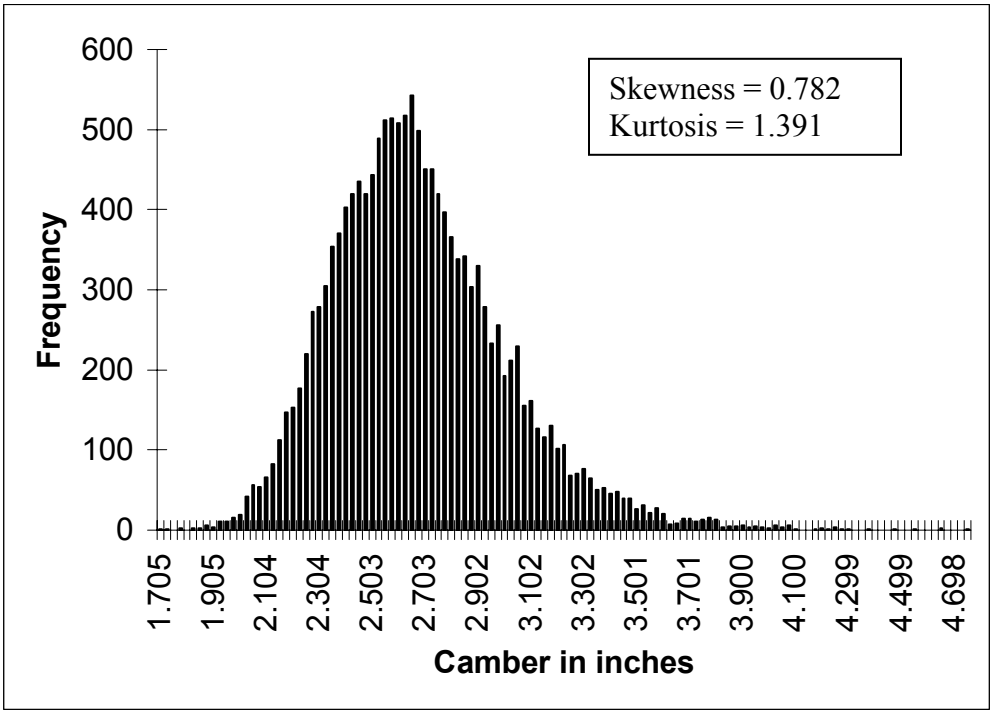

Figure A.13 Graph showing the probability density function of camber at release for beam number 7

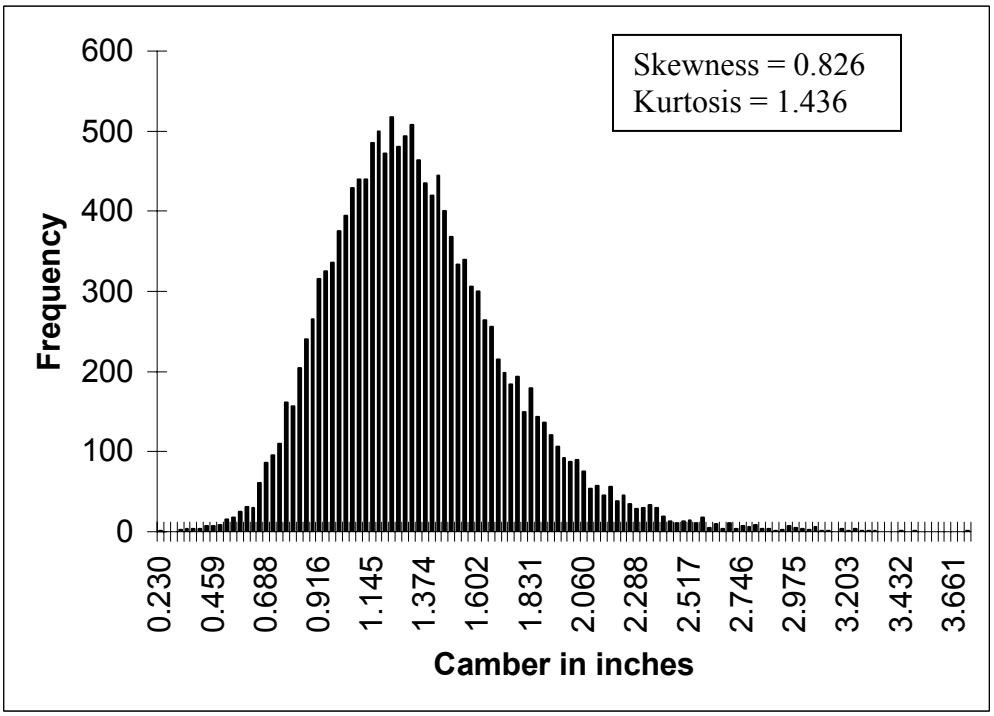

Figure A.14 Graph showing the probability density function of camber growth at 90 days for beam number 7

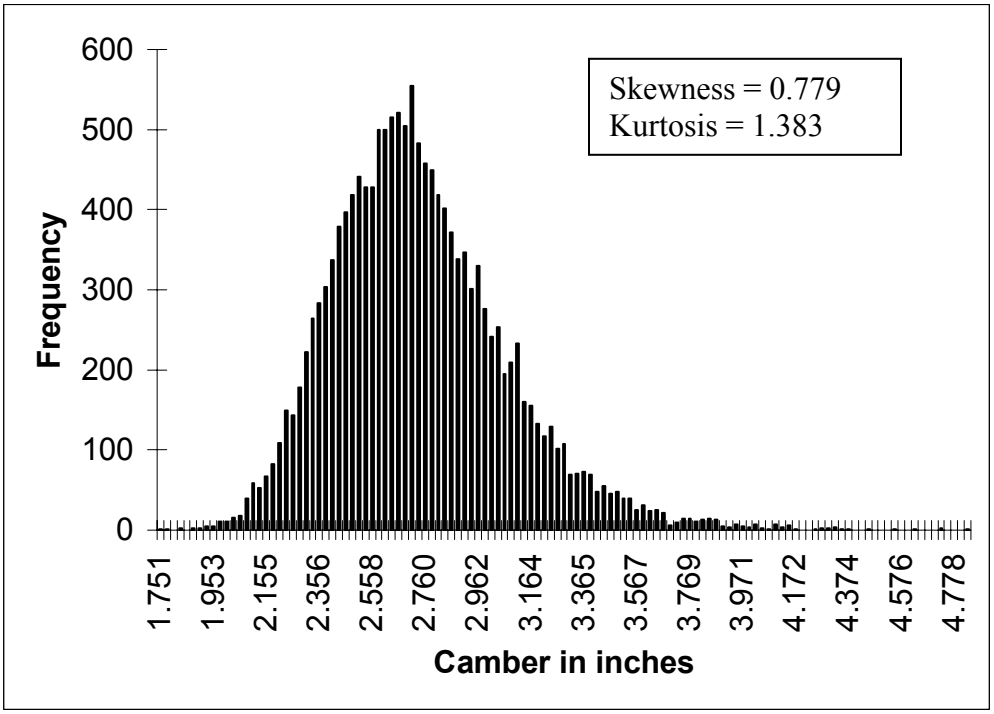

Figure A.15 Graph showing the probability density function of camber at release for beam number 8

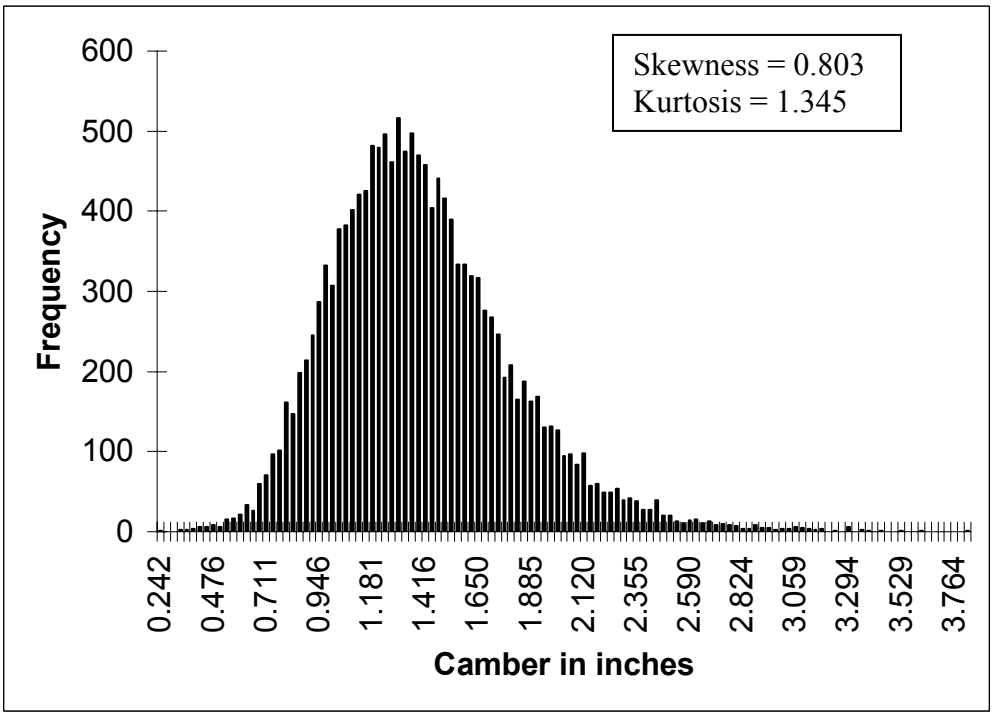

Figure A.16 Graph showing the probability density function of camber growth at 90 days for beam number 8

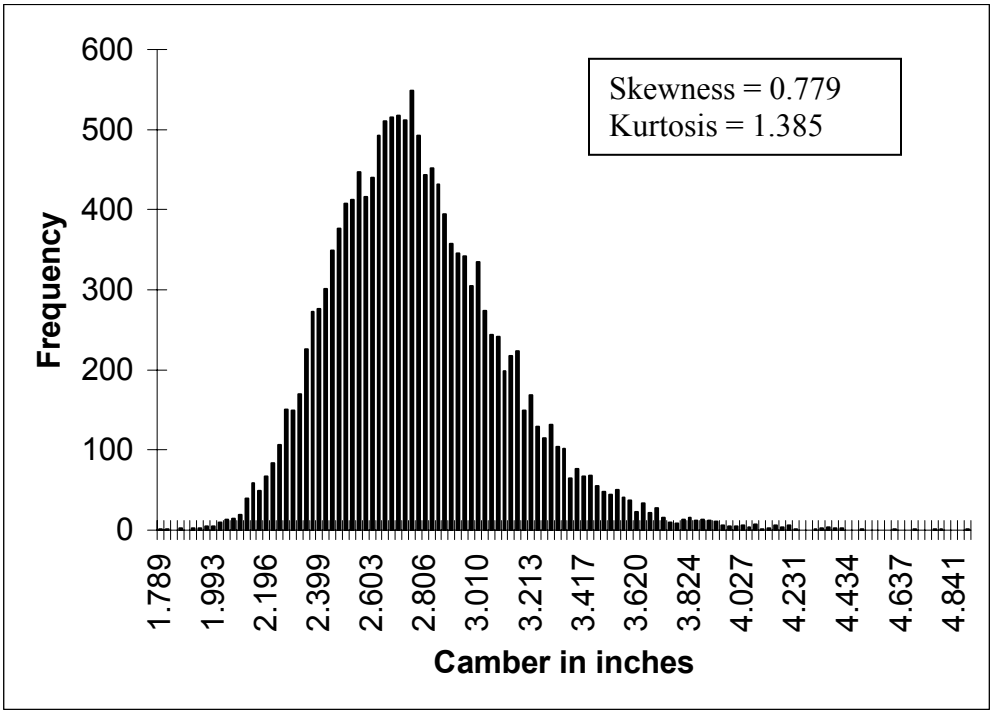

Figure A.17 Graph showing the probability density function of camber at release for beam number 9

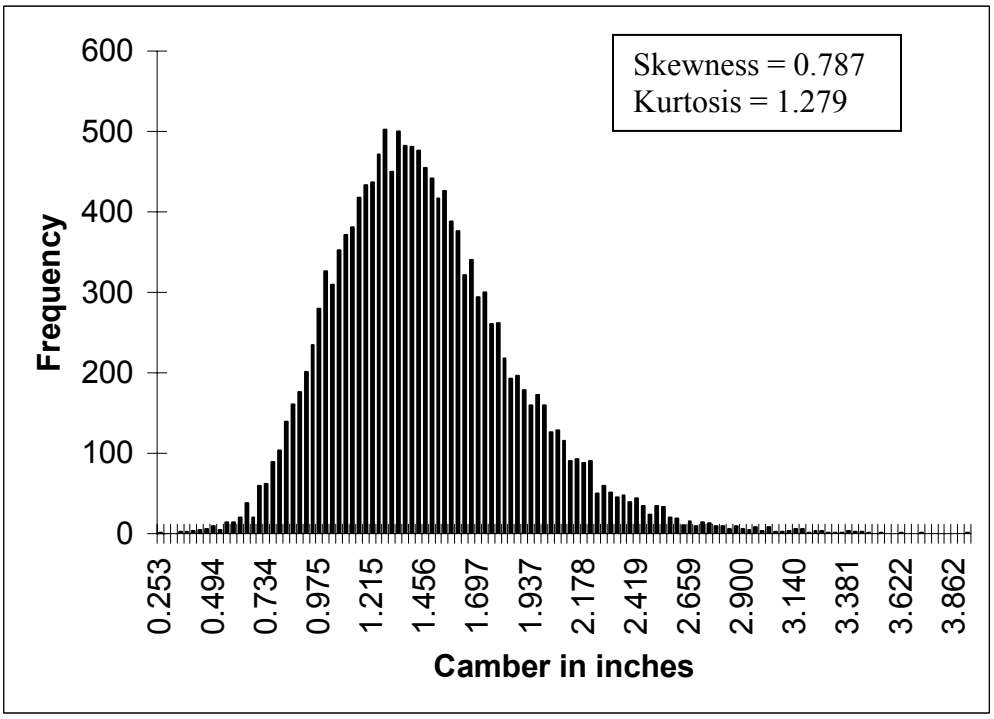

Figure A.18 Graph showing the probability density function of camber growth at 90 days for beam number 9

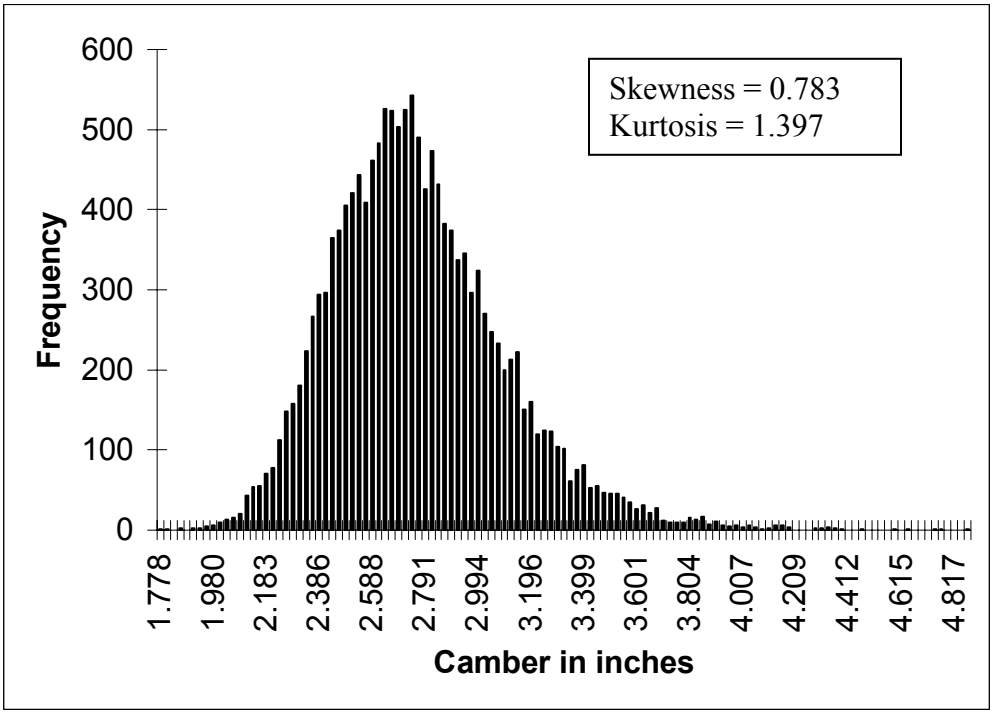

Figure A.19 Graph showing the probability density function of camber at release for beam number 10

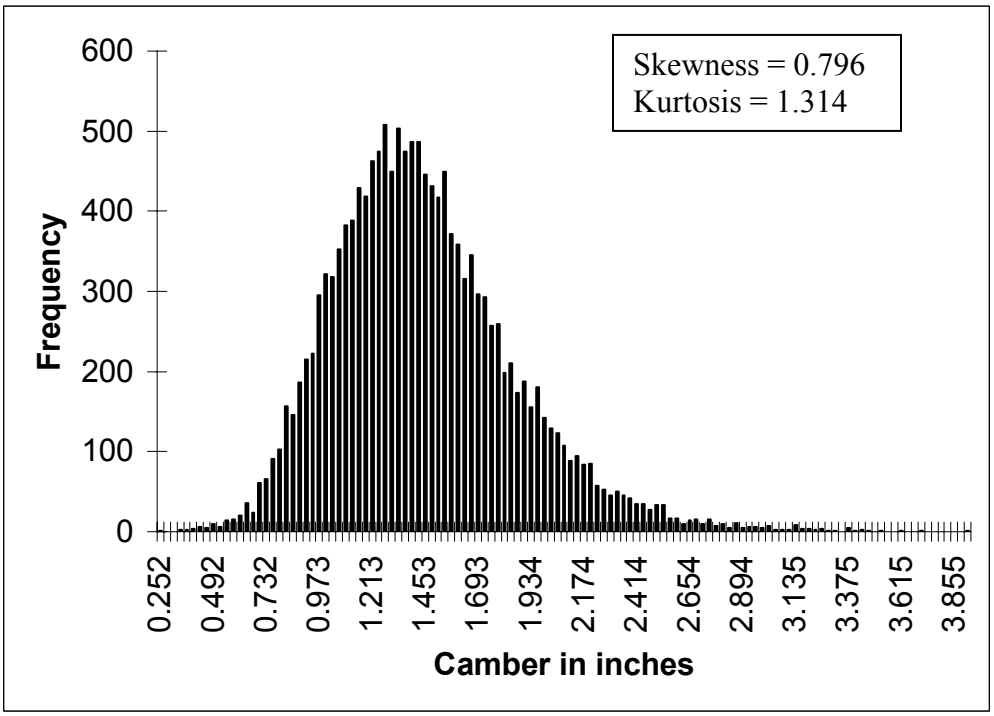

Figure A.20 Graph showing the probability density function of camber growth at 90 days for beam number 10

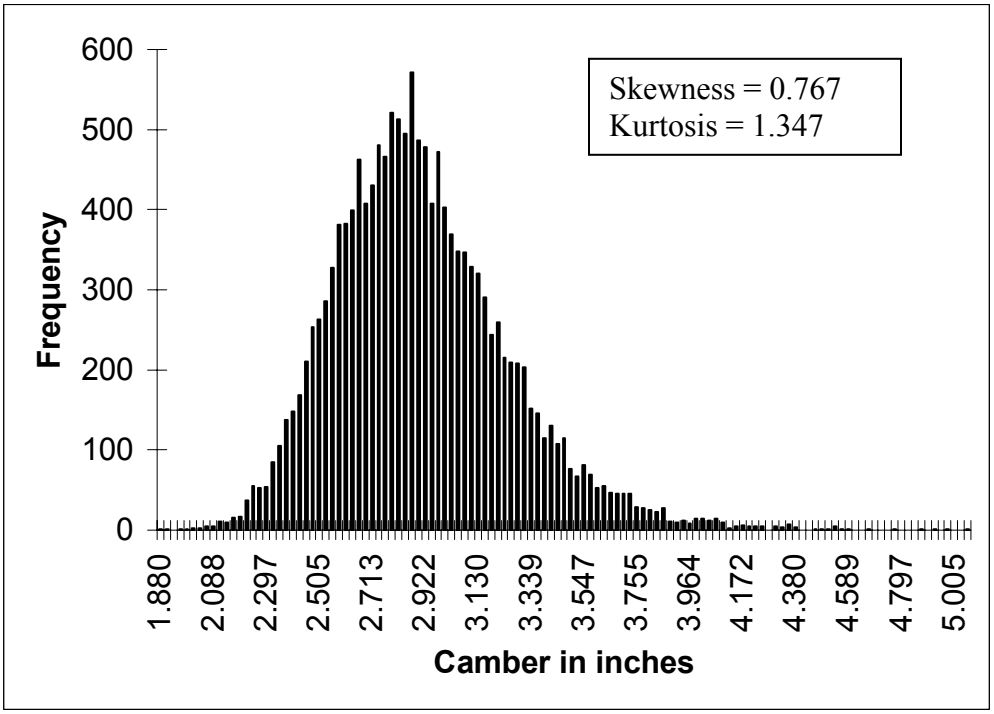

Figure A.21 Graph showing the probability density function of camber at release for beam number 11

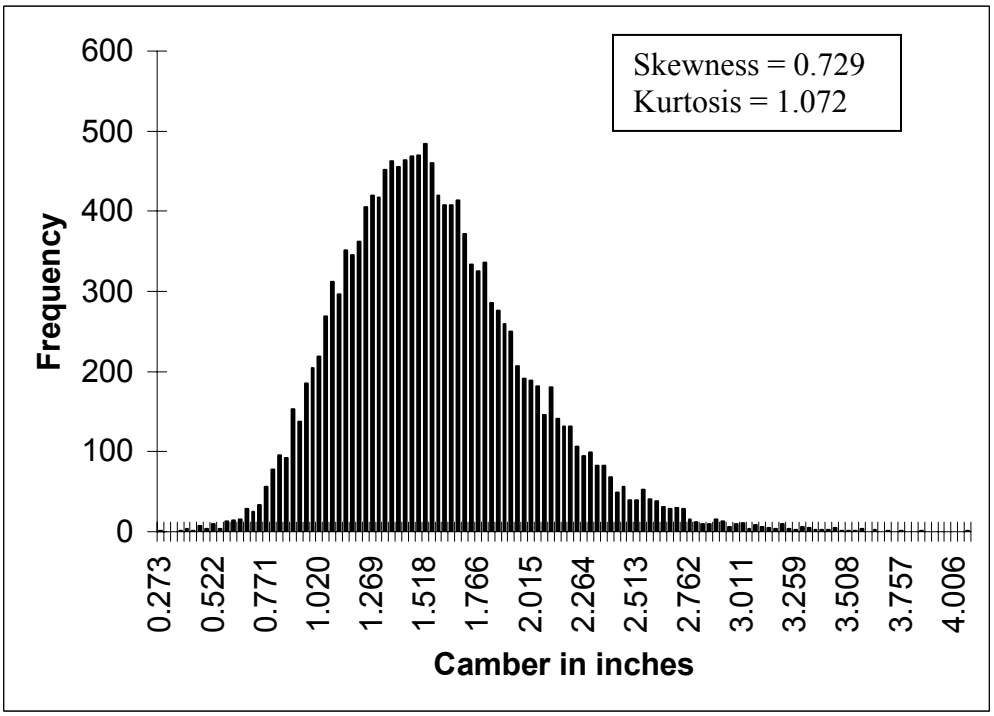

Figure A.22 Graph showing the probability density function of camber growth at 90 days for beam number 11

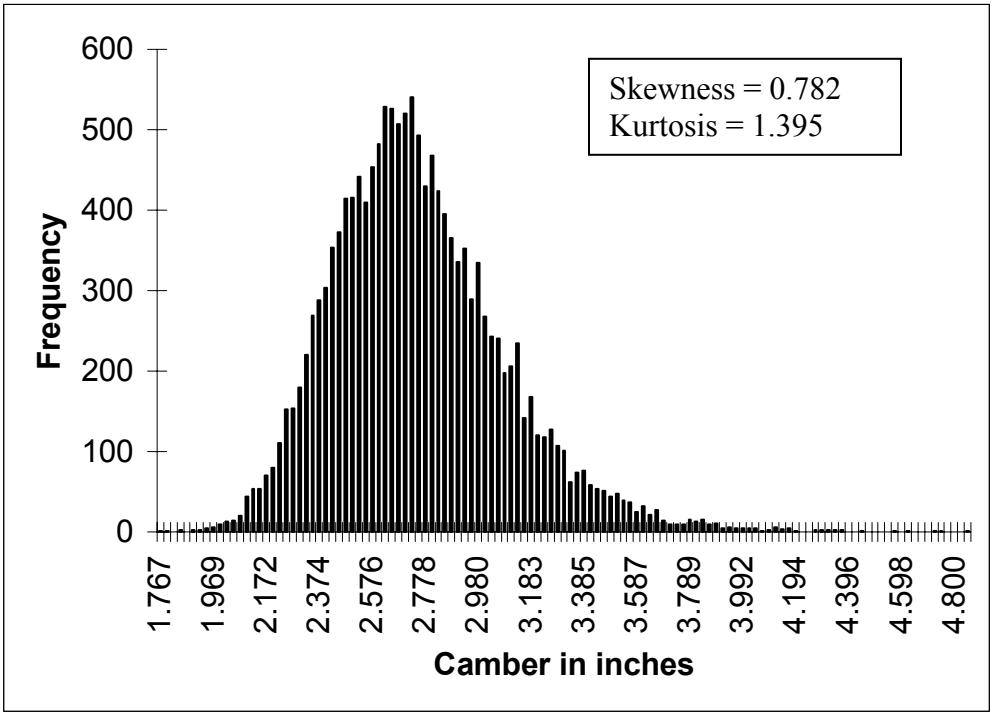

Figure A.23 Graph showing the probability density function of camber at release for beam number 12

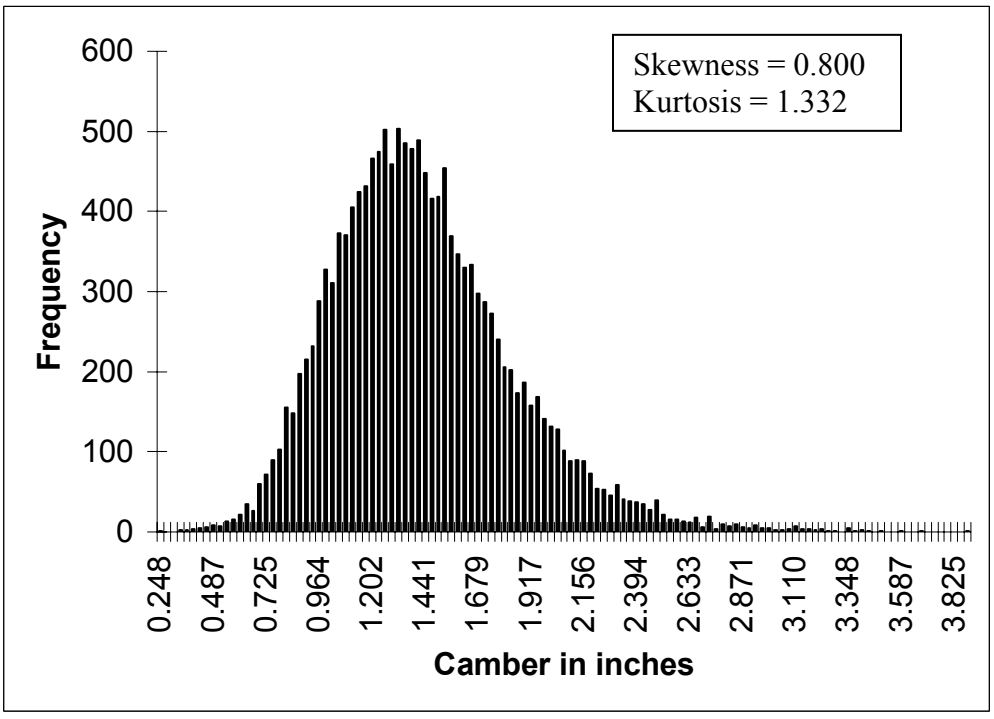

Figure A.24 Graph showing the probability density function of camber growth at 90 days for beam number 12

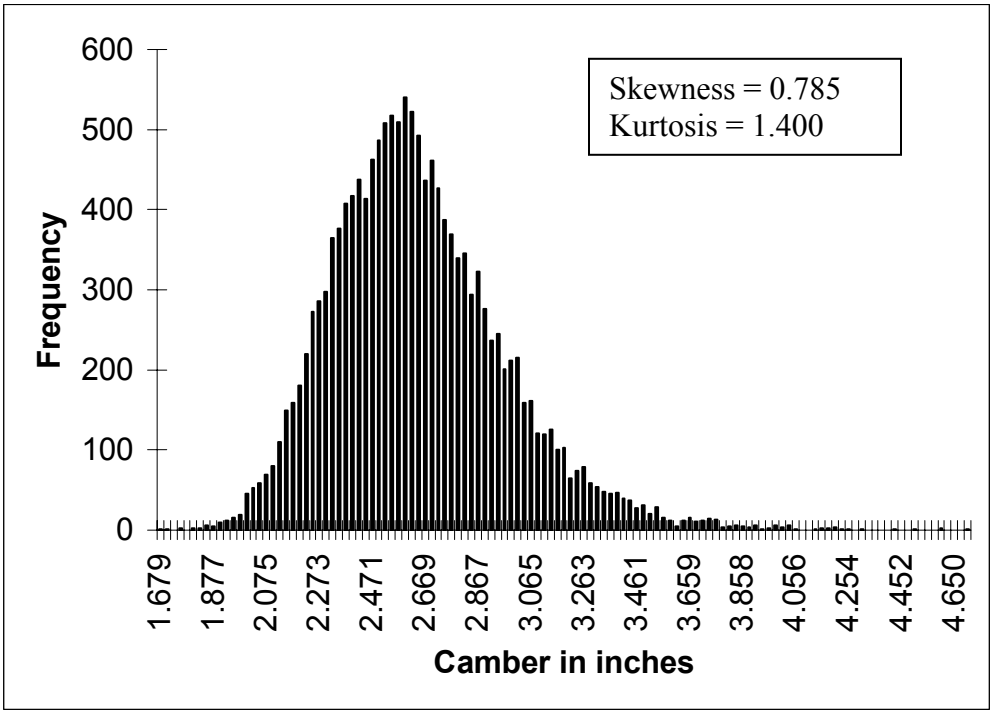

Figure A.25 Graph showing the probability density function of camber at release for beam number 13

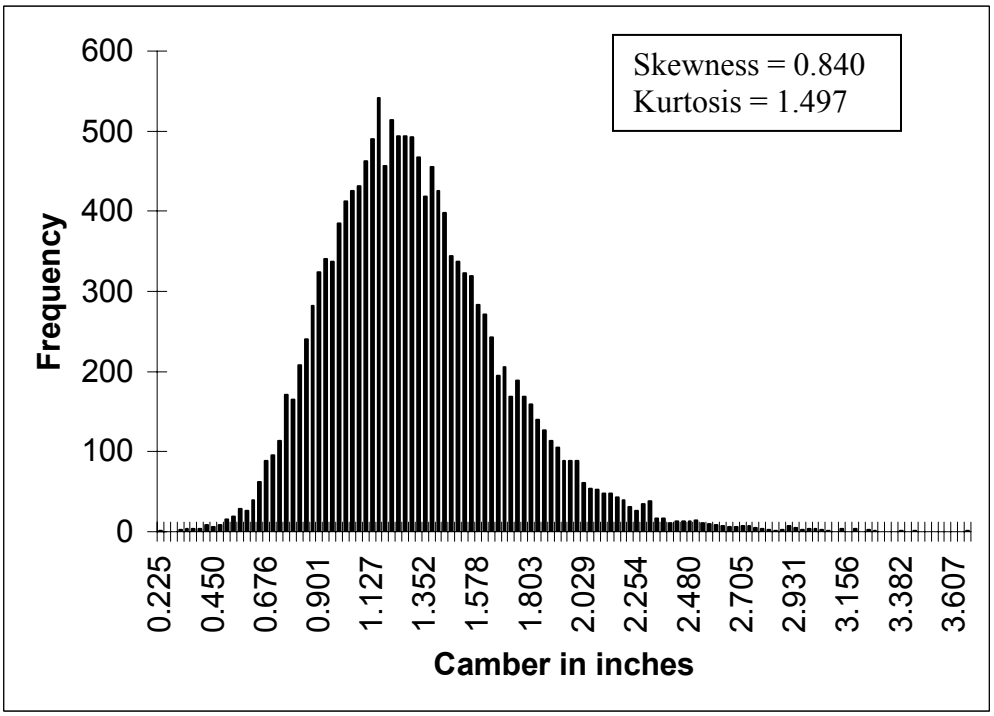

Figure A.26 Graph showing the probability density function of camber growth at 90 days for beam number 13

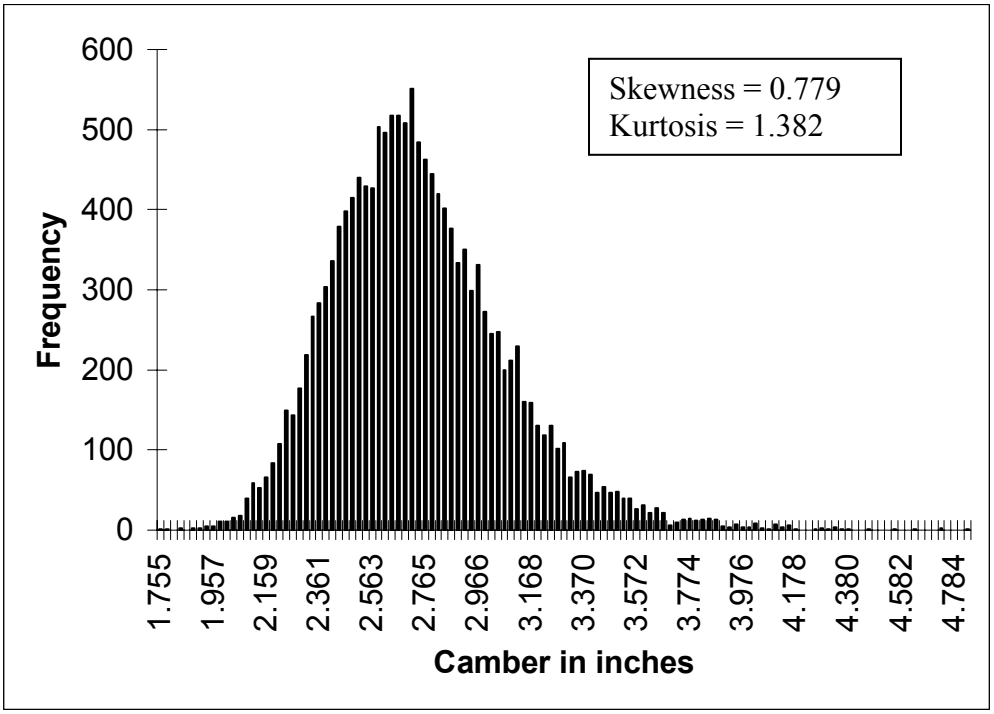

Figure A.27 Graph showing the probability density function of camber at release for beam number 14

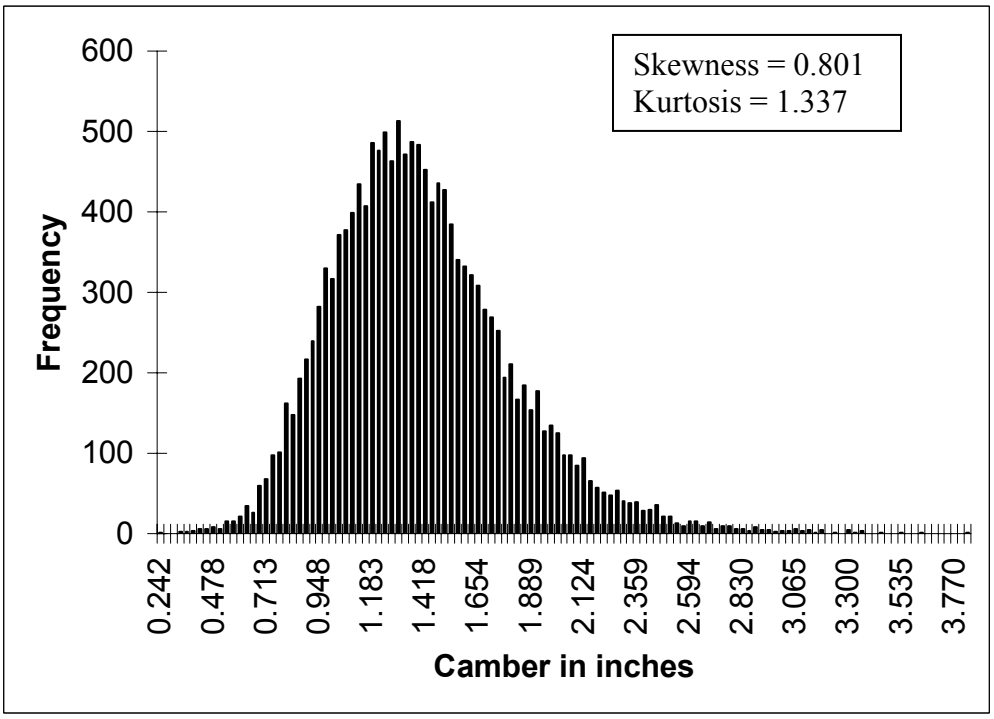

Figure A.28 Graph showing the probability density function of camber growth at 90 days for beam number 14

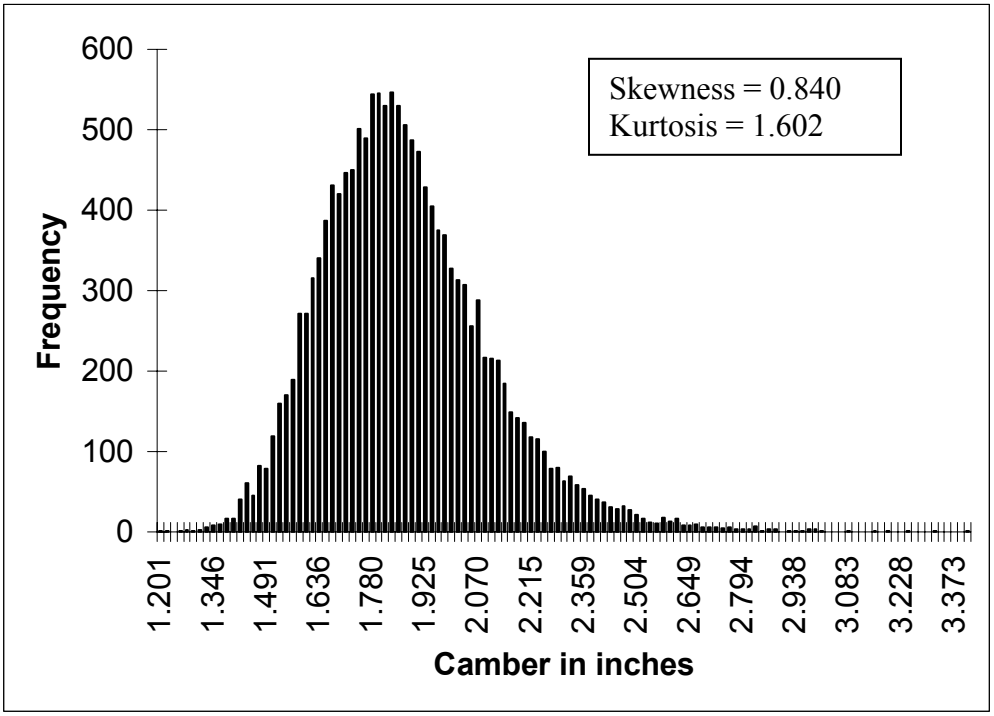

Figure A.29 Graph showing the probability density function of camber at release for beam number 15

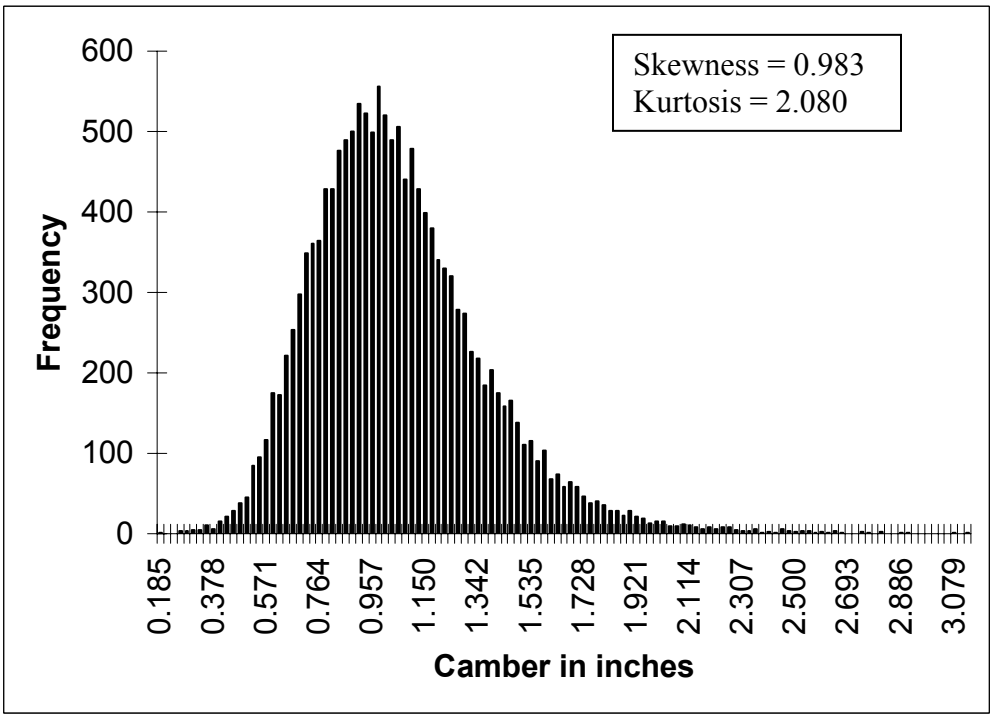

Figure A.30 Graph showing the probability density function of camber growth at 90 days for beam number 15

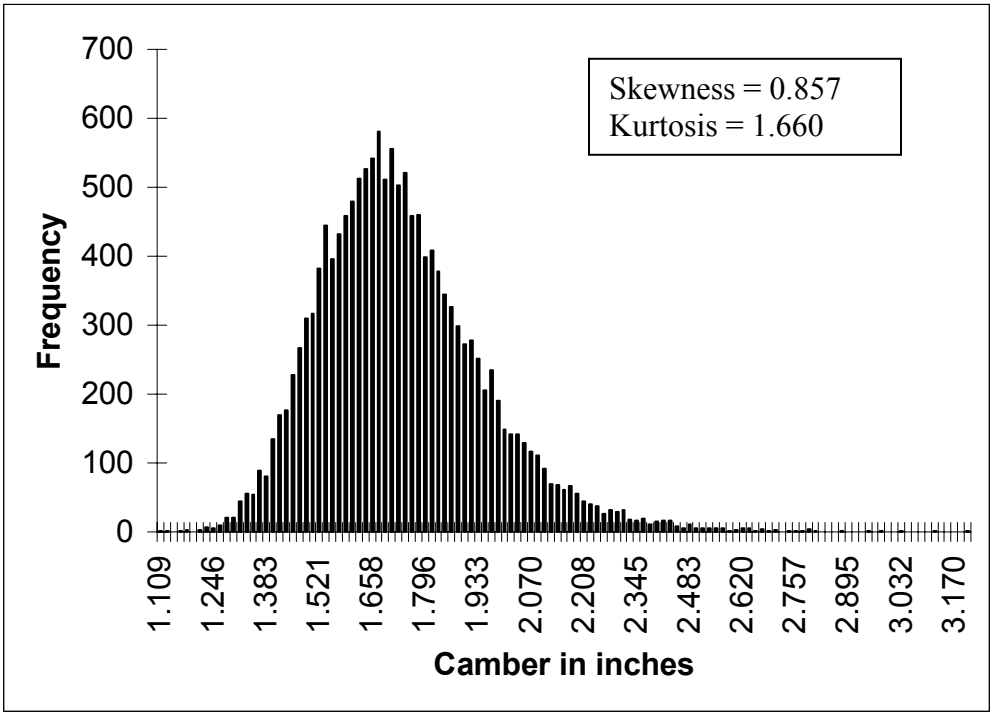

Figure A.31 Graph showing the probability density function of camber at release for beam number 16

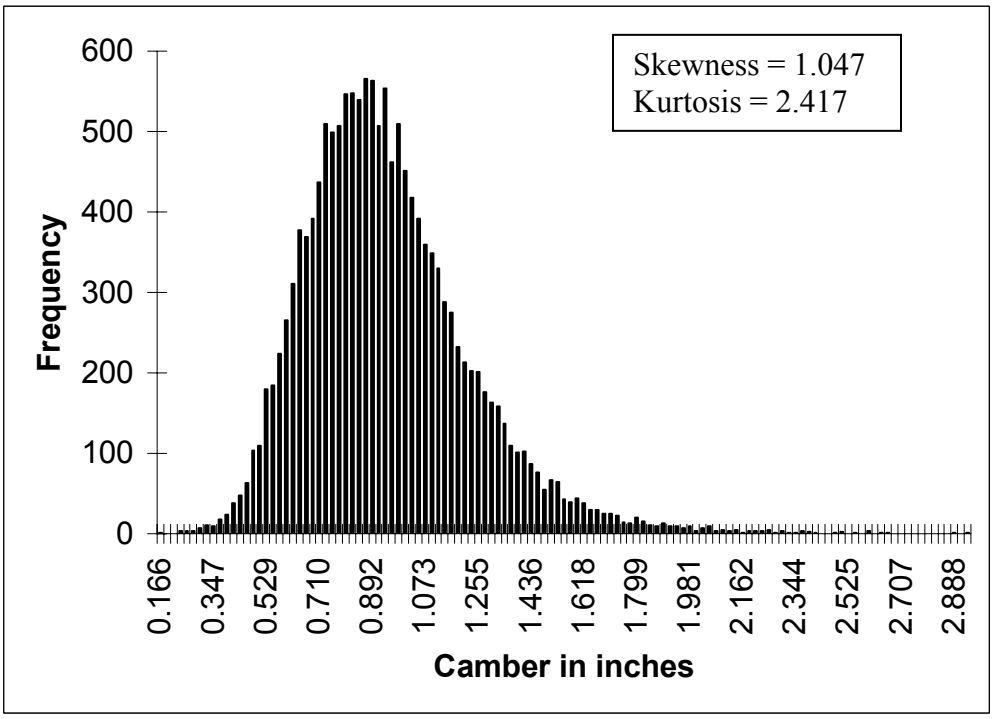

Figure A.32 Graph showing the probability density function of camber growth at 90 days for beam number 16

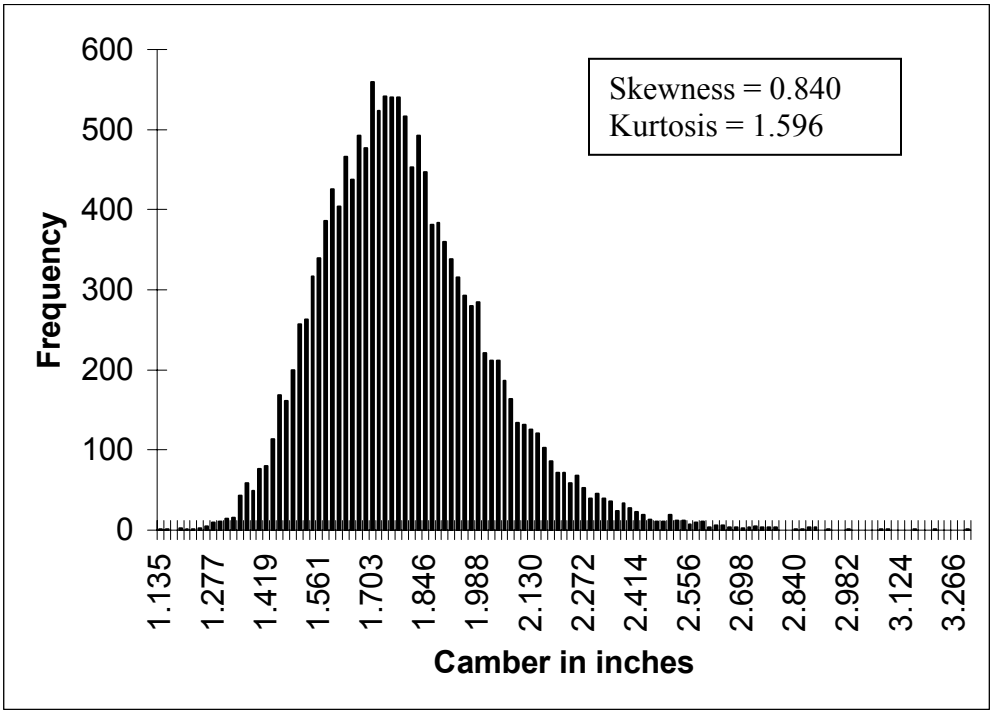

Figure A.33 Graph showing the probability density function of camber at release for beam number 17

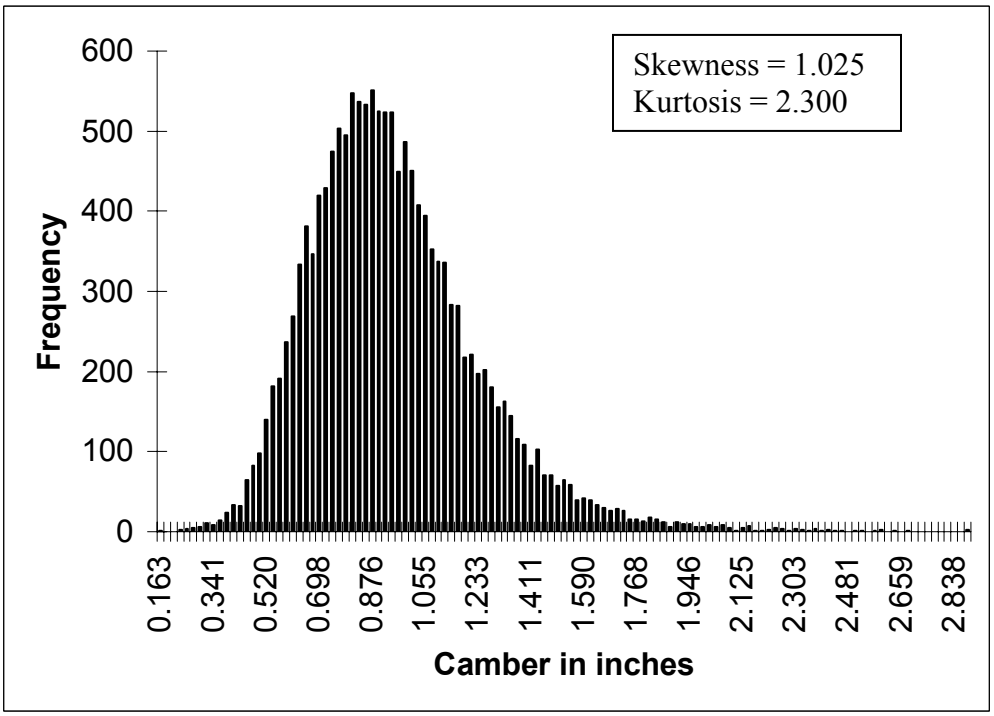

Figure A.34 Graph showing the probability density function of camber growth at 90 days for beam number 17

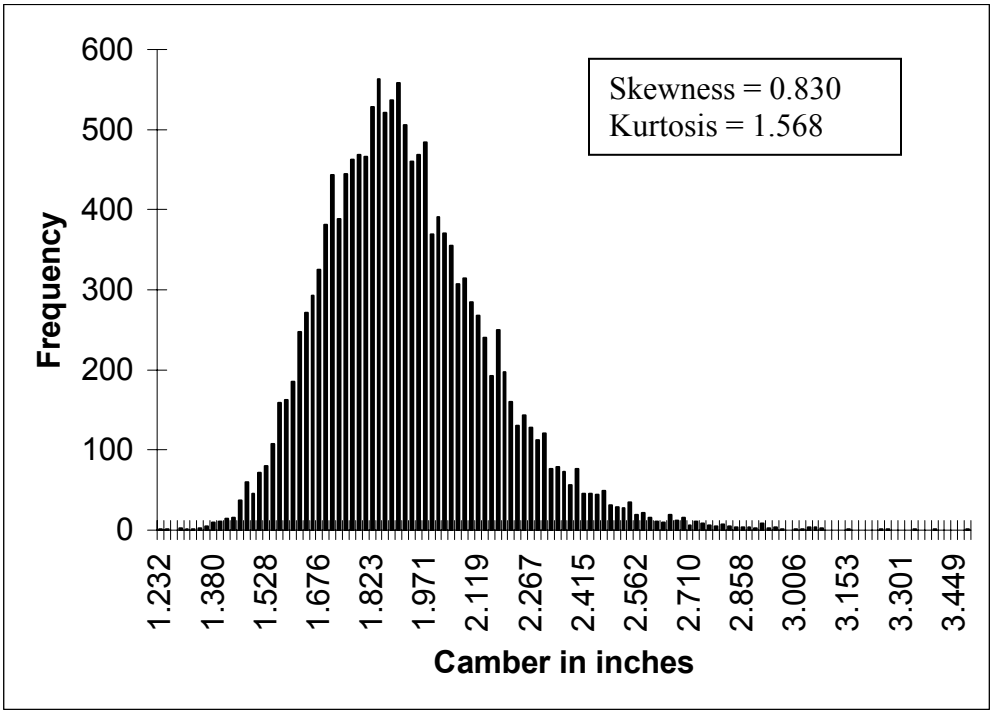

Figure A.35 Graph showing the probability density function of camber at release for beam number 18

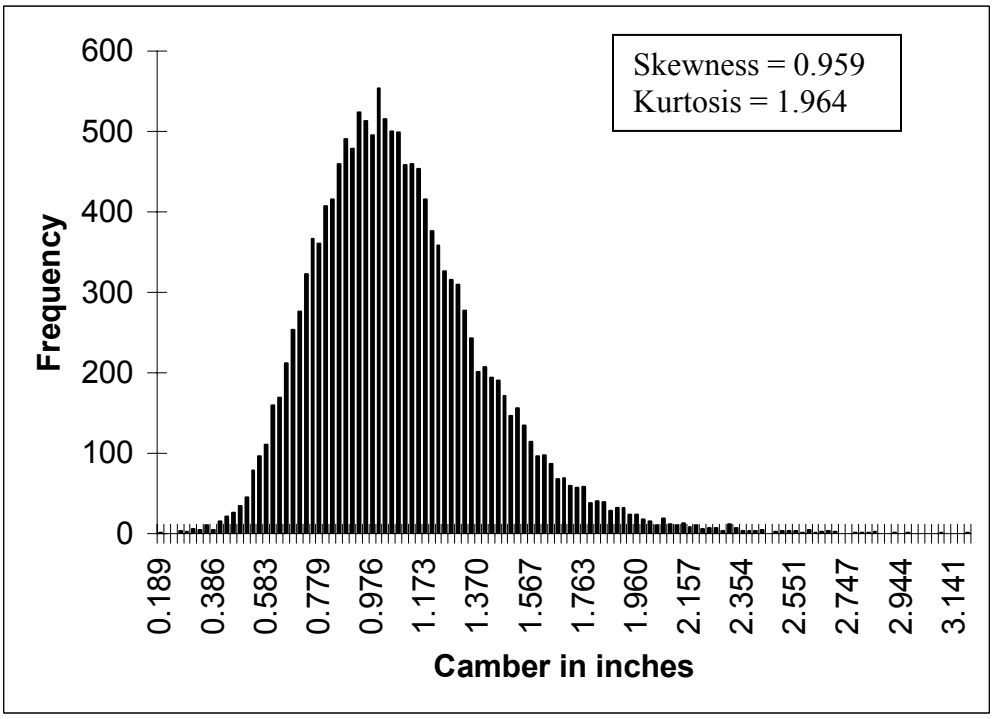

Figure A.36 Graph showing the probability density function of camber growth at 90 days for beam number 18

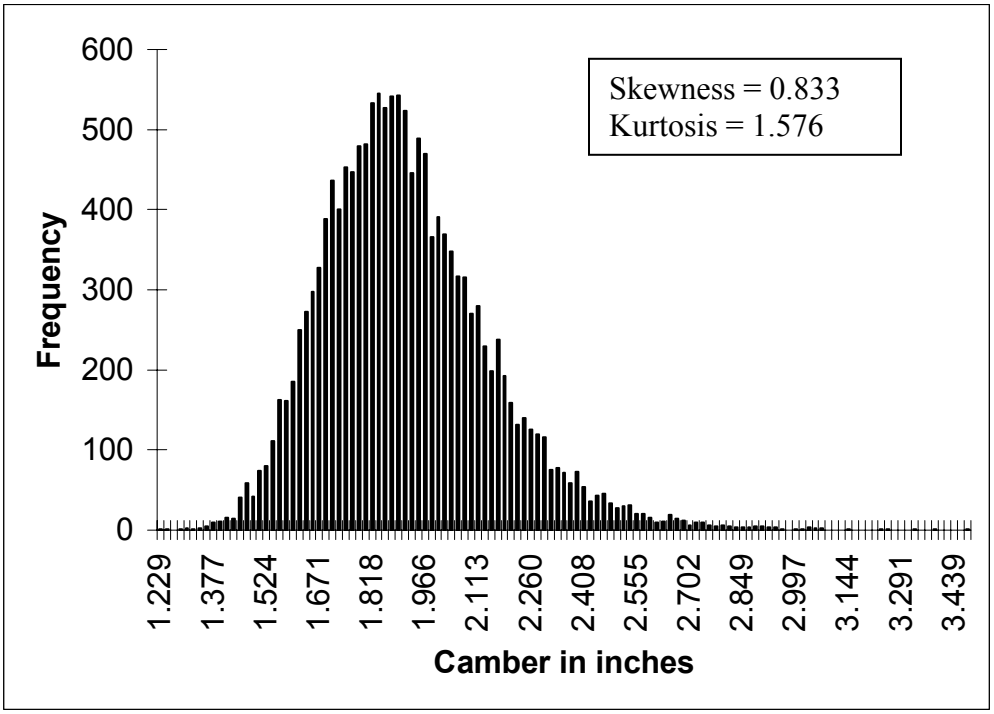

Figure A.37 Graph showing the probability density function of camber at release for beam number 19

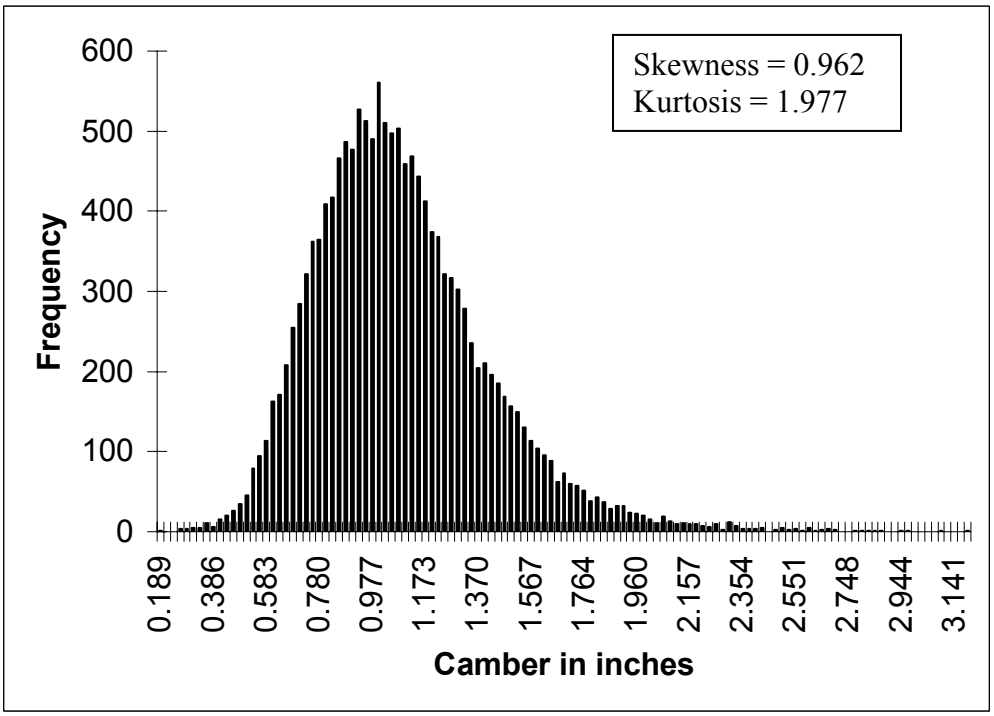

Figure A.38 Graph showing the probability density function of camber growth at 90 days for beam number 19

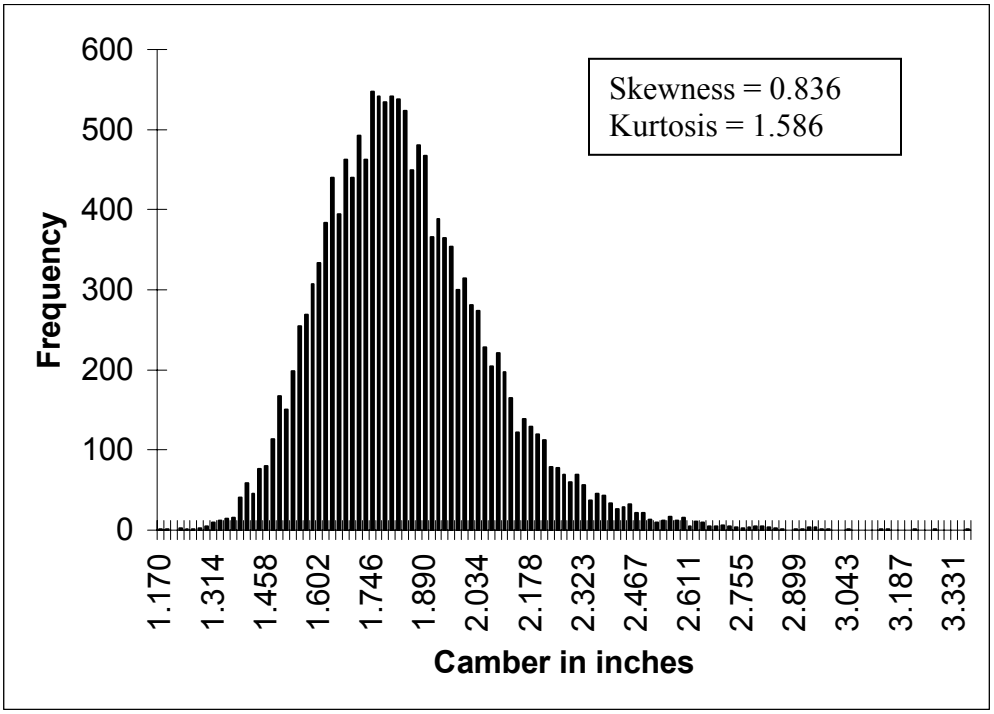

Figure A.39 Graph showing the probability density function of camber at release for beam number 20

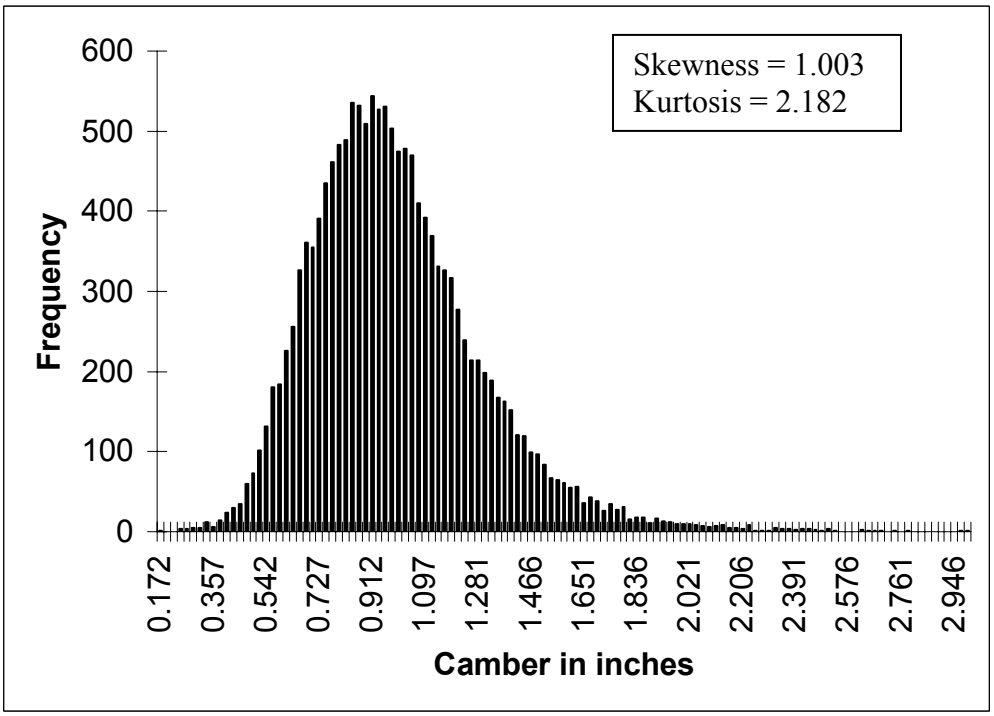

Figure A.40 Graph showing the probability density function of camber growth at 90 days for beam number 20

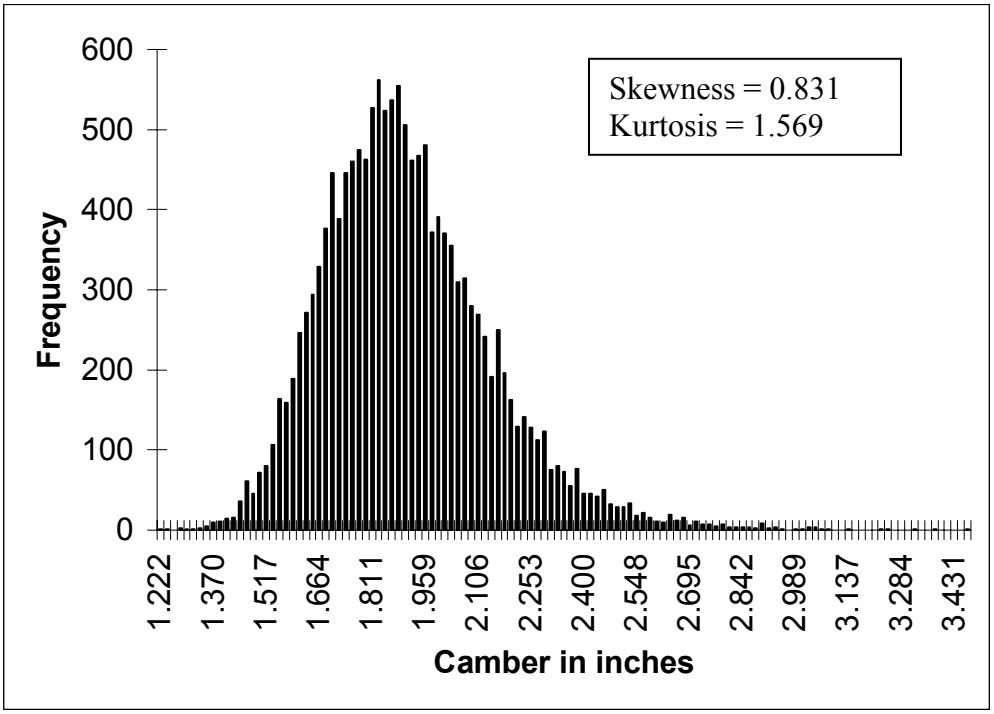

Figure A.41 Graph showing the probability density function of camber at release for beam number 21

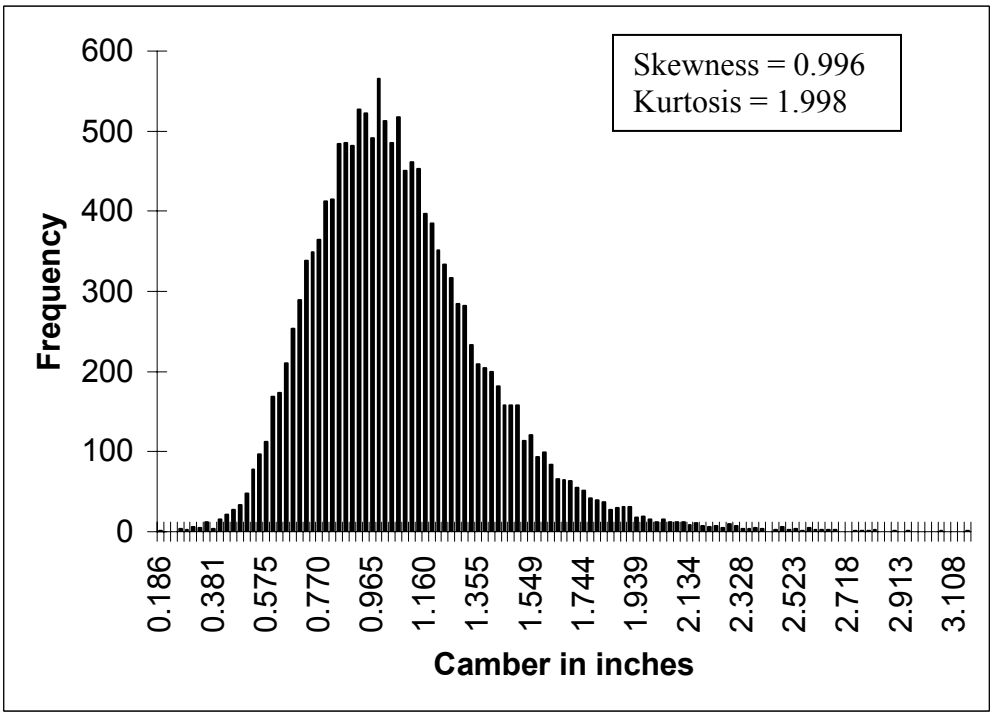

Figure A.42 Graph showing the probability density function of camber growth at 90 days for beam number 21

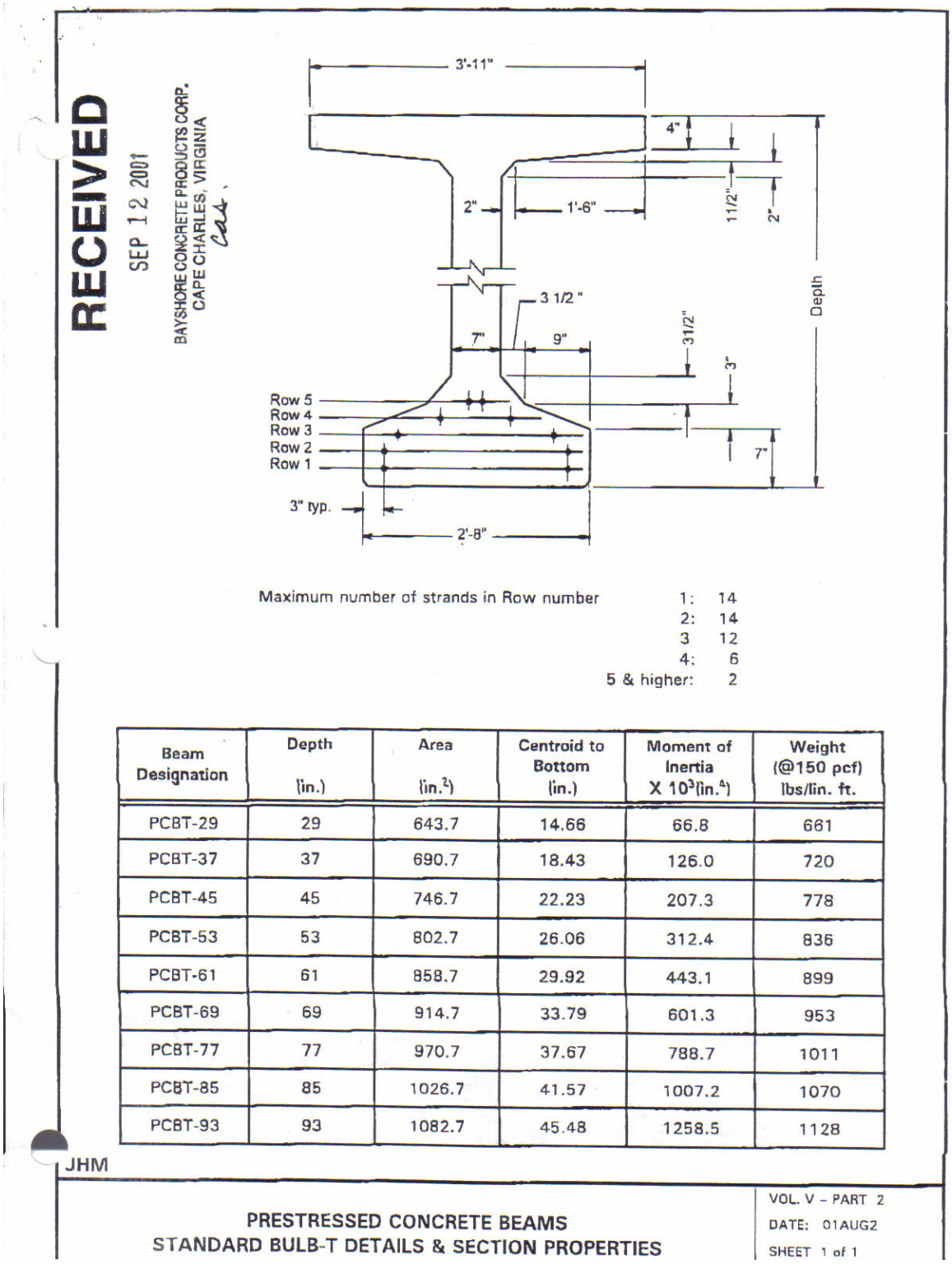

Beam Designation	Depth (in.)	Area (in.^{2})	Centroid to Bottom (in.)	Moment of Inertia X 10^3(in.^{4})	Weight (@150 pcf) lbs/lin. ft.
PCBT-29	29	643.7	14.66	66.8	661
PCBT-37	37	690.7	18.43	126.0	720
PCBT-45	45	746.7	22.23	207.3	778
PCBT-53	53	802.7	26.06	312.4	836
PCBT-61	61	858.7	29.92	443.1	899
PCBT-69	69	914.7	33.79	601.3	953
PCBT-77	77	970.7	37.67	788.7	1011
PCBT-85	85	1026.7	41.57	1007.2	1070
PCBT-93	93	1082.7	45.48	1258.5	1128

Figure A.43 Dimension details of a PCBT sections used by VDOT. (VDOT)

Table A.1 Details for number of strands used in PCBT sections.

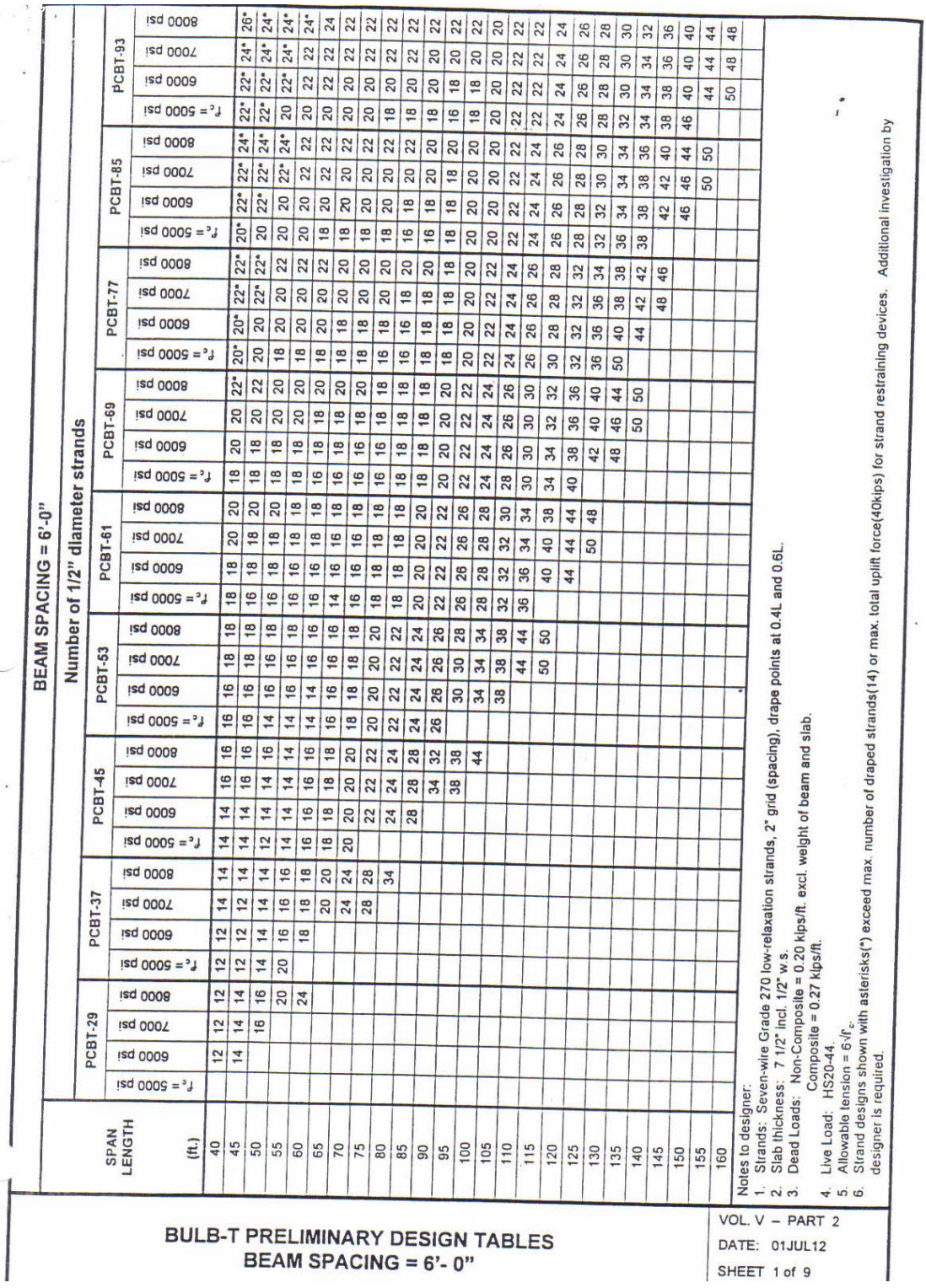

BEAM SPACING = 6'-0"

Number of 1/2" diameter strands

SPAN LENGTH (ft.)	PCBT-29			PCBT-37			PCBT-45			PCBT-53			PCBT-61			PCBT-69			PCBT-77			PCBT-85			PCBT-93		
	f'c = 5000 psi	6000 psi	7000 psi	f'c = 5000 psi	6000 psi	7000 psi	f'c = 5000 psi	6000 psi	7000 psi	f'c = 5000 psi	6000 psi	7000 psi	f'c = 5000 psi	6000 psi	7000 psi	f'c = 5000 psi	6000 psi	7000 psi	f'c = 5000 psi	6000 psi	7000 psi	f'c = 5000 psi	6000 psi	7000 psi	f'c = 5000 psi	6000 psi	7000 psi
40	12	12	12	12	12	14	14	14	16	16	16	18	18	18	20	18	20	20	20*	20*	22*	20*	22*	22*	22*	22*	24*
45	14	14	14	12	12	14	14	14	16	16	16	18	18	18	20	18	18	20	20	20	22*	20	22*	22*	22*	22*	24*
50		16	16	14	14	14	12	14	14	14	16	16	16	18	18	18	18	20	18	20	20	18	20	22	20	22*	24*
55				20	16	16	14	14	16	14	16	16	16	18	18	16	18	20	18	20	20	18	20	22	20	22*	24*
60			24		18	18	16	16	16	14	16	16	16	18	18	16	18	20	18	20	20	18	20	22	20	22*	24*
65					20	20	18	18	18	16	16	16	16	18	18	16	18	20	18	20	22	18	20	22	20	22	24*
70					24	24	20	20	20	16	16	16	16	16	18	16	18	18	18	20	20	18	20	22	20	22	24
75					28	28		22	22	20	20	18	16	16	18	16	16	18	18	18	20	18	20	22	20	22	22
80						34		24	24	22	22	20	18	18	18	16	16	18	16	18	20	18	20	22	20	22	22
85								28	28	24	24	24	20	20	20	18	18	18	18	18	20	16	18	20	18	20	22
90									34	26	26	26	22	22	22	20	20	20	18	18	20	16	18	20	18	20	20
95									38	30	30	28	26	26	26	22	22	22	20	20	20	18	18	18	16	18	20
100										34	34	34	28	28	28	24	24	24	22	22	22	20	20	20	18	18	20
105										38	38	38	32	32	30	28	26	26	24	24	24	22	22	22	20	20	20
110												44	36	34	34	30	30	30	26	26	26	24	24	24	22	22	22
115												50	40	40	38	34	32	32	30	28	28	24	24	24	22	22	22
120													44	44	40	38	36	36	32	32	32	28	28	28	24	24	24
125													50	48		42	40	40	36	36	36	32	32	32	26	26	26
130																48	46	44	40	38	38	34	34	34	28	28	28
135																	50	50	44	42	42	36	36	36	30	30	30
140																			48	46	46	38	38	38	34	34	32
145																						42	42	40	38	36	36
150																						46	46	44	40	40	40
155																							50	50	44	44	44
160																									50	48	48

Notes to designer:

1. Strands: Seven-wire Grade 270 low-relaxation strands, 2" grid (spacing), drape points at 0.4L and 0.6L.
2. Slab thickness: 7 1/2" incl. 1/2" w.s.
3. Dead Loads: Non-Composite = 0.20 kips/ft. excl. weight of beam and slab.
   Composite = 0.27 kips/ft.
4. Live Load: HS20-44.
5. Allowable tension = $6\sqrt{f'_c}$.
6. Strand designs shown with asterisks(*) exceed max. number of draped strands(14) or max. total uplift force(40kips) for strand restraining devices. Additional investigation by designer is required.

BULB-T PRELIMINARY DESIGN TABLES
BEAM SPACING = 6'- 0"

VOL. V – PART 2
DATE: 01JUL12
SHEET 1 of 9

APPENDIX B

Appendix B contains the data sheets showing the strand pattern and the girder details of the two samples used in the study done by Hinkle (2005).

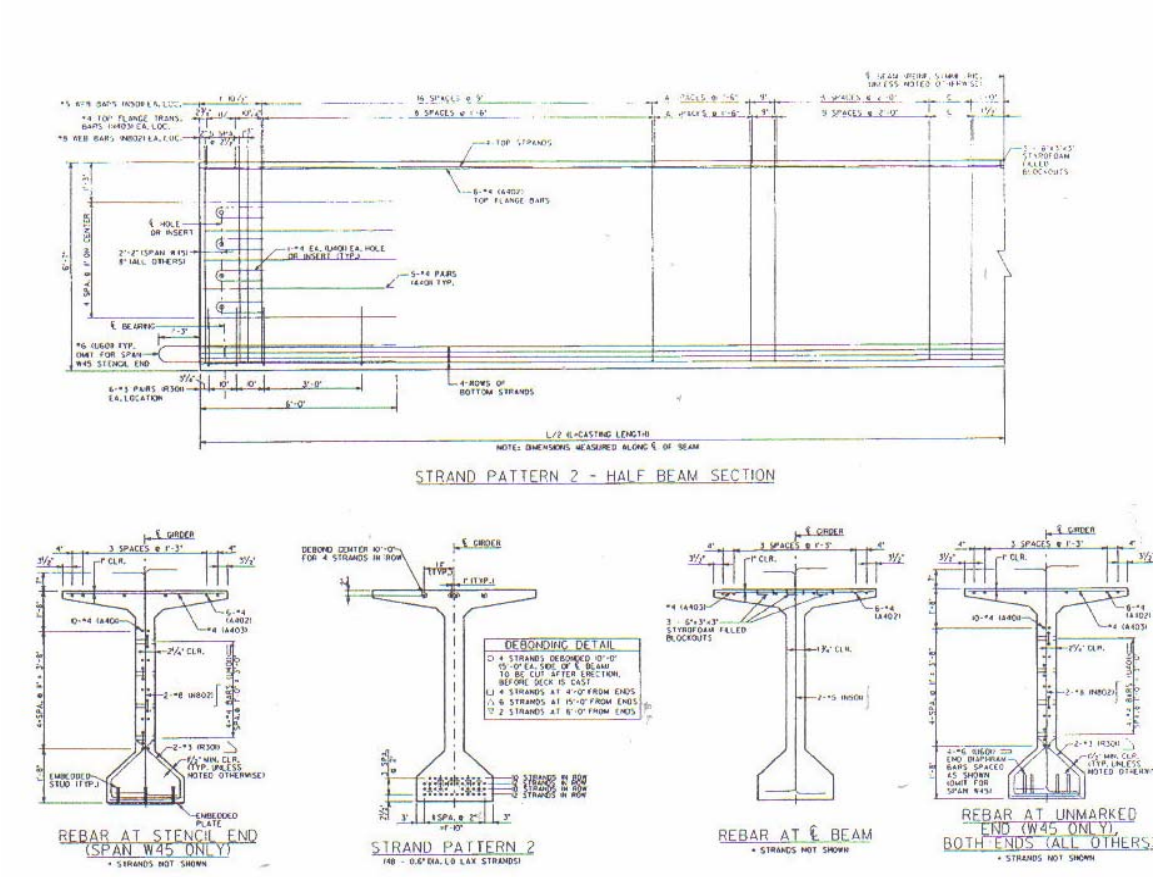

Figure B1 Strand Pattern of Sample 1

Table B1 Data of beams in Sample 1

Beam Number	Length	Strand Pattern	Date of Casting
W43-5	$127' - 5\frac{3}{4}"$	2	2/27/03
W43-8	$127' - 11\frac{1}{2}"$	2	2/27/03
W45-8	$127' - 5\frac{1}{2}"$	2	6/27/03
W45-7	$128' - 0\frac{3}{4}"$	2	6/27/03

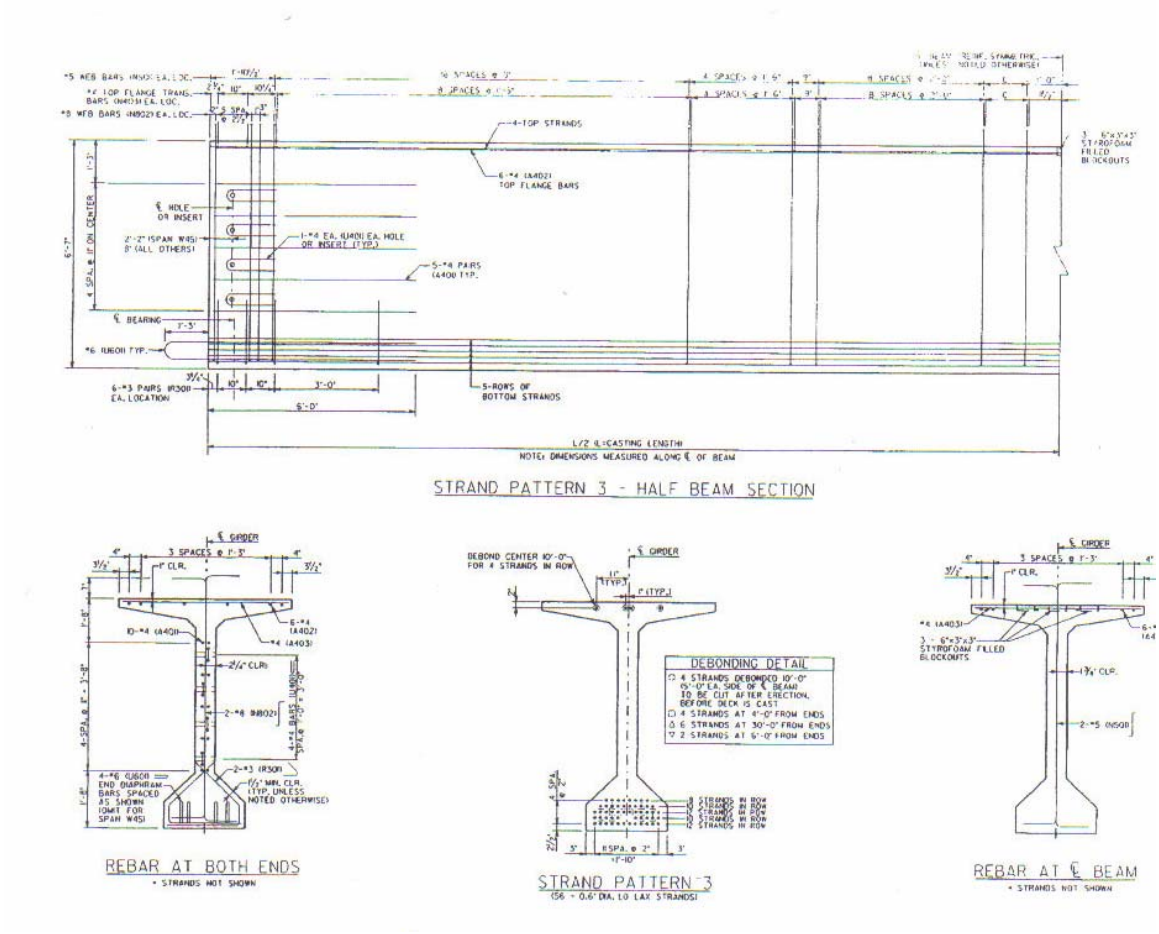

Figure B2 Strand Pattern of Sample 2

Table B2 Data of beams in Sample 2

Beam Number	Length	Strand Pattern	Date of Casting
W23-4	$136' - 6\frac{1}{2}"$	3	3/12/03
W24-3	$136' - 9\frac{1}{4}"$	3	2/26/03
W23-3	$136' - 9\frac{1}{4}"$	3	3/12/03
W27-7	$136' - 9\frac{1}{2}"$	3	7/3/03

APPENDIX C

Appendix C contains sample design calculations for the post-tensioned anchorage zone design for the unbonded monostrand anchorage. It also contains the procedure for determining the correction achieved by using the unbonded monostrands. In addition, it contains a data sheet showing the dimension details of the VSL type S6 monostrand anchorage.

C.1.1 Assumptions

The following assumptions were made to perform these calculations:

1. Rectangular section behavior is assumed.
2. The critical section behind the group of anchorages is assumed at h/3 from the first bearing surface of the anchorage.
3. The length of the local zone is assumed to be equal to the length of anchorage plus twice the edge distance of anchorage.
4. Rate of dispersion of compressive stress is assumed as 1:2 from the edge of bearing plate for e/b>3.

The size of type S6 anchorage is 4.13x2.95 inches.

C.1.2 Feasibility Check for Anchorage Arrangement in the PCBT Girder with No Draped Strands

C.1.2.1 Vertical Bearing Plates

Referring to Figure 5.9 and using the Guyon's method

$$P_{jack} = 0.80 A_{ps} f_s^{'} = 0.8\text{x}0.217\text{x}270 = 46.9 \text{ kips}$$

Calculate the bursting force and stress around the two vertical anchorages in the middle.

From Equation 5.6

$$T_{burst} = \frac{46.9}{4}\left(1 - \frac{4.13}{6.13}\right) = 3.82 kips$$

where

b is the bearing plate width and is equal to 4.13,

h is the member height and is equal to b plus twice the edge distance of 1 in. on each side,

P is the jacking force applied to one strand.

Calculate max f_t using Equation 5.8

$$\max f_t = \frac{T_{burst}}{0.55hw} = \frac{3.82}{0.55 \times 6.13 \times 9.0} = 0.251 \text{ ksi}$$

where, w is the member width calculated using assumptions 2 and 4.

The c/c distance of the middle two anchorages is 4 in.

Therefore w = 4+2.95+2.04(h/3) = 9.0 in.

Check this bursting stress against the allowable bursting stress

Allowable bearing stress is given by Equation C.1

$$allowable\ f_t = 4\sqrt{f_{ci}'} \qquad \text{(C.1)}$$

where f'_{ci} concrete strength at the time of stressing in psi.

The concrete strength chosen here is 5000 psi as this is the lowest concrete strength used in the PCBT's used by VDOT.

Therefore allowable f_t = 0.283 ksi.

For vertical anchorages allowable f_t is greater than max f_t therefore it is ok.

C.1.2.2 Bearing Stresses Behind Vertical Anchorages

Bearing stress behind each anchorage is checked using Equations 5.4 and 5.5. The method of checking the bearing stress is as follows: first the bearing stress under the first vertical anchorage is checked and then the bearing stress under the adjacent vertical anchorage is checked. Then the bearing stress under the two anchorages combined is checked.

Using Equation 5.4, the allowable bearing stress under the bearing plate is:

$$f_{cpi} = 0.5 \times 5 \times \sqrt{\frac{36.167}{12.183}} = 4.30\text{ksi} < 5.0\text{ksi}$$

where

f'_{ci}=5 ksi, is the concrete strength at the time of stressing,

A=36.167, is the distribution area given as $a_x a_y$,

A_g = 12.183 is the gross bearing plate area given as $b_x b_y$.

$a_x = b_x + 2e_x \leq 2b_x$

$a_y = b_y + 2e_y \leq 2b_y$

where b_x, b_y are the dimensions of the bearing plate and e_x, e_y are the edge distances to the bearing plates.

The limitation on the above equation is $\frac{1}{4} \leq \frac{e_x}{e_y} \leq 4$

The average bearing stress using Equation 5.3 is

$$\frac{46.9}{4.13 \times 2.95} = 3.84 \text{ ksi} < 4.30 \text{ ksi.}$$ Hence Ok

For the second bearing plate stress adjacent to the first one, the allowable bearing stress is

$$0.5 \times 5 \times \sqrt{\frac{24.52}{12.183}} = 3.54 \text{ ksi.}$$

As the allowable stress is less than the actual average bearing stress under the plate, we need to check the combined bearing stress under the two anchorages.

The combined allowable average bearing stress is given as

$$0.5 \times 5 \times \sqrt{\frac{8.95 \times 6.13}{2 \times 12.183}} = 3.75 \text{ ksi} < 5.0 \text{ ksi}$$

where a_x = 8.95, is equal to the out to out edge distance of the two bearing plates plus the edge distance of one inch on either side.

a_y = 6.13 is the length of the bearing plate plus the edge distance of 1 in. on either side.

The dimensions for a_x, a_y are chosen in such a way that they lead to conservative design values.

The average bearing stress under the two plates is

$$\frac{2 \times 46.9}{4.13 \times 6.95} = 3.26 \text{ ksi} < 3.75 \text{ ksi}$$

where, 6.95 is the out to out edge distance of the bearing plates in inches.

Therefore, the stress under the combined action of plates is ok and no confinement reinforcement is required.

C.1.2.3 Horizontal Bearing Plates

Referring to Figure 5.9, the bursting stress for horizontal anchorage is

$$T_{burst} = \frac{46.9}{4}\left(1 - \frac{2.95}{5}\right) = 4.80 kips$$

where

b is the bearing plate width equal to 2.95 in.,

h is the member height and is equal to b plus twice the edge distance of 1 inch on each side,

P is the same as above.

The maximum bursting stress is

$$\max f_t = \frac{T_{burst}}{0.55hw} = \frac{4.80}{0.55 \times 5 \times 5.80} = 0.300 \text{ ksi}$$

where, w is the member width calculated using assumptions 2 and 4,

Therefore w = 4.13+1.67(h/3) =9.0 in.

Checking this bursting stress against the allowable bursting stress gives

0.300 ksi > 0.283 ksi therefore the flange requires bursting reinforcement behind this anchorage.

C.1.2.4 Bursting Reinforcement

Using 1.2 as the load factor and 0.85 as the resistance factor the required bursting reinforcement is (Wollmann et al. 2000)

$$A_s = \frac{1.2 \times 4.80}{0.85 \times 60} = 0.11 in^2 \qquad \text{(C.2)}$$

Therefore, provide #3 bars vertical tie behind each horizontal anchorage

C.1.2.5 Bearing Stress Behind Horizontal Anchorage

From Equation 5.4 the allowable bearing stress under the horizontal anchorage is

$$0.5 \times 5 \times \sqrt{\frac{8.26 \times 5}{12.183}} = 4.60 \text{ ksi} < 5.0 \text{ ksi} \qquad \text{Ok}$$

where $a_x = 2x2.17 + 4.13 = 8.67 > 8.26\ (2b_x)$; $a_x = 8.26$ in.

$a_y = 2x1 + 2.95 = 4.95 < 5.9\ (2b_y)$; $a_y = 5$ in.

The average bearing stress under the horizontal anchorage is

$$\frac{46.9}{4.13 \times 2.95} = 3.84 \text{ ksi} < 4.60 \text{ ksi} \qquad \text{Ok}$$

C.1.2.6 Compressive Stress at the End of Local Zone

The length of the local zone for a conservative design is taken as the smaller dimension of the anchorage plus twice the edge distance of one inch.

Therefore $L_{lz} = 2.95 + 2x1 = 4.95$ in.

Using assumption 4 for rate of dispersion, the length at the end of the local zone for all the four anchorages is given as 19.55 + 4.95 = 24.5 in.

The depth at the end of local zone is 5 inches i.e. the maximum depth available for horizontal anchorages for a conservative design.

So the stress at the end of the local zone is

$$\frac{4 \times 46.9}{24.5 \times 5} = 1.53 \text{ ksi} < 2.5 \text{ ksi}\ (0.5f'_{ci})$$

Therefore, it is feasible to provide four anchorages in the top flange of a PCBT, which does not have any draped strands.

C.1.3 Feasibility Check for Anchorage Arrangement in PCBT Girder with Draped Strands

Referring to Figure 5.10 and using a similar approach as used in Section C.1.2.3 for horizontal bearing plates we would have to provide a #3 vertical tie behind each anchorage.

C.1.3.1 Bearing Stress Behind Horizontal Anchorage

Using Equation 5.4 the allowable bearing stress under the horizontal anchorage is

$$0.5\times 5\times\sqrt{\frac{8.26\times 5}{12.183}} = 4.60 \text{ ksi} < 5.0 \text{ ksi} \qquad \text{Ok}$$

where $a_x = 2x2.17 + 4.13 = 8.67 > 8.26\ (2b_x)$; $a_x = 8.26$ in.

$a_y = 2x1 + 2.95 = 4.95 < 5.9\ (2b_y)$; $a_y = 5$ in.

The average bearing stress under the horizontal anchorage is

$$\frac{46.9}{4.13\times 2.95} = 3.84 \text{ ksi} < 4\ 60 \text{ ksi} \qquad \text{Ok}$$

For the second bearing plate adjacent to the first one the allowable bearing stress is

$$0.5\times 5\times\sqrt{\frac{5.13\times 5}{12.183}} = 3.84 \text{ ksi} < 5.0 \text{ ksi} \qquad \text{Ok}$$

where $a_x = 2x0.5 + 4.13 = 5.13 < 8.26\ (2b_x)$; $a_x = 5.13$ in.

$a_y = 2x1 + 2.95 = 4.95 < 5.9\ (2b_y)$; $a_y = 5$ in.

The average bearing stress under the horizontal anchorage is

$$\frac{2\times 46.9}{8.76\times 2.95} = 3.63 \text{ ksi} < 4.60 \text{ ksi} \qquad \text{Ok}$$

where 8.76in., is the out to out edge distance of the horizontal bearing plates.

C.1.3.2 Compressive Stress at the End of Local Zone

The length of the local zone for conservative design is taken as the smaller dimension of anchorage plus twice the edge distance of one inch.

Therefore $L_{lz} = 2.95 + 2x1 = 4.95$ in.

Using assumption 4 for rate of dispersion, the length at the end of the local zone for all the four anchorages is given as 23.00 + 4.95 = 27.95 in.

The depth at the end of local zone is 5 in. i.e. the maximum depth available for horizontal anchorages for a conservative design value.

So the stress at the end of the local zone is

$$\frac{4 \times 46.9}{27.95 \times 5} = 1.342 \text{ ksi} < 2.5 \text{ ksi } (0.5f'_{ci})$$

Therefore, it is feasible to provide four anchorages in the top flange of a PCBT, which has draped strands.

C1.4 Camber Control Using Unbonded Monostrands

For controlling camber, the following steps were followed to determine the camber controlled by four 0.6 in. monostrands.

1. Calculate the transformed section properties of the beam.

$$A_{tr} = A_g + (n_{pc} - 1)A_{ps} \tag{C.3}$$

$$y_{btr} = \frac{A_g y_{bg} + (n_{pc} - 1)A_{ps} y_{cg}}{A_{tr}} \tag{C.4}$$

$$I_{tr} = I_g + A_g (y_{btr} - y_{bg})^2 + (n_{pc} - 1)A_{ps} (y_{btr} - y_{cg})^2 \tag{C.5}$$

where

A_g is the gross sectional area of the beam, in.^{2},

A_{ps} is the total area of prestressing strands, in.^{2},

y_{bg} is the distance of the center of gravity of the gross section of the beam from extreme fiber of bottom flange, in.,

y_{cg} is the distance of the center of gravity of the prestressing strands from extreme fiber of bottom flange, in.,

A_{tr} is the area of the equivalent transformed section of the beam, in.^{2},

$$n_{pc} = \frac{E_p}{E_c} \tag{C.6}$$

n_{pc} is the modular ratio,

E_p is the modulus of elasticity of prestressing strands, ksi,

E_c is the modulus of elasticity of concrete at the time of stressing of steel, ksi,

y_{btr} is the distance of the center of gravity of the equivalent transformed section of the beam from the extreme fiber of the bottom flange, in.,

I_{tr} is the second moment of area of the equivalent transformed section, in.^{4}.

2. Calculate the effective force in monostrands

$$P_{monostrands} = 0.70 f_{pu} A_{ps\_monostrands} \tag{C.7}$$

The above Equation calculates the effective force in monostrands after instantaneous friction and seating losses.

3. Calculate the stresses at the extreme fibers of the beam

$$f_{top} = \frac{P_{monostrands}}{A_{tr}} + \frac{P_{monostrands} e(h - y_{btr})}{I_{tr}} \tag{C.8}$$

$$f_{bot} = \frac{P_{monostrands}}{A_{tr}} - \frac{P_{monostrands} e y_{btr}}{I_{tr}} \tag{C.9}$$

where

f_{top} is the stress at extreme top fiber of the beam,

e is the eccentricity of the post tensioned monostrands with respect to the center of gravity of the equivalent transformed section,

h is the height of the section,

f_{bot} is the stress at the extreme bottom fiber of the beam.

4. Calculate strains at the extreme fibers of the beam using the Hooke's law

$$\varepsilon_{top} = \frac{f_{top}}{E_c} \tag{C.10}$$

$$\varepsilon_{bot} = \frac{f_{bot}}{E_c} \tag{C.11}$$

5. Calculate curvature of the transformed section

$$\phi = \frac{\varepsilon_{bot} - \varepsilon_{top}}{h} \tag{C.12}$$

6. Calculate the curvature at various sections along the length of beam up to midspan using the above steps and plot the curvature diagram.
7. Calculate the downward deflection using the moment area method.

Monostrand Post-Tensioning

Stressing Anchorage VSL Type S-6

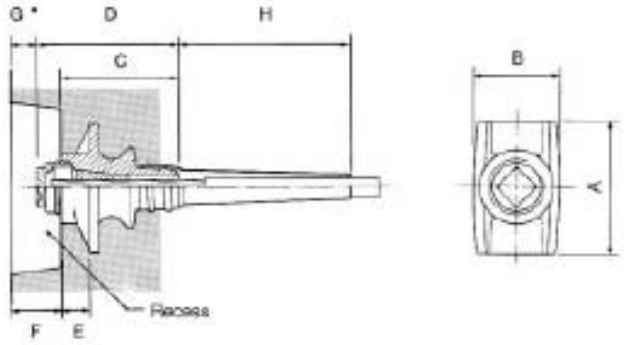

Type	A	B	C	D	E	F	G	H
S-6	4.13	2.95	4.33	4.53	0.91	1.57	0.79	6.25

* for 0.79" cover, to be adjusted for other values as needed

Dimensions in inches.

Dimensions are valid for nominal concrete strength: 3,000 psi (20 MPa), at the time of stressing, for a maximum stressing force of 80% of the tendon breaking load.

Dead-End Anchorage VSL Type SF-6

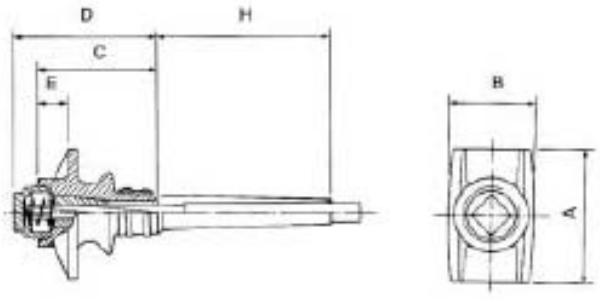

Type	A	B	C	D	E	H
SF-6	4.13	2.95	3.74	4.53	0.91	6.25

Dimensions in inches.

Dimensions are valid for nominal concrete strength: 3,000 psi (20 MPa), at the time of stressing, for a maximum stressing force of 80% of the tendon breaking load.

Figure C.1 Data sheet showing the dimension details of type S6 anchorage used.

VITA

Vivek Sethi was born on May 30, 1980 in Madras, India. He completed his high school from Ramjas School- Pusa Rd, New Delhi in 1997. He graduated with Bachelor of Engineering in Civil Engineering from Punjab Engineering College, Chandigarh in 2001. He worked for 3 years in Simplex Concrete Piles (I) Ltd. as Assistant Engineering (Civil) on a large-scale infrastructure project. Vivek Sethi joined Virginia Tech for pursuing Master of Science in Civil Engineering in August 2004.